# TUNNELS AND UNDERGROUND CITIES: ENGINEERING AND INNOVATION MEET ARCHAEOLOGY, ARCHITECTURE AND ART

Volume 5

Innovation in underground engineering, materials and equipment - Part 1


Editors:

Daniele Peila

Giulia Viggiani

Tarcisio Celestino



CRC Press
Taylor & Francis Group
A BALKEMA BOOK

TUNNELS AND UNDERGROUND CITIES: ENGINEERING AND INNOVATION MEET ARCHAEOLOGY, ARCHITECTURE AND ART

Taylor & Francis
Taylor & Francis Group
http://taylorandfrancis.com

PROCEEDINGS OF THE WTC2019 ITA-AITES WORLD TUNNEL CONGRESS, NAPLES, ITALY, 3-9 MAY, 2019

# Tunnels and Underground Cities: Engineering and Innovation meet Archaeology, Architecture and Art

## *Volume 5: Innovation in underground engineering, materials and equipment - Part 1*

*Editors*

Daniele Peila

*Politecnico di Torino, Italy*

Giulia Viggiani

*University of Cambridge, UK*
*Università di Roma "Tor Vergata", Italy*

Tarcisio Celestino

*University of Sao Paulo, Brasil*

CRC Press
Taylor & Francis Group
Boca Raton London New York

CRC Press is an imprint of the
Taylor & Francis Group, an **informa** business
A BALKEMA BOOK

Cover illustration:

View of Naples gulf

*CRC Press/Balkema is an imprint of the Taylor & Francis Group, an informa business*



*Typeset by Integra Software Services Pvt. Ltd., Pondicherry, India*



Published by: CRC Press/Balkema
Schipholweg 107C, 2316XC Leiden, The Netherlands
e-mail: Pub.NL@taylorandfrancis.com
www.crcpress.com – www.taylorandfrancis.com

ISBN: 978-0-367-46870-5 (Hbk)
ISBN: 978-1-003-03161-1 (eBook)

*Tunnels and Underground Cities: Engineering and Innovation meet Archaeology, Architecture and Art, Volume 5: Innovation in underground engineering, materials and equipment - Part 1 – Peila, Viggiani & Celestino (Eds)*
*© 2020 Taylor & Francis Group, London, ISBN 978-0-367-46870-5*

# Table of contents

*Tunnels and Underground Cities: Engineering and Innovation meet Archaeology, Architecture and Art, Volume 5: Innovation in underground engineering, materials and equipment - Part 1 – Peila, Viggiani & Celestino (Eds)*
 *ISBN 978-0-367-46870-5*

# Preface

The World Tunnel Congress 2019 and the 45th General Assembly of the International Tunnelling and Underground Space Association (ITA), will be held in Naples, Italy next May.

The Italian Tunnelling Society is honored and proud to host this outstanding event of the international tunnelling community.

Hopefully hundreds of experts, engineers, architects, geologists, consultants, contractors, designers, clients, suppliers, manufacturers will come and meet together in Naples to share knowledge, experience and business, enjoying the atmosphere of culture, technology and good living of this historic city, full of marvelous natural, artistic and historical treasures together with new innovative and high standard underground infrastructures.

The city of Naples was the inspirational venue of this conference, starting from the title Tunnels and Underground cities: engineering and innovation meet Archaeology, Architecture and Art.

Naples is a cradle of underground works with an extended network of Greek and Roman tunnels and underground cavities dated to the fourth century BC, but also a vibrant and innovative city boasting a modern and efficient underground transit system, whose stations represent one of the most interesting Italian experiments on the permanent insertion of contemporary artwork in the urban context.

All this has inspired and deeply enriched the scientific contributions received from authors coming from over 50 different countries.

We have entrusted the WTC2019 proceedings to an editorial board of 3 professors skilled in the field of tunneling, engineering, geotechnics and geomechanics of soil and rocks, well known at international level. They have relied on a Scientific Committee made up of 11 Topic Coordinators and more than 100 national and international experts: they have reviewed more than 1.000 abstracts and 750 papers, to end up with the publication of about 670 papers, inserted in this WTC2019 proceedings.

According to the Scientific Board statement we believe these proceedings can be a valuable text in the development of the art and science of engineering and construction of underground works even with reference to the subject matters "Archaeology, Architecture and Art" proposed by the innovative title of the congress, which have "contaminated" and enriched many proceedings' papers.

Andrea Pigorini
SIG President

Renato Casale
*Chairman of the Organizing Committee WTC2019*

*Tunnels and Underground Cities: Engineering and Innovation meet Archaeology, Architecture and Art, Volume 5: Innovation in underground engineering, materials and equipment - Part 1 – Peila, Viggiani & Celestino (Eds)*
 *ISBN 978-0-367-46870-5*

# Acknowledgements

REVIEWERS

The Editors wish to express their gratitude to the eleven Topic Coordinators: Lorenzo Brino, Giovanna Cassani, Alessandra De Cesaris, Pietro Jarre, Donato Ludovici, Vittorio Manassero, Matthias Neuenschwander, Moreno Pescara, Enrico Maria Pizzarotti, Tatiana Rotonda, Alessandra Sciotti and all the Scientific Committee members for their effort and valuable time.

SPONSORS

The WTC2019 Organizing Committee and the Editors wish to express their gratitude to the congress sponsors for their help and support.

*Tunnels and Underground Cities: Engineering and Innovation meet Archaeology, Architecture and Art, Volume 5: Innovation in underground engineering, materials and equipment - Part 1 – Peila, Viggiani & Celestino (Eds)*
*© 2020 Taylor & Francis Group, London, ISBN 978-0-367-46870-5*

# WTC 2019 Congress Organization

## HONORARY ADVISORY PANEL

Pietro Lunardi, President WTC2001 Milan
Sebastiano Pelizza, ITA Past President 1996-1998
Bruno Pigorini, President WTC1986 Florence

## INTERNATIONAL STEERING COMMITTEE

Giuseppe Lunardi, Italy (Coordinator)
Tarcisio Celestino, Brazil (ITA President)
Soren Eskesen, Denmark (ITA Past President)
Alexandre Gomes, Chile (ITA Vice President)
Ruth Haug, Norway (ITA Vice President)
Eric Leca, France (ITA Vice President)
Jenny Yan, China (ITA Vice President)
Felix Amberg, Switzerland
Lars Barbendererder, Germany
Arnold Dix, Australia
Randall Essex, USA
Pekka Nieminen, Finland
Dr Ooi Teik Aun, Malaysia
Chung-Sik Yoo, Korea
Davorin Kolic, Croatia
Olivier Vion, France
Miguel Fernandez-Bollo, Spain (AETOS)
Yann Leblais, France (AFTES)
Johan Mignon, Belgium (ABTUS)
Xavier Roulet, Switzerland (STS)
Joao Bilé Serra, Portugal (CPT)
Martin Bosshard, Switzerland
Luzi R. Gruber, Switzerland

## EXECUTIVE COMMITTEE

Renato Casale (Organizing Committee President)
Andrea Pigorini, (SIG President)
Olivier Vion (ITA Executive Director)
Francesco Bellone
Anna Bortolussi
Massimiliano Bringiotti
Ignazio Carbone
Antonello De Risi
Anna Forciniti
Giuseppe M. Gaspari

Giuseppe Lunardi
Daniele Martinelli
Giuseppe Molisso
Daniele Peila
Enrico Maria Pizzarotti
Marco Ranieri

## ORGANIZING COMMITTEE

Enrico Luigi Arini
Joseph Attias
Margherita Bellone
Claude Berenguier
Filippo Bonasso
Massimo Concilia
Matteo d'Aloja
Enrico Dal Negro
Gianluca Dati
Giovanni Giacomin
Aniello A. Giamundo
Mario Giovanni Lampiano
Pompeo Levanto
Mario Lodigiani
Maurizio Marchionni
Davide Mardegan
Paolo Mazzalai
Gian Luca Menchini
Alessandro Micheli
Cesare Salvadori
Stelvio Santarelli
Andrea Sciotti
Alberto Selleri
Patrizio Torta
Daniele Vanni

## SCIENTIFIC COMMITTEE

Daniele Peila, Italy (Chair)
Giulia Viggiani, Italy (Chair)
Tarcisio Celestino, Brazil (Chair)
Lorenzo Brino, Italy
Giovanna Cassani, Italy
Alessandra De Cesaris, Italy
Pietro Jarre, Italy
Donato Ludovici, Italy
Vittorio Manassero, Italy
Matthias Neuenschwander, Switzerland
Moreno Pescara, Italy
Enrico Maria Pizzarotti, Italy
Tatiana Rotonda, Italy
Alessandra Sciotti, Italy
Han Admiraal, The Netherlands
Luisa Alfieri, Italy
Georgios Anagnostou, Switzerland
Andre Assis, Brazil
Stefano Aversa, Italy
Jonathan Baber, USA
Monica Barbero, Italy
Carlo Bardani, Italy
Mikhail Belenkiy, Russia
Paolo Berry, Italy
Adam Bezuijen, Belgium
Nhu Bilgin, Turkey
Emilio Bilotta, Italy
Nikolai Bobylev, United Kingdom
Romano Borchiellini, Italy
Martin Bosshard, Switzerland
Francesca Bozzano, Italy
Wout Broere, The Netherlands
Domenico Calcaterra, Italy
Carlo Callari, Italy

Luigi Callisto, Italy
Elena Chiriotti, France
Massimo Coli, Italy
Franco Cucchi, Italy
Paolo Cucino, Italy
Stefano De Caro, Italy
Bart De Pauw, Belgium
Michel Deffayet, France
Nicola Della Valle, Spain
Riccardo Dell'Osso, Italy
Claudio Di Prisco, Italy
Arnold Dix, Australia
Amanda Elioff, USA
Carolina Ercolani, Italy
Adriano Fava, Italy
Sebastiano Foti, Italy
Piergiuseppe Froldi, Italy
Brian Fulcher, USA
Stefano Fuoco, Italy
Robert Galler, Austria
Piergiorgio Grasso, Italy
Alessandro Graziani, Italy
Lamberto Griffini, Italy
Eivind Grov, Norway
Zhu Hehua, China
Georgios Kalamaras, Italy
Jurij Karlovsek, Australia
Donald Lamont, United Kingdom
Albino Lembo Fazio, Italy
Roland Leucker, Germany
Stefano Lo Russo, Italy
Sindre Log, USA
Robert Mair, United Kingdom
Alessandro Mandolini, Italy
Francesco Marchese, Italy
Paul Marinos, Greece
Daniele Martinelli, Italy
Antonello Martino, Italy
Alberto Meda, Italy
Davide Merlini, Switzerland
Alessandro Micheli, Italy
Salvatore Miliziano, Italy
Mike Mooney, USA
Alberto Morino, Italy
Martin Muncke, Austria
Nasri Munfah, USA
Bjørn Nilsen, Norway
Fabio Oliva, Italy
Anna Osello, Italy
Alessandro Pagliaroli, Italy
Mario Patrucco, Italy
Francesco Peduto, Italy
Giorgio Piaggio, Chile
Giovanni Plizzari, Italy
Sebastiano Rampello, Italy
Jan Rohed, Norway
Jamal Rostami, USA
Henry Russell, USA
Giampiero Russo, Italy
Gabriele Scarascia Mugnozza, Italy
Claudio Scavia, Italy
Ken Schotte, Belgium
Gerard Seingre, Switzerland
Alberto Selleri, Italy
Anna Siemińska Lewandowska, Poland
Achille Sorlini, Italy
Ray Sterling, USA
Markus Thewes, Germany
Jean-François Thimus, Belgium
Paolo Tommasi, Italy
Daniele Vanni, Italy
Francesco Venza, Italy
Luca Verrucci, Italy
Mario Virano, Italy
Harald Wagner, Thailand
Bai Yun, China
Jian Zhao, Australia
Raffaele Zurlo, Italy

*Innovation in underground engineering, materials and equipment*

*Tunnels and Underground Cities: Engineering and Innovation meet Archaeology, Architecture and Art, Volume 5: Innovation in underground engineering, materials and equipment - Part 1 – Peila, Viggiani & Celestino (Eds)*
*© 2020 Taylor & Francis Group, London, ISBN 978-0-367-46870-5*

# Artificial intelligence technique for geomechanical forecasting

M. Allende Valdés, J.P. Merello & P. Cofré
*SKAVA Consulting, Santiago, Chile*

ABSTRACT: After every blast, rock mass classification is performed. However, no person can see beyond the face. There are methods commonly used for this purpose: core drilling, measurement while drilling and probe holes. In this project, machine learning techniques (Artificial Intelligence), were applied to geotechnical information from probe hole drilling and face mappings, in order to find patterns and infer functions based on data used for training. Information had to be organized to be accessed by the machine learning method. The model learns from training data; it is understood that non-experienced situations cannot be predicted. Because of this, it was assumed that every project would need its own training. Data from a testing tunnel was considered. Once the model was trained, it was used as a forecasting tool during the performance of new Probe Holes. Results show that the model has an accuracy of +85% forecasting rock mass classification.

## 1 INTRODUCTION

For the construction of every underground facility in rock, the site's geology is the most important condition to consider for every stage of the project, from feasibility studies to detail engineering and construction. Prospecting and studies are performed following the level of certainty required for the project subjected to technical requisites and budget. For tunnels, in the early stages of engineering, core drilling is by far the most used method of prospecting. Depending on the overburden of the tunnel, a large total of meters of core drillings will be needed to reach a single point of the axis of the tunnel. However, there are other forms of prospecting available and used worldwide.

The geology to consider for the design of a project is the result of the interpretation of all prospections, review of references, studies and all available information, generally resulting in a Geotechnical Baseline Report. However, this information gives a general overview and does not cover the drastic variations that geology can have within a matter of meters during the construction of underground facilities resulting in changes in support conditions and in most severe cases, tunnel collapses.

This is the reason why during the construction of tunnels the forecasting of rock mass is always wanted in order to perceive in advance the changes in the geology that could result in construction delays and in worst case scenarios, damage to equipment or loss of life. In other words, a trustworthy forecast of the rock mass to be excavated will result in the reduction of geological risk.

This paper describes some of the current methods for rock mass forecasting and how the application of Artificial Intelligence (AI) improves rock mass forecasting.

## 2 ROCK MASS FORECASTING METHODS

Currently, rock mass forecasting is performed by several methods. Each method has advantages and disadvantages.

### 2.1 *Core drillings*

Core drilling can be precise, but expensive and slow (Chapman 2000). Only specific conditions will justify the investment, because advancing face has to be halted to perform the task. If it is done in parallel, then the advance rate of the face will probably be higher than that of the core drilling, returning useless information. This occurred during the construction of the tunnel detailed in this paper. At the end, a special niche had to be constructed to perform the core drilling without stopping the excavation face advance. Due to the complex logistics and numerous interferences between core drilling and advance teams, the drill & blast cycle had important delays while coexisting with each other. The advance rate of the core drilling was only a couple of meters a week faster than the advance face, so the useful information provided was good only to forecast one or two rounds. Also, a joint system subparallel to the core drill was not detected, producing small deviations in the forecasting information.

At the end, core drilling was a very expensive tool (a special niche had to be built) that contributed with limited forecasting information. Nevertheless, this was high quality information.

### 2.2 *Measurement while drilling*

Measurement while drilling (MWD) is a very powerful tool. The interpretation of digital drilling parameters can give useful information about what lies behind the face, but the investment in computerized equipment, and training of personnel imposes a huge constraint (Rivera 2012). Even when the MWD is considered for tunnel construction, the interpretation of the parameters must be done by a geologist with special training in such tools. In most of the cases the geologist is in charge of the drilling equipment while the MWD is in use. This can generate difficulties when the geologists in charge of the definition of the rock mass support belong to an independent third party, because the contractor must allow an external member to use their equipment.

In the case study presented in this paper, the drilling equipment (Jumbo) did not offer the option to include automated MWD tools, so this option was not considered.

### 2.3 *Probe holes*

Probe holes, on the other hand, are cheap, fast and easy to perform (Bilgin 2016). The problem is that the data interpretation is very subjective, generally leaving the responsibility in the hands of the operator. The analysis will vary depending on which shift, equipment and operator is drilling. Probe holes are destructive perforations (i.e. no core recovery), so all information is gathered during the drilling process. Also, in old drilling equipment like the one used in the project listed in this paper, maintenance operations can modify the jumbo's performance.

All the information resulting from probe holes will be summarized and interpreted by the operations manager or geologist in charge. This will create a large scattering of information if no unified criteria are applied to the project. Also, as mentioned before, the handling by the drilling operator plays a very important role, because the perforation with old equipment like that used in the study case depends on 2 variables: drilling pressure and rotation speed. So, the operator has to modify these 2 variables to drill most effectively.

### 2.4 *Others*

Nowadays, there are other methods available for the forecast of rock mass. Just to name one, Tunnel Seismic Prediction (TSP) uses seismic induced waves and geophysics to interpret properties of the upcoming rock mass and significant changes (i.e. faults, shear zones, etc.).

## 3 DEFINITION OF THE DATA

In order to work on new forecasting options, a set of data was needed. A project located in Perú was selected for this purpose. The project consists of a river diversion tunnel of 7.7 km in length and with a cross section of 23 $m^2$. The construction method selected for the project was Drill & Blast.

During the engineering stages of the project, the rock mass support was to be qualified using Barton's Q Index. In total, 6 support types were defined, assigning support type 1 to the best rock mass competency and support type 6 to the weakest rock mass. The following table shows the support classes limits.

The support consisted in combinations of sprayed shotcrete (with and without fiber), passive rock bolts, steel mesh and lattice girders.

The geology in the project area was largely dominated by igneous rocks, mainly granodiorite and riolite. There was an altered zone near the project, which produced a large number of geologic faults with very poor geotechnical conditions. The variation of geotechnical conditions were abrupt in many cases, changing from support type 3 to support type 6 in a matter of meters. These variations had a high impact in the coordination of construction directly impacting the advance rates and stability of the tunnel between blasting and support installation. Also, during rainy seasons, a significant amount of infiltration waters entered the excavation section, producing a decrease in the geotechnical rock mass quality.

### 3.1 *Rock mass face mapping and probe holes*

Due to contractual requirements and the site conditions previously described, a geological face mapping had to be performed after every blast during construction by an independent third party (this was SKAVA's role in this project). In such face mapping, a geologist had to evaluate the geological conditions of the rock mass and calculate the Barton's Q Index. Also, in the face mapping a full register of joint systems, shear zones, infiltrations and pictures were included, giving a very complete set of data on the excavated rock mass.

Also due to contractual requirements and site conditions, the contractor had to perform Probe Holes (destructive) 30 meters long with a minimum overlap of 5 meters. The contractor used 3-meter rods for perforation, so each probe hole had a total of 10 perforation rods. The independent third party geologists were responsible for the parameter measurements and interpretation.

While performing the probe holes, the following data were recorded:

- Initial chainage of the probe hole.
- Date and time of the probe hole.
- Orientation of the probe hole.
- Equipment used for the probe hole (jumbo)
- Boring pressure for each rod.
- Advance speed for each rod, in meters per minute
- Advance speed for each rod, in seconds per meter
- Detritus colour
- Water inflow

After the total completion of the probe hole, the third party geologist had to write a report and inform the Owner and the contractor of the project about the findings obtained from the probe hole. Such report was purely factual and not interpretative.

Table 1. Rock mass support types limits (Q index).

| Support Type | Lowest Q Value | Highest Q Value |
|---|---|---|
| Type 1 | 10 | |
| Type 2 | 5 | 10 |
| Type 3 | 0.4 | 5 |
| Type 4 | 0.1 | 0.4 |
| Type 5 | 0.03 | 0.1 |
| Type 6 | | 0.03 |

## 4 FIRST APPROACH OF FORECAST

During the construction of the tunnel an important number of overbreaks resulted after blasting, the drastic changes in the geology being one of the most important root causes. In this scenario, the forecast performed through probe holes was studied in detail by the third party geologist in order to give this database a more useful purpose.

The first action was to gather, standardize, label, organize, and store all the existing information obtained from all historic probe holes of the project. A total of 560 sets of information were analysed, each dataset comprised all the information corresponding to one perforation rod.

Since the focus of this research was to improve the information behind the excavation face, a first examination of the data showed that for this purpose the boring pressure and the advance speed of the rod were the most useful information.

After selecting what information to consider, an historical review of the existing information was performed. As a way to simplify the forecast expected, the first correlations were made looking for support types to be installed, thus all information selected was compared with the actual support type installed. In other words, a linear comparison was performed, aligning information from the probe holes and the rock mass support type effectively installed for the same chainages.

In this line, the following Figures 1, 2 and 3 present, graphically, the history of the database from the probe holes of the project (the aforementioned 560 data sets) and the effectively installed rock mass support type.

Through visual and numerical processing of the information plotted, it was decided that the boring pressure was the most representative information obtained from probe holes to relate to support type. Figure 4 shows how the simple average of the boring pressures relate to the support type for the 560 data sets considered. Also, a simple linear regression was included in this graph to show that the average boring pressure and the support type relation has a $R^2$ value of 0,692. As expected, the boring pressure increased with the highest rock mass quality. An important fact is that for all the data sets considered, no support type 6 had been installed, thus this support type was not statistically considered in this first approach. As shown in Figure 4, the average boring pressures are within a range of 20 bars, from 60 bars for support type 5, to 80 bars for support type 1.

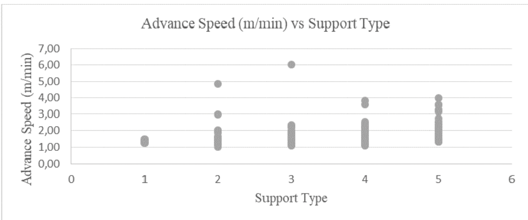


Figure 1. Advance speed (m/min) vs support type.

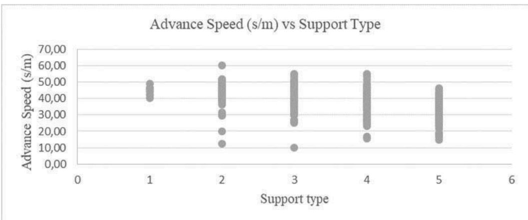


Figure 2. Advance speed (s/m) vs support type.

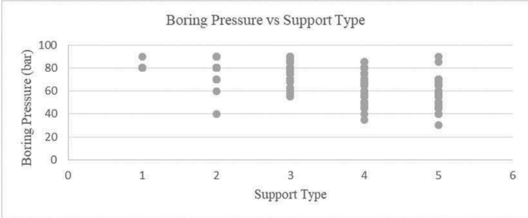


Figure 3. Boring pressure vs support type.

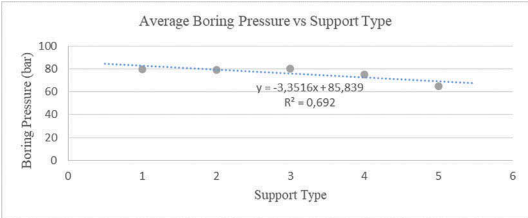


Figure 4. Boring pressure vs support type.

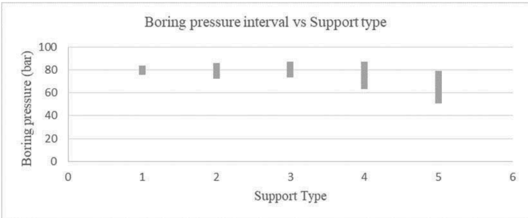


Figure 5. Boring pressure interval vs support type, “Abacus”.

Table 2. First results using the “Abacus”.

| Forecasts | Unit | (%) |
|---|---|---|
| Correct | 158 | 74,2% |
| Incorrect | 55 | 25,8% |
| Total | 213 | 100,0% |

The next step was to generate an simple tool for rock mass forcasting. So, an “abacus” that had a pressure interval for each support type was generated. Each interval consisted of the average boring pressure plus and minus a single standard deviation (Figure 5). The abacus was applied as follows: The geologist supervising the probe hole recorded the average boring pressure for each rod and then through the abacus determined the support types that are contained in such boring pressure. Since the boring pressure intervals have common values, simple boring pressure data could forecast 2 or 3 support types. And so a single boring pressure measurement was used for a single forecast, but such forecast included 2 or 3 support types.

After some time forecasting with the “Abacus” a review of the forecast results was analyzed. A total of 213 forecasts were made using the “Abacus”. Table 2 shows the results obtained

Table 3. Error analysis.

| Incorrect forecasts | Unit | (%) |
|---|---|---|
| Conservative | 5 | 9,1% |
| Non-conservative | 50 | 90,9% |
| Total | 55 | 100,0% |

with its usage. From all the forecasts, a 74,2% proved to be correct, the forecasted support types with the real mapped support type were a perfect match.

The incorrect forecasts were analyzed to realize whether the errors were conservative or non-conservative. A conservative error was defined as when the forecasted support type having a lower Q value than the real Q value mapped. Table 3 shows the analysis of the errors made.

## 5 MACHINE LEARNING APPROACH

After the first approach for forecasting the support type using single average values, the idea of including Artificial Intelligence (AI) was implemented.

### 5.1 *Method used and data considered*

Supervised Learning is the machine learning task of inferring a function from labelled training data (Mohri et al 2012). The goal of this project was to apply Supervised Learning to geotechnical information, in order to find patterns and infer functions based on training data. The chosen technique was Support Vector Machine (Kotsiantis 2006), and the data from Geotechnical Mapping and Probe Holes drilling was used for training.

Information from both sources had to be standardized, labelled, organized and stored in such a way that it would be easily accessed by the supervised learning method. The model only learns from that training data, and it is understood that non-experienced situations cannot be predicted. Because of this, it was assumed that every project would need its own training process.

As mentioned before, the testing tunnel was located mainly in a Granodiorite region from Superior Cretaceous-Tertiary, with a Rhyolite unit from Cretaceous-Tertiary, and some presence of Dacite. Geomechanical stability was structurally dominated, with a periodical appearance of two fault systems. Water and stresses were not dominant factors.

### 5.2 *First models*

After the selection of the AI method to use, a model needed to be developed. This time the model should forecast the Q index value, not the support type. Once the model was complete and ready to forecast, in order to get an idea on how fast the model learned, 4 different models were trained with different sample sizes. Figure 6 shows, in red, the Q value forecasted and in black the real Q value mapped for four different training models with sample size 100, 200, 300 and 500.

As can be seen in Figure 6, more data available (i.e. sample size increases), the more accurate the trained model becomes. For the same models analyzed at this time, a support type forecast was made considering the forecasted Q value that would assign a support type. This was compared with the real support type mapped in the tunnel. The result was found correct within the exact support type or within 2 consecutive support types from the real ones mapped. Table 4 shows the results from this initial 4 models.

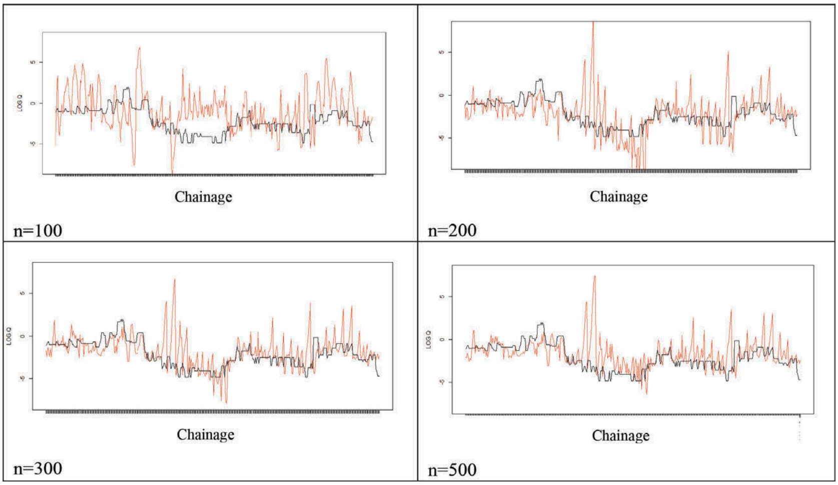


Figure 6. Improvement of forecast with Machine Learning.

Table 4. First Machine Learning results.

| Sample Size | Exact support type | 2 support types range |
|---|---|---|
| 100 | 35% | 45% |
| 200 | 50% | 69% |
| 300 | 51% | 71% |
| 500 | 54% | 75% |

### 5.3 *Trained model*

The final model considered 1692 registers that were used to train it, and 423 registers were used as test set, all from the same tunnel. Once the model was trained, it was used as a forecasting tool during the performance of new Probe Holes. Results show that the model has an accuracy of +85% forecasting rock mass classification behind the face in a way that is suitable for advising a decision maker. Figure 7 shows the results obtained with the final model.

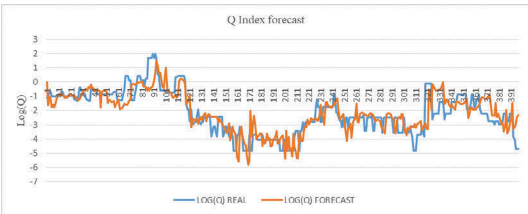


Figure 7. Final forecast with trained model.

## 6 CONCLUSIONS

Forecasting the rock to be excavated has been always a crucial tool during tunnel construction. Current methods offer some predictions, but all of them have certain limitations. Data used from an existing project showed that an historical analysis was a good tool to forecast the rock mass quality, but the inclusion of Artificial Intelligence offers more accurate results.

## REFERENCES


Bilgin, N. & Ates, U, 2016. Probe Drilling Ahead of Two TBMs in Difficult Ground Conditions in Turkey. *Rock Mechanics Rock Engineering* Volume 49 (Issue 7): pages 2763–2772.

Chapman, R.E., (ed) 2000. Petroleum Geology, Developments in Petroleum Science. Amsterdam: Elsevier.

Kotsiantis, S.B., 2006, Supervised Machine Learning: A Review of Classification Techniques. *Artificial Intelligence Review* Volume 26 (Issue 3): pages 159–190.

Mohri, M, and Rostamizadeh A. & Talwalkar, A, 2012, Foundations of Machine Learning. Cambridge, MA, USA: MIT Press.

Rivera, D, 2012, Aplicación de la tecnología Measurement While Drilling en Túneles. Santiago, Chile: Universidad de Chile Repository.

*Tunnels and Underground Cities: Engineering and Innovation meet Archaeology, Architecture and Art, Volume 5: Innovation in underground engineering, materials and equipment - Part 1 – Peila, Viggiani & Celestino (Eds)*
*© 2020 Taylor & Francis Group, London, ISBN 978-0-367-46870-5*

# TBM drive along curved alignments: Model based prognosis of shield movement

A. Alsahly, A. Marwan & G. Meschke
*Institute for Structural Mechanics, Ruhr-University Bochum, Bochum, Germany.*

ABSTRACT: In current mechanized tunneling practice, the position of the shield machine during TBM-advancement is controlled by the shield driver with the aid of monitoring-based guidance systems. This results in an uneven movement of the machine. This contribution proposes a computational model able to support the TBM-steering during tunnel drives along curved alignments. A computational framework is developed to simulate the advancement and excavation processes, and to enable an efficient and realistic 3D-modeling of the advancement process and the shield-soil interactions during tunneling along arbitrarily curved alignments using the finite element method. The proposed framework combines a newly developed steering algorithm to simulate the TBM-movement during the excavation process. The steering algorithm serves as an artificial guidance system to automatically determine the exact position and the driving direction of the TBM in 3D-space. This modeling approach allows for better prediction of the shield behavior and thrusting forces during the advancement process.

## 1 INTRODUCTION

In numerical simulations of shield driven tunneling processes, the realistic modeling of both the excavation process and the advancement of the Tunnel Boring Machine (TBM) is a challenge. For a better understanding of these processes during tunnel construction, the interactions between the shield machine and the surrounding soil need to be investigated, yet this excavation process is difficult to model with existing finite element models. In addition, the simulation of the advancement of the machine as an independent body, that interacts with all relevant component of the model, requires a realistic kinematics model of the shield machine which is often not included (Sugimoto & Sramoon 2002). A prototype for a process-oriented three-dimensional finite element model for simulations of shield-driven tunnels in soft, water-saturated soil has been developed and successfully used for systematic numerical studies of interactions in mechanized tunneling (Kasper & Meschke 2004). This model has been reformulated and extended to partially saturated soils and more advanced constitutive models for soils in the context of a integrated design support system for mechanized tunneling (see, e.g. Meschke et al. 2011). Furthermore, several finite element models have been proposed, addressing the difficulties inherent in the simulation of the excavation process. Many of these models account for excavation by removing finite elements from the excavated volume in front of the machine, and then by applying the nodal forces necessary to preserve equilibrium (Bernat & Cambou 1998, Clough et al. 1983). A more realistic representation of the excavation process, based on mesh adaptation, using so-called “excavating elements” in front of the machine has been proposed by (Komiya et al. 1999). In this paper, a steering algorithm is presented in the context of 3D modeling TBM advancement processes. The algorithm serves as an virtual guidance system which automatically determines the exact position and the driving direction of the TBM in three dimensional space. Hereby, the model provides the vertical and horizontal deviations of the machine, its shield orientation, and provides direct input for the jacking cylinders. In addition, a problem specific re-meshing procedure is introduced for the

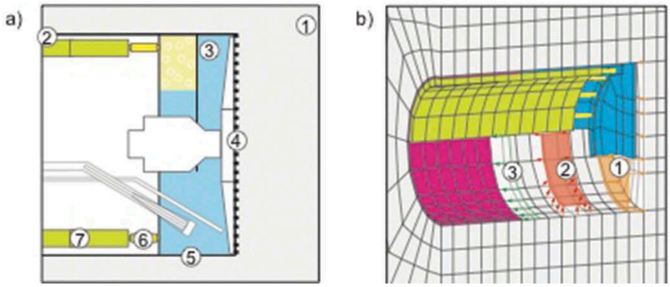

Figure 1. a) Main components involved in mechanized tunneling: (1) soil, (2) tail gap, (3) pressurized support medium, (4) cutting wheel, (5) shield skin, (6) hydraulic jacks and (7) segmented lining. (b) Modeling of interactions between soil and TBM in the simulation model ***ekate***: (1) heading face support, (2) frictional contact between shield skin and soil and (3) grouting of the tail gap) and components of the simulation model: TBM, hydraulic jacks, lining and grouting mortar.

simulation of the excavation process. In this process, a hybrid mesh generation procedure adapts the spatial discretization in the vicinity of the tunnel face, according to the actual position of the TBM, in order to better capture the excavated geometry and predict more realistic shield behavior.

## 2 COMPUTATIONAL MODEL

The numerical 3D finite element method for shield tunneling used here as a basic framework for the new TBM advancement model has been presented in a number of publications (see, e.g. Alsahly et al. 2016). It has been implemented in the object-oriented finite element framework KRATOS and is denoted as ekate (Enhanced Kratos for Advanced Tunneling Engineering). This finite element model takes into account all relevant components involved in shield tunneling such as the tunnel boring machine (TBM), the hydraulic jacks, the lining structure, the frictional contact between the shield skin and the soil and the supporting measures at the face and the tail gap, respectively, and their interactions.

Figure 1 shows the main components involved in mechanized tunneling (left) and their representation in the finite element model (right). These components are considered as independent sub-models interacting with each other. The interaction between the surrounding soil and the shield machine is accounted for by means of a surface-to-surface frictional contact formulation in the framework of geometrically nonlinear analysis. The hydraulic jacks are represented as CRISFIELD truss elements connected to the surface of tunnel lining element from one side and to the pressure wall of the TBM by tying utility. The simulation of the tunnel advances is performed in a step wise procedure. The soil and the grout are formulated within the framework of the theory of porous media (TPM) as two-phase materials.

## 3 FINITE ELEMENT MODELING OF THE ADVANCING PROCESS

The modeling of the advancement process in mechanized tunneling is one of the most complex processes, since it requires a good understanding of the real kinematics of the shield machine and its interaction with the surrounding environment (Finno & Clough, 1985). Therefore, a nonlinear kinematic analysis of the shield, based on the action forces imposed on the shield and on the inertial forces due to the shield, is performed. The action forces result from hydraulic jacks pushing against the machine, earth/slurry pressure at the cutting face, friction with surrounding soils, and the fluid flow of processes of the support fluid and grouting mortar, whereas the inertial forces are due to the self-weight of the shield and of the equipment. Furthermore, the taper and the thickness of the shield skin are accounted for in the geometrical representation of the TBM, guaranteeing a realistic distribution of the ground reaction forces in both circumferential and longitudinal directions. The TBM is advanced by hydraulic jacks that are attached to the machine and work as groups in different sectors which push against the previously installed lining ring. From the physical point of view, the minimum pressure exerted by these jacks must overcome the resistance generated by the surrounding soil.

In accordance with tunneling practice, a reliable steering algorithm that provides the numerical model with the required information to keep the TBM on the track is developed. This TBM advancement algorithm serves as an artificial guidance system which automatically determines the exact position and the driving direction of the TBM in 3D space providing the vertical and horizontal deviation, shield orientation and direct input for the jacking cylinders (Figure 2).

The simulation of the advancing process for arbitrary alignments by means of the proposed steering algorithm requires a continuous adaption of the finite element mesh in the vicinity of the tunnel face. Furthermore, the finite element mesh should match the actual motion path of the shield machine resulting from the FE-analysis in each excavation step. For this purpose, a re-meshing algorithm is developed in order to automate the process of mesh generation in a domain in the vicinity of the tunnel face within the advancing process (Figure 3).

Both the steering and the re-meshing algorithm represent the main components of the proposed framework for modeling the excavation process during the advancement of the tunnel

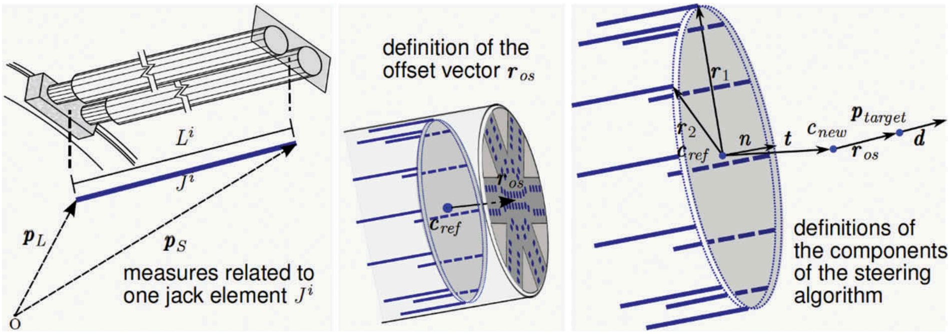


Figure 2. Geometrical quantities involved in the steering algorithm.

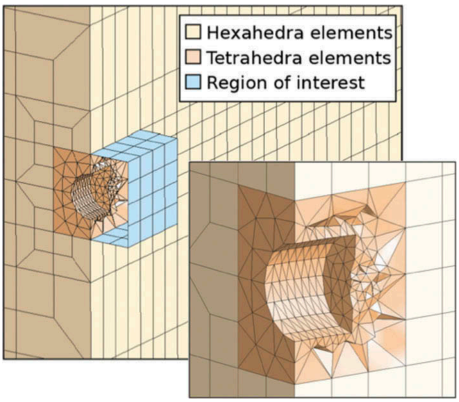


Figure 3. Non-overlapping subdomains and the region of interest (ROI) constituting a compatible hybrid finite element mesh.

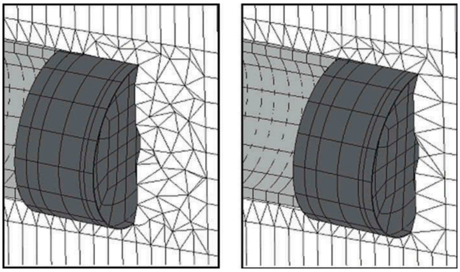

Figure 4. Automatically generated mesh at the tunnel face for two advancement and excavation steps.

boring machine. The advancement of the TBM involves a change in geometry and removal of excavated soil. The kinematic analysis of the shield within the steering procedure provides the exact position and geometry of the new facets as well as the center of the cutting wheel and the updated positions of reference points. In order to avoid over or under excavation it is necessary to adapt the finite element mesh ahead of the shield face. This is accomplished by generating a new finite element mesh ahead of the shield face such that the excavated volume matches the geometric shape and size of the incremental shield advance as provided by the steering algorithm, see Figure 4.

## 4 NUMERICAL APPLICATION TO WEHRHAHN LINE METRO IN DÜSSELDORF

The applicability of the proposed approach to a large scale simulation of a mechanized tunneling project, is demonstrated using the real project data from Wehrhahn-Line (WHL) metro in Düsseldorf. The ground model is characterized by three geological layers that mainly consist of sandy soil. These layers are the filling layer at the surface (2–3 m), the Rhine terrace (17–29 m), and the tertiary (30 m). The machine is driven in the Rhein terrace layer with an overburden which varies between 12 m and 16 m. The soil parameters are derived from the available soil reports and listed in Table 1. In the numerical analysis, Drucker-Prager plasticity model with non-associative flow rule is employed to represent the soil behavior.

During the simulation of this complete section of WHL, the proposed steering algorithm (Alsahly et al. 2016) is employed for the advancement of the TBM along the complex tunnel path which contains several straight and curved parts, see Figure 5. According to the machine data, the TBM was driven by means of 14 pairs of hydraulic jacks, working in 6 groups: A (2 pairs with 26° cw), B (3 pairs with 90° cw), C (2 pairs with 154°), and D, E and F symmetrical to A, B and C w.r.t. the vertical axis. In order to replicate the real movement of the TBM and predict more realistic distributions of thrusting forces, the steering algorithm is adapted in

Table 1. Material parameters for the finite element model for the selected section of the Wehrhahn-Line.

| Soil parameters | Layer 1 | Layer 2 | Layer 3 |
|---|---|---|---|
| Unit weight | 17.32 | 20.38 | 21.40 |
| Young modulus | 21.0 | 50.0 | 67.0 |
| Poisson ratio | 0.25 | 0.25 | 0.3 |
| Friction angle | 30.0 | 35.0 | 33.0 |
| Cohesion | 2.0 | 0 | 0 |
| Hardening modulus | 5.80 | 50.0 | 67.0 |
| Porosity | 0.4 | 0.25 | 0.3 |
| Permeability | 0.01 | 0.001 | $10^{-6}$ |

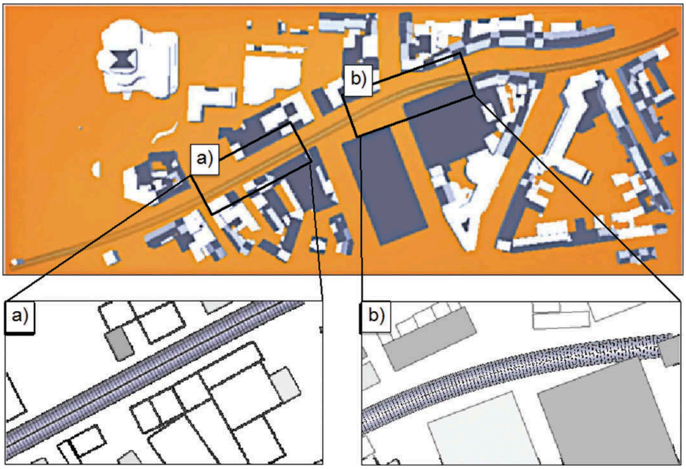


Figure 5. WHL tunnel route, a) section with straight alignment b) section with curved alignment.

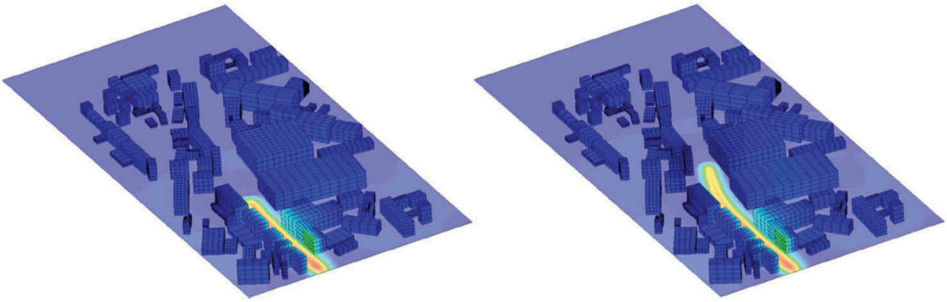

Figure 6. Selected results for different advancement steps obtained from the numerical analysis of the selected section of the Wehrhahn-Line in Düsseldorf.

order to account for these Jack's grouping systems during the simulation by enforcing equal elongation for all jacks of the same group. Figure 6 presents selected results for different advancement steps obtained from the parallelized numerical analysis of the selected section of WHL.

In order to investigate the influence of the remeshing procedure during the advancement process, two sections (each of 100 m long) located along different parts of the tunnel route of the WHL project are analysed and observed. These two sections are located at the straight and the curved parts of the tunnel route as shown in Figure 5a and Figure 5b, respectively. As the simulations contain both straight and curved alignment, they suit well to demonstrate the capabilities of the develop simulation model with respect to the steering algorithm and the soil-shield interactions. Furthermore, the predicted shield behaviors and thrusting forces are validated using the real machine data.

### 4.1 *Straight tunnel section*

This tunnel section considers a horizontal straight alignment located between Ring-Nr. 1260 and Ring-Nr. 1335 with 75 lining rings. Within the simulation, the TBM (D = 9:49 m) is driven with an overburden of 16 m applying a constant face support pressure equal to 240 [kPa] and grouting pressure equal to 300 [kPa]. The steering algorithm is employed during the simulation of the advancement process in order to push the machine forward and account to the drift-off phenomena. Figure 7 shows a comparison between the real excavated geometry, and the one stemming from the finite element model for the straight section of the tunnel. The real excavated geometry is schematically shown in Figure 7 (top). As can be seen, the machine moves along the straight path with a wriggling movement confirming the so-called “snake-like” motion. This motion results in an uneven excavation boundaries. Similarly, it is noticed from the result of the finite element analysis in Figure 7 (bottom) that the predicted movement of the TBM and the excavation geometry follow a pattern similar to the real ones. It is also apparent that machine drives in a zig-zag pattern along the target alignment which leads to the uneven excavation boundaries obtained from the FE model.

In addition, Figure 7 also demonstrates the downward tilting of the TBM. This can be also deduced from observing the trend lines of the vertical positions of the two reference points. Similar behavior of a shield machine driven along straight path was reported by (Festa et al. 2015). It is noticed from the results of the numerical analysis that the behavior of the TBM resulting from the FE model follows similar patterns to the ones recorded from the machine data. Moreover, it can be seen from the predicted vertical deviation of the two reference points in Figure 7 (as obtained from the steering algorithm during the numerical analysis of the tunneling process) that the tilt of the TBM is trending downward. Hence, the FE model predicts reasonably well the actual shield behavior during the advancement process along straight path.

A further investigation considering TBM-soil interactions is performed employing a similar simplified geometrical approach proposed by (Festa et al. 2015) using machine data. This approach utilizes the reference points (front and rear) to determine shield position and orientation within the obtained theoretical excavated profile at each tunnel advancement step. Assuming a rigid TBM body, the relative distance between the shield periphery and the theoretical excavated soil profile will be quantified. Here, two specific points on the shield tail (top and bottom) are investigated, and the results are presented in Figure 8a. It can be shown from Figure 8a that, upon driving, the top point on the shield tail (point B) is always in contact with the excavated geometry and displacing the soil, whereas the bottom point on the shield tail (point A) originates a gap between the shield and the excavated profile. This is fully

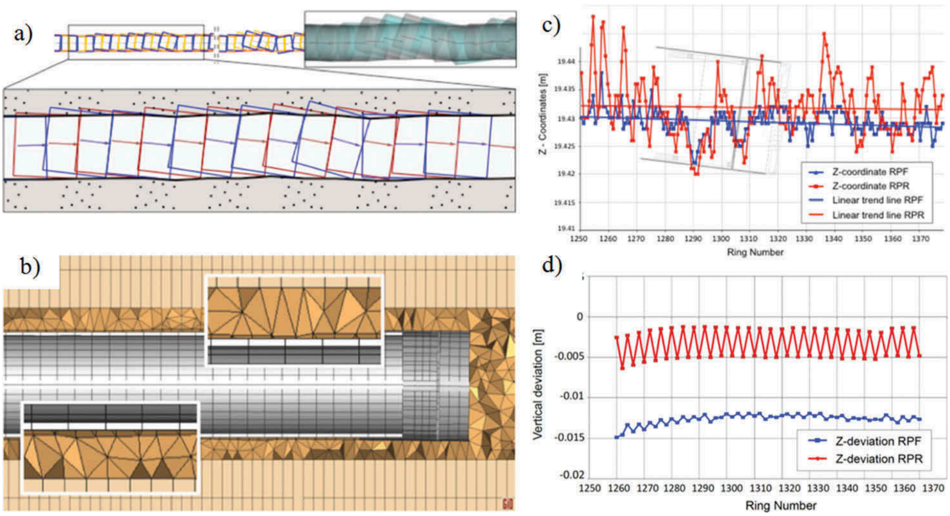


Figure 7. a) Schematic representation of the real excavated geometry, b) The excavated geometry obtained from FE model, c) Monitored vertical position of two reference points along shield axis, i.e. Reference Point Front (RPF) and Reference Point Rear (RPR), during all advancement steps, d) Computed vertical deviation (position) of two reference points RPF & RPR along shield axis as obtained from FE-analysis employing steering algorithm during the simulation of the advancement process.

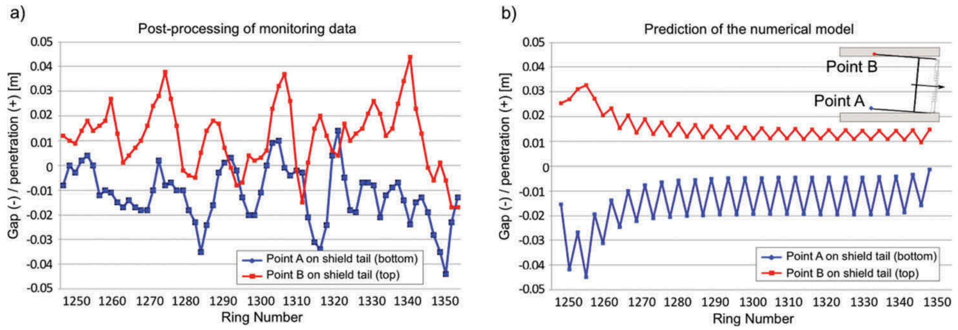


Figure 8. TBM-soil interactions: a) the relative distance between the shield tail and the theoretically excavated soil profile at two selected points (A & B) computed from monitoring data, b) the computed gap distribution from the FE-analysis for the two points during the simulation of the advancement process.

consistent with the reported vertical tendency of the TBM movement along this tunnel section. As for the theoretical, two specific points on the shield tail (B at top and A at bottom) are monitored within the numerical model during the simulation. It can be seen from Figure 8b that the numerical model tends to predict similar pattern of these points which is again consistent with the predicted TBM vertical tendency.

Applying the developed steering algorithm during the simulation of the advancement process, the distribution of jack thrusts exerted by each group, i.e. groups A, B, C, D, E and F, within the thrusting system are obtained. These are visualized and compared with their counterparts value from the machine data in Figure 9. The predicted values are obtained during the advancement of the shield considering a constant face support pressure equal to 240 [kPa] and the cutting forces required to excavate the soil, which are crucial for valid comparison with the measurements. In the numerical model, these cutting forces are considered as a constant static loading on the pressure wall and adopted from the recorded machine data with a mean value of 20 [kPa].

As expected, the thrusting forces of the groups at the invert (group C and group D) are the highest and conversely the thrusting forces of the groups at the crown (group A and group F) are the lowest to prevent the TBM from diving, and to correct the tilting of the machine. From Figure 9, it is evident that the predicted distribution of the jack forces is in reasonably good agreement with the measured thrusting forces. These results demonstrate that enhanced prediction capabilities of the numerical model can be obtained by applying the developed steering algorithm.

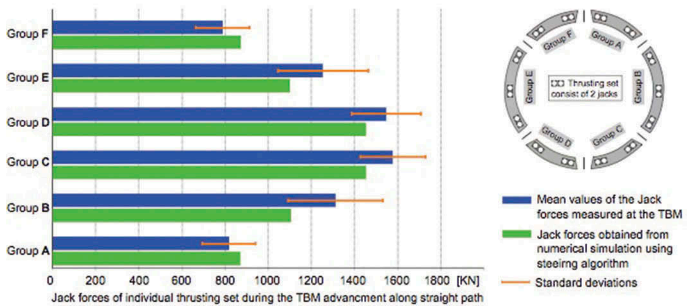


Figure 9. Comparison between the measured thrusting forces of each individual group (obtained from machine data) and the predicted thrusting forces from FE model applying the steering algorithm during the simulation of the advancement process.

### 4.2 *Curved tunnel section*

The simulation model of this example considers a curved section of the tunnel route as shown in Figure 5b. This tunnel section simulates rightward curve alignment with a radius of 500m located between Ring-Nr. 1400 and Ring-Nr. 1480 with 80 lining rings. Within the simulation, similar to the straight case, the TBM (D = 9:49 m) is driven with an overburden of 16 m applying a constant face support pressure equal to 240 [kPa] and grouting pressure equal to 300 [kPa]. The steering algorithm in conjunction with the remeshing technique are employed during the simulation of the advancement process in order to drive and steer the machine along the designed curved path by means of 14 pairs of truss elements working in 6 groups A, B, C, D, E and F. This approach allows the TBM to move independent of the soil and, thus, allows for better prediction of the shield behavior within the excavated curved path during the advancement process. Figure 10 shows the generated FE model for the selected curved tunnel section together with the so-called excavated domain or "region of interest".

In this FE model, the TBM is driven along the curved path employing the steering algorithm. Simultaneously, the finite element mesh of the excavation domain is automatically generated according to the actual position of the TBM after each advancement representing the complete curved path of the excavated geometry. Furthermore, the position and orientation of the shield machine within the excavated domain is demonstrated in Figure 10 at three different advancement steps.

An indication of the actual shield behavior during the advancement process is given by the relative positions of the front and rear reference points, defined as RPF and RPR respectively, at each step. In order to understand the actual behavior of the shield upon driving along the given rightward curved path, the horizontal tendency of the TBM-shield is demonstrated using the real machine data in Figure 11 for all advancement steps. The real machine tendency can be deduced by observing the horizontal deviation of the front and rear reference points from the designed path. It can be observed that the TBM is driven with continuous horizontal rightward tilting. A similar behavior of the shield machine driven along curved path was also reported in (Festa et al. 2015).

It is noticed from the results of the numerical analysis that the behavior of the TBM resulting from the FE model (Figure 11-left) follows similar patterns to the ones recorded from the machine data in Figure 11-right. Moreover, it can be seen from the predicted horizontal deviation of the two reference points in Figure 11-left (as obtained from the steering algorithm during the numerical analysis of the tunneling process) that the tilt of the TBM is trending rightward following the curved path. Hence, the FE model reasonably predicts the actual shield behavior during the advancement process along curved path as well. It should, however, be noted that obtained oscillation in the results using FE methods, is due to the application of the steering algorithm, which corresponds to the deviation-correction procedure during the advancement steps. It is evident that the steering algorithm tries to correct the position of the machine during the advancement process in order to follow the defined curved path which explains this oscillation.

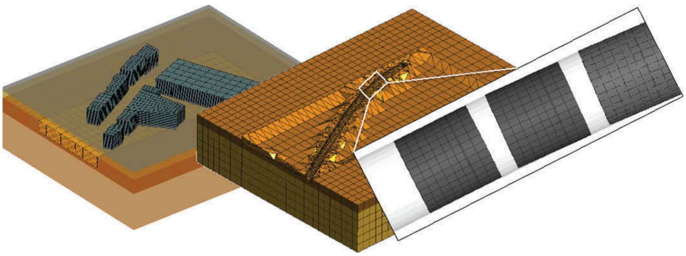

Figure 10. The excavated geometry obtained from FE model employing the developed steering algorithm in conjunction with the automatic remeshing technique and the shield position and orientation within the excavated profile at three different advancement steps. process.

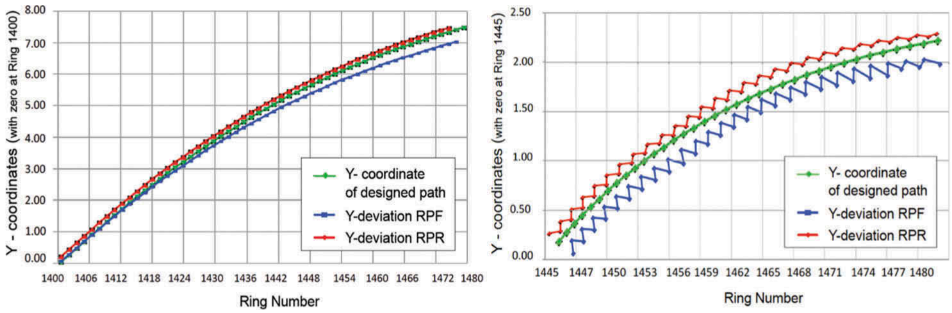


Figure 11. Monitored horizontal position (Y - coordinate) of two reference points (RPF & RPR) along shield axis during all advancement steps as obtained from machine data (left) demonstrating the rightward horizontal tilting and the computed horizontal position (deviation) of the same reference as obtained from FE-analysis (right) employing steering algorithm during the simulation of the advancement process.

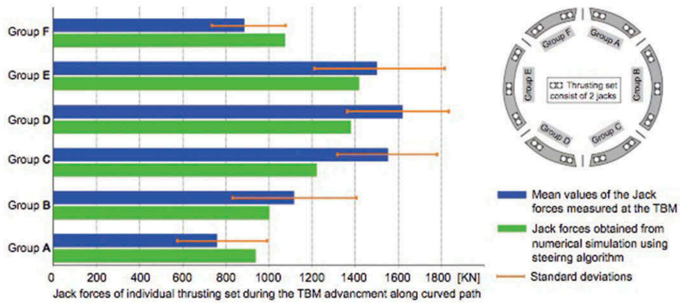


Figure 12. Comparison between the measured thrusting forces of each individual group (obtained from machine data) and the predicted thrusting forces from FE model applying the steering algorithm during the simulation of the advancement process.

Applying the developed steering algorithm during the simulation of the advancement process, the distribution of jack thrusts exerted by each group, i.e. groups A, B, C, D, E and F, within the thrusting system is obtained. These jack thrusts are visualized and compared with their counterparts value from machine data in Figure 12. The predicted thrusting forces of the groups at the invert (group C and group D) are higher than the thrusting forces of the groups at the crown (group A and group F) to prevent the TBM from diving and correct the vertical tilting of the machine due to its self weight. Additionally, in comparison to the obtained thrusting forces for the case of the straight path, higher thrusting forces in group E is predicted, as expected. These results are consistent with the designed curved path where higher thrusting forces on the left side of the shield are required for driving along rightward curvature. From Figure 12, it is evident that the predicted distribution of the jack forces are in reasonably good agreement with the measured thrusting forces.

## 5 CONCLUSION

In this work, a new computational framework for the simulation of the advancement and the excavation process of tunnel boring machines (TBMs) during mechanized tunneling was proposed using the finite element method. Within this framework, the TBM advancement and excavation processes are simultaneously simulated in such a manner to enable the efficient and realistic three-dimensional modeling of the tunneling process for an arbitrary alignment. The stepwise excavation process is modeled by means of an adaptive spatial discretization strategy used in conjunction with a steering algorithm. This combination of algorithms provides a high resolution of the stress and deformations in the direct vicinity of the TBM and thus also a realistic kinematic description of the movement of the TBM during advancement. The coupled re-meshing– TBM steering procedure embedded in the simulation model takes the actual deformations of the soil and the TBM-soil interactions into account. This method automatically corrects "drift-off" phenomena, as are often observed in TBM tunneling, and continuously keeps the TBM on the desired course during the simulation. The applicability and effectiveness of the proposed computational framework for the advancement and excavation process was demonstrated and verified by 3D numerical simulations of tunnel drives along both straight and curved tunnel paths. The thrust force distribution predicted by the proposed adaptive re-meshing and steering strategy along the shield of the TBM has been shown to be in good agreement with the observed field data for both cases. The machine drives along a zig-zag pattern around the target alignment, which corresponds well with data collected from TBM guidance systems. The applicability of the proposed technique is shown by means of a case-study in which the a TBM was driven along a curved alignment. This study has shown that the proposed framework is able to realistically simulate the motion of the TBM and the TBM-soil interactions along an arbitrary path with minimum effort.

## ACKNOWLEDGEMENTS

Financial support was provided by the German Research Foundation (DFG) in the framework of project C1 of the Collaborative Research Center SFB 837 Interaction modeling in mechanized tunneling. This support is gratefully acknowledged.

## REFERENCES

Alsahly, A & Staschei, J. & Meschke, G. 2016. Advanced finite element modeling of excavation and advancement processes in mechanized tunneling. Advances in Engineering Software 100: 198–214.

Festa, D., W. Broere, & J. Bosch. Kinematic behaviour of a Tunnel Boring Machine in soft soil: Theory and observations. Tunnelling and Underground Space Technology 49, 208–217, 2015.

Finno, R. & G. Clough (1985). Evaluation of soil response to EPB shield tunneling. Journal of Geotechnical Engineering 111(2),155–173

G. Clough, B. Sweeney, & R. Finno. Measured soil response to EPB shield tunneling. Journal of Geotechnical Engineering, 109(2):131–149, 1983.

G. Meschke, F. Nagel, & J. Stascheit. Computational simulation of mechanized tunneling as part of an integrated decision support platform. Journal of Geomechanics (ASCE), 11(6):519–528, 2011.

K. Komiya, K. Soga, H. Akagi, T. Hagiwara, and M. Bolton. Finite element modelling of excavation and advancement processes of a shield tunnelling machine. Soils and Foundations, 39(3):37–52, 1999.

M. Sugimoto & A. Sramoon. Theoretical model of shield behaviour during excavation. I: Theory. Journal of Geotechnical and Geoenvironmental Engineering, 128(2):138–155, 2002

S. Bernat & B. Cambou. Soil - structure interaction in shield tunnelling in soft soil. Computers and Geotechnics, 22(3/4):221–242, 1998.

T. Kasper & G. Meschke. A 3D finite element model for TBM tunneling in soft ground. International Journal for Numerical and Analytical Methods in Geomechanics, 28:1441–1460, 2004.

*Tunnels and Underground Cities: Engineering and Innovation meet Archaeology, Architecture and Art, Volume 5: Innovation in underground engineering, materials and equipment - Part 1 – Peila, Viggiani & Celestino (Eds)*


# Soil conditioning adaptation to the heterogeneous volcanic geology of Mt. Etna, Sicily, Italy

A. Alvarez, S. Mancuso & N. Bona
*Cooperativa Muratori e Cementisti, Ravenna, Italy*

ABSTRACT: In the TBM world, one of the most important key success factors is soil conditioning. While many TBM projects encounter mixed geology, the case of Mt. Etna and the volcanic geology of the Catania Metro is truly singular. Soil conditioning can change the balance of a project, that is economical and feasibility balance. Especially in EPB projects, this factor defines the rules to lead the excavation, it could enhance our performance, decrease our wear drastically and also help us make important savings. In most projects, soil conditioning parameters rarely change. These parameters follow the primary characteristics of the site´s geology. In our Catania Metro tunnel, soil conditioning has changed continuously, and we have had to adapt to the changing mixed face. The aim of this article is to show how the heterogeneous geology of Etna has been excavated and the problems found during this challenge.

## 1 INTRODUCTION

The following article aims to highlight a recent and increasingly common fact, the use of EPB TBMs in mixed excavation faces with high presence of hard rock, and how conditioning is fundamental to bore in these complicated conditions.

The Catania project has given us a rich experience of conditioning in mixed faces, a critical situation for an EPB, mainly designed to work in soft ground. In this scenario, conditioning is even more important than normal, and its continual adaptation to a constantly changing mixed face has been a reality, every meter of excavation.

The use of chemical agents like foams, polymers and natural agents like bentonite can make a radical difference in the excavation parameters and especially in the wear of tools and contact surfaces. For this reason we will describe some aspects encountered during the construction of the tunnel of the metropolitan area called Nesima-Misterbianco lot 1, linking the differences between the lithology forecast by the geological studies and the geology actually encountered.

## 2 PROJECT GEOLOGY

The Nesima-Misterbianco tunnel is the first tunnel to be bored by an EPB TBM in the soil particular to Etna, but also in an urban context. The tunnel runs with an overburden of between 12 to 20 meters. The geological profile in Figure 1 and the photographs in Figure 2 show the constantly changing lithology characteristic of this project.

The excavation commenced in a geology mainly characterised by a mixed face with non-coherent materials in the upper section and under the ground water table. In particular, the upper part of the tunnel is affected by the presence of alluvial materials, mainly characterised by clayey silts, while the central and lower portions are made up of lava rocks with a significant degree of fracturing and the presence, within them, of terrigenous materials combined with beige silts.

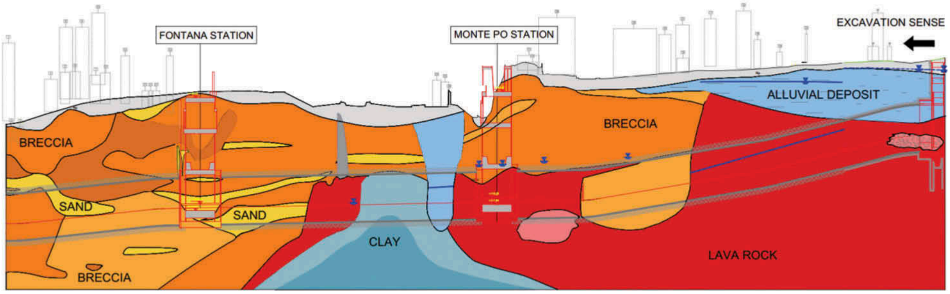


Figure 1. Geological profile updated after excavation.

Figure 2. Different excavation faces: Lava-clay, lava, breccia, rifusa.

As excavation advances, the front presents a predominantly rocky terrain interrupted by sections of breccia and consecutive reappearances of rock near the Monte Po station. In addition, the water table and the tunnel soffit gradually align.

The next tunnel section is affected significantly by the heterogeneous excavation face, with materials having different physical-mechanical behaviors. In particular, in the area immediately after Monte Po station the face is characterised by the presence of lava in the upper section and clayey and alluvial materials in the lower section. Near the Fontana station the tunnel is in turn affected by not very compact breccia. The remaining excavation is characterised by the presence of mixed faces consisting of compact lava-volcanoclastic breccia (lava in the upper section and breccia in the lower section) and breccia alternating with layers of volcanoclastic sands. In particular, the so-called "Rifusa" which was predominant in the final section of tunnel and shows a reddish colour due to thermal factors of contact between lava flows and clays. This mixed face was also characterized for the presence of voids, which creates serious risk to the stability of the excavation, and of course a big risk for the environment over the tunnel.

The article will describe the high degree of fracturing of the rock mass, as well as the abundant and unexpected water inflows which characterised the excavation, this fact caused difficulties due to the incessant application of the adaptation measures necessary to deal with these changes.

## 3 PREVIOUS STUDIES

### 3.1 *Cutter head*

For the construction of the tunnel of it has been foreseen the use of an EPB TBM with an excavation diameter of 10.60 m.

The cutter head tools include 63 cutters with a diameter of 19", including 4 bi-discs, as well as 182 scraper blades and 16 buckets. Its degree of opening is 33–36%.

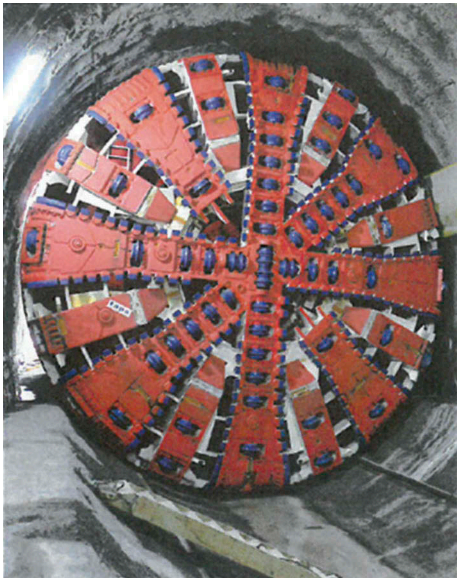

Figure 3. Cutter head view.

### 3.2 *Conditioning tests*

After the design of the TBM head, the studies focused on the conditioning of the soil. Numerous tests were carried out in order to reproduce the excavation conditions on a reduced scale. A full range of preliminary tests was performed to define the correct excavation procedure in order to establish the exact balance between the machine parameters and the geology.

However, due to the strong level of subsoil heterogeneity, from the first stage of progress, the conditions represented by the studies were not completely reliable both for the sequence of the different geological formations, and for the configuration of the discontinuities and the percentage of fracturing rock.

For the conditioning tests, the terrains studied were representative of the three geological formations prevalent in the excavation of the Catania tunnel: lava, sand and clayey silt, with different percentages of water added in order to analyse the behaviour of the ground in the different conditions of natural saturation.

In collaboration with the University of Torino, it has been made an in-deep study of the different lithology.

The soil samples were mixed with different foaming agents, using a foam generator that allowed the control of water, foam and airflow, as well as the control of the dosage of the foaming agent. For each lithology an in-depth study using slump testing was carried out with the aim of identifying an optimal conditioning set (foam, added water and polymer) for each combination of foaming agent and type of soil studied. The polymer was also used to evaluate conditioning in the presence of the ground water. The objective was to find the optimum plasticity condition for the fluid to maintain the chamber pressure, and also to be transported by the screw conveyor.

The testing confirmed the feasibility of the conditioning to obtain acceptable levels of plasticity.

These tests were therefore developed as a tool to indicate parameters and levels of reference for conditioning.

However, as already described previously, during excavation the front was rarely composed of homogeneous material, but characterised by constantly changing percentages of lithotypes (mixed faces), making impossible to follow the indications developed by the experimental study. The consistency of paste required for transportation could not be achieved and more importantly, it was truly complicated to maintain pressure in the excavation chamber, especially in the case of rock.

### 3.3 *Analysis of the wear phenomenon*

Laboratory tests were carried out to evaluate the phenomenon of wear caused by the excavated soil, simulating the interaction between tools and the excavated material, to verify the effect of water content and conditioning.

The tests were carried out using a steel container filled with soil, inside of which a disc made of the same steel used to manufacture the cutter head was placed and rotated, to reproduce at a reduced scale the cutter head of the TBM, measuring rpm and torque and plotting them on a graph.

Before carrying out the test, the weight of the disc was measured. The disc was then rotated inside the steel container for 10 minutes and finally weighed again, to determine the weight loss.

The results obtained were plotted in terms of average weight-loss and torque related to differing water contents, comparing the wear of metal tools in sand and lava rock with the data obtained in a quartz granular soil.

From the results we learnt that fractured rock is more abrasive than volcanic sand and that a higher water content decreases the wear, but only up to a certain value, after which, the abrasiveness is accentuated, especially in the case of sand.

This aspect was confirmed during excavation, in areas where a high water content combined with abrasive volcanic sand caused abnormal wear of the cutting tools.

## 4 CONDITIONING

Although the guidelines for good conditioning of the ground traversed during the excavation had been defined, it was truly complicated to follow the established procedures.

The high degree of fracturing of the rock, the high presence of water and the frequent lithological changes prevented standard excavation as the values of the machine parameters were never constant due to the incessant interruptions of the production activity.

The reduced excavation speed made the conditioning even more problematic as it was not possible to maintain constant foam flow rates. The low excavation speed meant that the foam flow rates were also low and that created several blockages of the foam lines as the pressure in the excavation chamber was higher than the pressure in the foam lines.

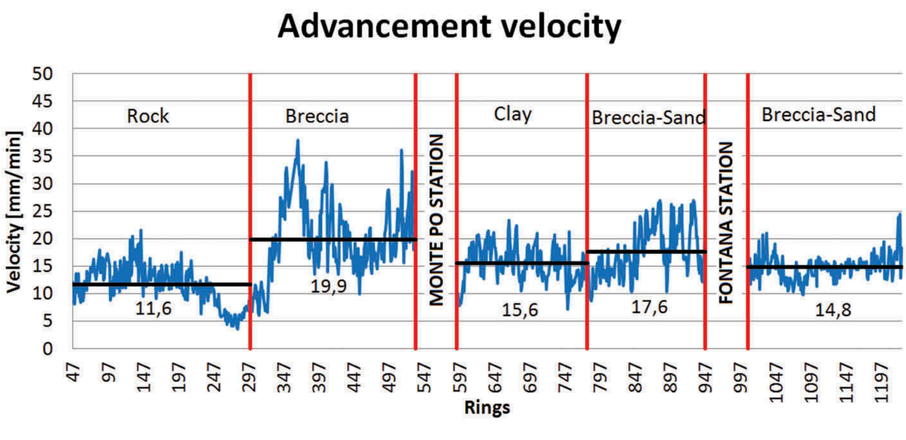


Figure 4. Average boring speed in the different geologies.

In correspondence with the hard rock, the TBM produced a material with an abnormally low presence of fines. That fact, in addition to the large quantity of water affluent in the tunnel, determined the difficulty of correct conditioning of the ground and therefore the difficulty to operate in EPB mode.

In fact, the abundant presence of water separating the fine material from the blocks and thus the difficulty of adequate conditioning forced the operation of the TBM with an open face. Despite the use of foaming agents we rarely obtained the expected fluid material.

Even the use of the polymer was not sufficient to create the pasty mixture typical of good conditioning. However, the use of the polymer was essential to absorb the excessively liquid material and for it to be conveyed by the screw conveyor, avoiding its accumulation at the point of discharge on the belt, facilitating the activity of the material conveyor.

In these conditions, all attempts to excavate the rock under pressure failed. As the excavation chamber filled with rocky material there was a proportional decrease of the torque, and a decrease of the penetration until reaching the complete stop of the TBM as shown in the graphic below, Figure 5.

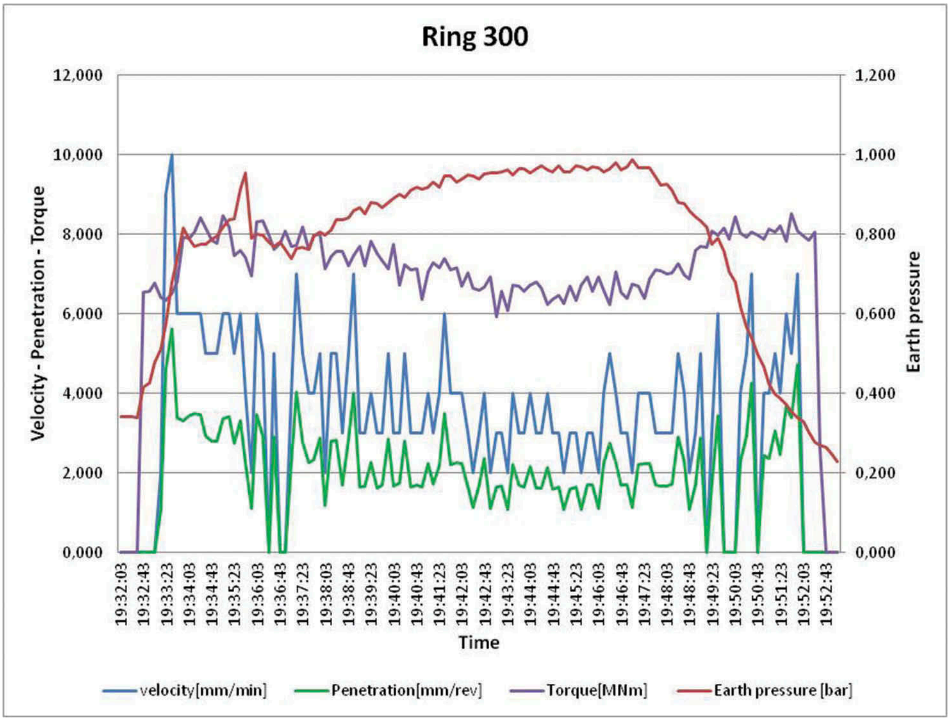


Figure 5. TBM parameters.

As for the tunnel excavation in EPB mode in the lava and with the presence of a large amount of water, the fundamental issue was that of adequate conditioning. Not reaching it easily, we repeated on site the scale studies carried out previously in the laboratory, with a sample of material taken directly from the face and using the foam generator of the TBM. These tests showed the extreme difficulty of conditioning once again.

In the case of clay, conditioning was less problematic even though the sticky nature of this type of material requested a continuous survey of parameters in order to avoid clogging. The effect of conditioning were specially monitored in the TBM parameters, especially in the torque.

Compounding this situation was the absence of suitable excavation tools, which had previously been disassembled in anticipation of boring though rock showed in the geological profile. In fact, the lack of action of the scraping knives did not allow the correct fragmentation of the clayey chips, hindering the action of the conditioning agents.

Also, the irregularity of the excavation and the consequent variation of the abnormal low speed did not allow the correct adaptation of the parameters of the foam system in terms of flow rate and injection pressure to the conditions required by the geology found.

## 5 ADAPTATION OF THE TBM

As already described, the excavation face was mainly a mix of different materials, and as shown in the photographs, the face was almost always presented with different percentages of these lithotypes (mixed faces).

Although the TBM had all the necessary equipment to excavate all the geological formations present, it was not expected that the changes would be so sudden, and so frequent, rendering very difficult to adequately organise the correct configuration of the cutter head and tools.

As is known, when passing from rock materials to clay materials or vice versa, the replacement of tools involves a forecast and important stoppage of excavation in a stable or consolidated foreseen area. Instead, during our experience, we had to continuously adapt the cutter head configuration to the geological conditions of the moment without ever reaching the optimal configuration for the excavation, and unfortunately having serious delays in our production due to the continual stoppages.

In the beginning of the excavation due at the mix face mainly characterised by fractured lava, the openings of the cutter head has to be reduced also because of the entry into the screw of the boulders, that reached dimensions of up to 60–80 cm, and could have compromised the integrity of the whole conveyor system.

However, when the TBM excavated through loose materials in EPB mode it was necessary to re-establish the original opening ratio of the head, removing the closures to allow the passage of the spoil.

All attempts to limit the breakage of the discs due to the impacts that they received at each turn of the head in the fractured rock, by reducing the rotation speed or reducing the penetration, proved ineffective, as the consequent increase in the excavation time favoured breaking due to continuous non-uniform contact with the face.

Limiting the size of the pieces of rock that could pass through the cutting head was also important to reduce the risk of blockage of the screw conveyor and of the cutter head.

On the other hand, by closing these openings the torque and thrust were increased and the penetration of the machine was reduced, increasing also the wear of tools and cutter head and increasing also the consumption of energy.

Figure 6. Modification of the cutter head opening.

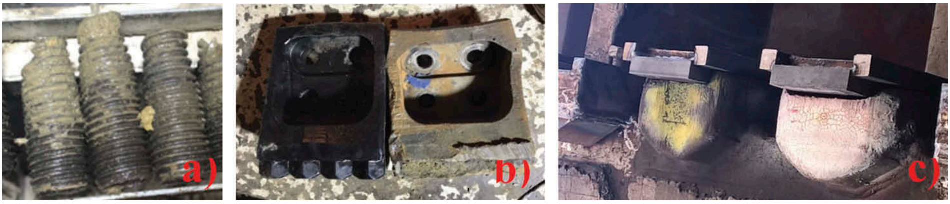


Figure 7. a) Bolt deformation; b) knife deformation; c) cover plates.

Many of the stoppages of the production activity were caused by the locking of the cutter head as large blocks interlocked between the openings of the cutter head.

This fact led us to an abundant replacement of tools, always trying to adapt the cutter head to the geological situation found.

Owing to the excessive breaking of the scraping knives due to the continuous impacts against the fractures in the rocky face and boulders in correspondence with the fractured rock formations, we replaced the knives by protection plates. The knives were literally torn from their housing, materialised by the screws suffering an elongation effect.

The objective of the new configuration was not only to avoid the deformation and breakage of the knives and fixing tools, but also to avoid the damage caused by the broken off parts that interfered with the cutter traces, which in turn were also damaged, causing a chain effect that created significant damages and delays.

This new configuration with the protection plates was installed during the TBM stoppage in Monte Po station in parallel to the various maintenance activities. The knives were replaced by cover plates that protected the knife bases, avoiding in this way the loss of knives and the damages that they can generate.

This intervention was carried out in anticipation of a face mainly composed of lava, as represented in the geological profile obtained during the project phase. However, after the restart from the station, subsequently to a very short stretch of rock, the TBM bored through clayey-silty terrain for about 200 meters, as opposed to the geology forecast by the studies.

The cutter head configuration was therefore not suited to the type of soil to be excavated, with the difficulty of replacing tools in a hyperbaric environment or consolidated area.

Without the knives, and with the clay in direct contact with the support protections, the clay was torn out mainly in big blocks causing significant wear of the protection and bases of the knives. As the clay pouring from the screw conveyor onto the conveyor belt, it clogged and obstructed the flow of material at the different discharge hoppers between the belt

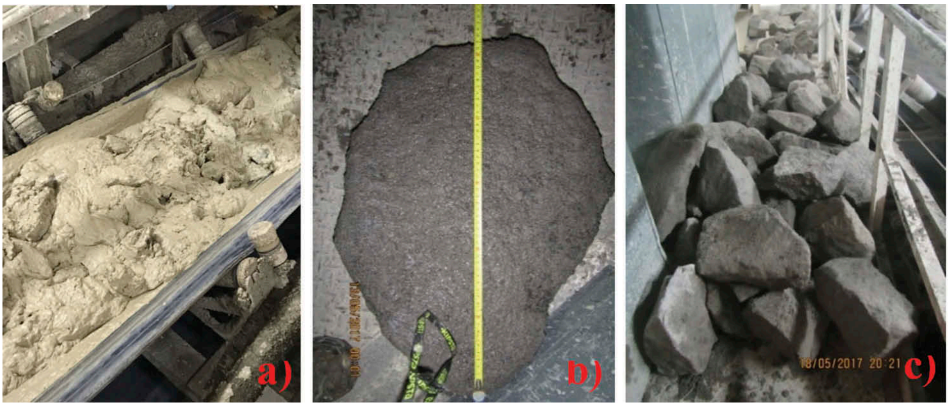


Figure 8. a) Clay blocks; b,c) boulders.

sections of the entire plant. In addition, the big shapes of the silty sticking masses caused breakdowns in the conveyor system, especially in the vertical conveyor belt.

## 6 PROBLEMS DURING EXCAVATION

Some of the problems related to the excavation have already been described in the last chapter, as they are related to modifications made to the TBM.

### 6.1 *Excessive water flow*

The presence of the water table in correspondence with the lava mass was detected during the preliminary investigation phase.

The excavation experience confirmed that the crushed lava, which remains in suspension in the water present in the chamber, constitutes an abrasive mix that accumulates in the lower part of the face of the excavation chamber, inside which the cutting tools of the head and the screw conveyor must operate.

Also the significant amount of ground water flowing into the excavation chamber in an irregular and discontinuous way through underground fracture systems and the accumulation of water present randomly in the subsoil, led to constant slowdowns in production due to the

Figure 9. Tunnel floods.

impossibility of creating a plastic material leaving the screw. The overflow of the liquid material forced a stoppage at each ring to clear the shields and the dewatering system.

The difficult operating conditions described were not localised, but, as mentioned, they gradually became normal as the excavation progressed through the lava.

In order to reduce the amount of liquid sludge coming out of the conveyor belt it was necessary to modify its inclination and speed.

### 6.2 *Clogging*

Clogging is another issue that affected the excavation. The mix between clay and rock, and the high temperatures produced by the excavation of hard rock, generated sticky material in the central part of the material chamber.

In fact on many occasions, due to the high temperatures reached in the material chamber, the excavated material, became "cooked" creating a dehydrated crust on the whole metal surface of the cutter head. Therefore, to unlock the head it was necessary to reach the maximal rotation force to obtain values of torque equal to 9000 KN/m.

Different chemical agents were tested in order to avoid this effect, with significant impact. However this still slowed down the excavation rate, and it was continuously necessary to first modify the foam parameters, and when that solution didn't work to directly clean the chamber with high pressure water.

### 6.3 *Cutter break because of impacts*

Another problem found was the continuous breakage of cutters. It was necessary to work on the cutter head, replacing the excavation tools damaged by the diffused structural discontinuities. The cutters, covering the circular trajectory of the whole excavation section and passing on materials of different compactness, from soft soil to stone, were subjected to impacts that would break the cutting edge, which was often lost inside the excavation chamber and created consequently damage to other cutters and knives.

Even though a significant consumption of cutters was expected, especially near the joints between different geologies throughout the tunnel path, the actual consumption was exponential compared to the previsions.

### 6.4 *Mechanical breakdown*

The frequent clogging of the cutter head, as well as the presence of rock blocks that did not allow the correct turning of the cutter head, created very high values of torque that caused damage to the main systems of the TBM.

Going beyond the normal levels of the machine parameters led to failures of the pumps that supply the rotation, motors and reducers of the main drive, and also of the screw, with consequential financial impact.

The extreme wear produced by the combination of water and sand already described above, caused damage to the main drive joint seal system. This failure produced contamination of gear oil that has been monitored throughout the excavation of the tunnel.

### 6.5 *Continuous adaptation of the team*

Interruptions due to mechanical failures produced by the extremely geological conditions together with all the geological stoppages (flooding, etc.), influence the continuity of the excavation.

The recovery of the boring pace, was always long due to the continuous change in the typology of works, cleaning shields for the coming of sand and water, mechanical or electrical repairs, consolidation works, works demolition for head unlocking.

The adaptation of the team and the supply of what was necessary for each task described above was a complicated forecasting mission.

Also the continuous changes to the logistics needed to face the different works were a real challenge for the external supply team that feeds all requested materials as well as the warehouse and procurement department.

All of these facts made it almost impossible to keep a rhythm of excavation that allow us to improve the excavation parameters.

## 7 CONCLUSION

The TBM has been a radical innovation in the excavation method in Catania, allowing to schedule work phases and to predict the end of the excavation activities despite the significant heterogeneity of the ground that characterises the Catanese subsoil.

Moreover, the great change brought about by the first mechanized excavation in Catania concerns the homogeneity of the excavation sections, no longer variable depending on the lithology present but constant throughout the tunnel length.

It is very important to carry out an in-depth study of the geology before the excavation of a tunnel. Drill tests are fundamental in this study, and in the case of a heterogeneous soil like in Catania, it is very important not only to see the material extracted from the drills, but also to appreciate how the drill has been done. Today, with new technology, we can have full parameters of the drilling machine during the excavation, for example torque and penetration that can help us to understand the different joints between lithology and also the empty areas found.

## REFERENCES


Peila, D., Oggeri C., AND Borio L. (2009), Using the slump test to assess the behavior of conditioned soil for EPB tunneling, Environmental & Engineering Geoscience, XV (3), 167–174.

Borio, L. & Peila D. 2010. Study of the Permeability of Foam Conditioned Soils with Laboratory Tests, American Journal of Environmental Sciences, Vol. 6, 365–370.

Borio, L. & Peila, D. 2011. Laboratory test for EPB tunnelling assessment: results of test campaign on two different granular soils. Gospodarka Surowcami Mineralnymi, 27(1), 85–100.

Fiore, S. & Neri, S. 2017. The Circumetnea Metropolitan Underground Railway though the great variety of Etna Lava. *Gallerie e grandi opere sotterranee* 124: 21–29.

*Tunnels and Underground Cities: Engineering and Innovation meet Archaeology, Architecture and Art, Volume 5: Innovation in underground engineering, materials and equipment - Part 1 – Peila, Viggiani & Celestino (Eds)*


# Particularities of tunnel primary support modelling in BIM environment

M. Andrejašič, M. Huis, A. Likar, J. Likar & Ž. Likar
*Geoportal d.o.o., Ljubljana, Slovenia*

ABSTRACT: Karavanke tunnel is considered the most challenging tunneling project in recent time in Slovenian area. Nowadays the project execution design is prepared for the eastern tube and the construction phase will take place in the following years. One of the bigger challenges for tunnel designers was the client requirement for implementation of building information modelling (BIM). The present article discusses the implementation of BIM in tunnel excavation and primary support in the case of Karavanke tunnel project. Because of the uncertainties in tunnel construction, some different approaches had to be taken compared to standard BIM. In fact, lining deformation tolerance is expected to be up to 50 cm, which directly affect the changing of primary lining geometry during the construction phase. The article also compares two different modelling approaches. One approach emphasizes on tunnel support geometry, the other focuses on smart attribute/property attribution with less element modeled in 3D space.

## 1 INTRODUCTION OF BIM APPROACH IN THE FIELD OF CIVIL ENGINEERING

Building engineering industry has caught up with the digitalization process, taking place in the 21. century. This technological breakthrough was made possible by the engineers that have seen the benefits that the digitalization process is bringing and by the development of the hardware and dedicated BIM software. The process of digitalization in construction industry is known as BIM (Building Information Modelling/Model). As we can deduct from the name, it is a process of modelling the building environment with emphasis on information. If the goals of BIM are successfully followed, the result will be a well-structured database of the building. With BIM the client will get an organized, better defined and well-coordinated project, which will be useful from the construction phase, through the operating phase for the maintenance purposes and thill the demolition phase of the structure.

BIM approach brings many advantages, for example:

- Clear representation of the building elements, which are better understood by the less skilled project participants, who are not able to create a proper 3D structure appearance from the 2D drawings.
- Greater coordination of the project, especially in the case of multi-company project preparation.
- Better defined project quantities and execution schedules.
- Longer lasting digital project information compared to a printed copy
- Faster and easier accessible project information compared to manual searching through the archived printed project versions.

The advantages of BIM have been efficiently used in the field of building construction for some time now. On the other hand, BIM technology has spread into the field of civil engineering just recently. The main problem for BIM implementation in civil engineering projects was

| Tunnel segment | | | | | Top heading | | | | Bench | | | | Invert | | |
|---|---|---|---|---|---|---|---|---|---|---|---|---|---|---|---|
| Seg. | km | Length | BT | % | ST | % | Length | Invert compl. | ST | % | Length | Excav. | ST | % | Length |
| 15 | 2250.17 | 349.63 | BT3 | 15% | 2P-H-K-6/12,42 | 50% | 26.2 m | 200.0 m | 2P-H-S-5/7,08 | 50% | 26.2 m | 1/1 | 2P-H-TO-5/4-BB-25 | 50% | 26.2 m |
| | | | | | 2P-H-K-6/10,52 | 50% | 26.2 m | 200.0 m | 2P-H-S-5/8,21 | 50% | 26.2 m | 1/1 | 2P-H-TO-5/4-BB-25 | 50% | 26.2 m |
| | | | BT4 | 80% | 2P-H-K-6/14,32 | 20% | 55.9 m | 200.0 m | 2P-H-S-5/9,51 | 20% | 55.9 m | 1/1 | 2P-H-TO-5/4-BB-30 | 20% | 55.9 m |
| | | | | | 2P-H-K-6/16,23 | 20% | 55.9 m | 200.0 m | 2P-H-S-5/10,74 | 20% | 55.9 m | 1/1 | 2P-H-TO-5/4-BB-30 | 20% | 55.9 m |
| | | | | | 2P-H-K-6/18,11 | 30% | 83.9 m | 200.0 m | 2P-H-S-5/12,16 | 30% | 83.9 m | 1/1 | 2P-H-TO-5/4-BB-30 | 30% | 83.9 m |
| | | | | | 2P-H-K-7/16,42 | 30% | 83.9 m | 70.0 m | 2P-H-S-6/9,73 | 30% | 83.9 m | 1/1 | 2P-H-TO-6/4-BB-30-O3 | 30% | 83.9 m |
| | | | BT8 | 5% | 2P-H-K-7/18,69 | 40% | 7.0 m | 70.0 m | 2P-H-S-6/11,16 | 40% | 7.0 m | 1/1 | 2P-H-TO-6/4-BB-35 | 40% | 7.0 m |
| | | | | | 2P-H-K-7/20,89 | 30% | 5.2 m | 70.0 m | 2P-H-S-6/13,47 | 30% | 5.2 m | 1/1 | 2P-H-TO-6/4-BB-35 | 30% | 5.2 m |
| | | | | | 2P-H-K-7/23,44 | 30% | 5.2 m | 70.0 m | 2P-H-S-6/15,40 | 30% | 5.2 m | 1/1 | 2P-H-TO-6/4-BB-35 | 30% | 5.2 m |

Figure 1. Example of the tunnel supporting measures distribution for the tunnel segment.

lacking of software support for BIM modeling of civil structures. This was mainly cause by the changing project and therefore model boundary conditions represented by the geological strata.

## 2 PARTICULARITIES OF BIM IN THE FIELD OF TUNNEL CONSTRUCTION

A special segment of civil engineering is tunneling design. It can be divided in two parts based on the designing procedure. The inner-secondary tunnel lining has constant boundary conditions, maintained by the primary lining. On the other hand, primary lining is exposed to changing boundary conditions produced by changes in geological strata. Modelling of the tunnel secondary lining and other inner structures can be somehow compared to standard building modelling, since structure elements precise location and displacements can be defined in the project design phase. We can assume that in the case of inner lining, the challenge is mainly to coordinate concrete structure with electrical and mechanical equipment. These kinds of issues are common in the field of building engineering and are frequently solved with BIM programs.

Design of the primary tunnel support brings a different challenge. In this case the project boundary conditions are represented by the surrounding geological strata. The geological structure is investigated by specialists in the project design phase with geological, hydrological and geomechanical investigations. These investigations though, cannot predict the exact structure and mechanical characteristics of the surrounding ground. Moreover, geologist have a tough job of predicting all the locations and directions of fault zones, through which the planed tunnel would pass. The consequences of these uncertainties, are changing boundary conditions, which can be described with a certain probability of appearing. The result of this is a geological model (boundary condition model) which is defined with a certain probability of appearing on a particular tunnel segment. An example of such of distribution is shown in Figure 1. Every engineering decision is based on this probability geological model. Consequently, the distribution of the tunnel supporting measures is defined with a certain probability of appearance on a tunnel segment.

In essence, the distribution of primary support measures is not finalized in the design phase but is a probabilistic prediction that has to be confirmed in the execution phase. This uncertainty issue represents a significant difference compared to standard building projects. This kind of issues are not common in BIM environment and consequently, no tools are developed, which could make BIM modelling of tunnel support a standard BIM modelling workflow.

## 3 DESIGN OF BIM KARAVANKE TUNNEL PRIMARY SUPPORT FOR EASTERN TUBE

Nine companies have been involved in the process of designing the Slovene part of east tube of Karavanke tunnel with the length of 7.820 m of which 3.446 m are within Slovenian country borders. The client - DARS the Slovene national highway company, has concluded a contract with the joint venture group - Design group Karavanke. They have agreed that the project will be delivered in standard 2D drawings and in BIM technology. The project consists of a tunnel part and a daylight rode part. BIM should represent all the major building structures: tunnel primary support, inner lining, electrical and mechanical installations, rode structure and road equipment, drainage, bridges and locations of material disposal from tunnel excavation. BIM modelling has been a part of tunnel design throughout all the project phases. With the BIM requirement the client wanted to have a better coordinated and defined project, thus the total cost of the project would be lower, despite the higher initial financial input for a BIM modelling.

The project has been subjected to some particular circumstances, which have caused some issues during design phase:

– Nine companies which were using different software packages had to deliver a harmonized project
– Open BIM principles were adopted in the project
– First BIM project of such of magnitude in the region
– Different coordinate systems were used for the tunnel and daylight road
– The client did not prescribe the exact BIM project specification but has legitimately expected a unified project delivery
– IFC 2x3 format, in which the project is delivered, has no dedicated attributes for tunnel design
– This is a bilateral project between Slovenia and Austria with different national legislation and coordinate systems.

Because of all the mentioned project characteristics, the project resulted to be very complex and difficult to manage. For easier management of large data quantities, more than one hundred partial BIM models have been produced. They were divided into two larger groups. Models of daylight rode and model of tunnel structures. As mentioned before, models were based on different coordinate systems with an exactly defined joining point on the portal area. Furthermore, the tunnel model was divided into primary support models and inner lining models with all the related electrical, mechanical, drainage and road layer models.

This article focuses on the tunnel primary support model. The particularity of the model, because of which it significantly differs from other BIM models, is that the geometry of tunnel lining changes between the installation phase and the final construction phase. This is caused by large surrounding rock mass stresses and the deformation capacity of primary support and surrounding rock mass. In fact, the location in 3D space (x, y, z coordinates) for every structure element of the primary lining change for various centimeters up to 50 cm, during construction works and this represents a collision with one of the basic BIM principles that states that every element in the model has a precisely defined location in actual space.

This discrepancy represents a big challenge for the engineer and the client to find a solution, that will efficiently solve the issue. It has to be practical, accurate and has to produce correct material takeoff quantities.

The Karavanke tunnel project was supposed to be developed based on the LOD description in the internationally adopted specifications »LOD Specification 2015«. Tunnel elements are not separately described in the specifications (2015). Nevertheless, it was written that in case of tunnel structure it is advised to refer to the basic principles based on the development level of the model. For LOD 300, required by the client, it is written: »The Model Element is graphically represented within the model as a specific system, object or assembly in terms of quantity, size, shape, location, and orientation. Non-graphic information may also be attached to the Model Element«. This raises a question about which is the exact location of the tunnel support elements? Is this the location of the installed elements or the final location at the end of construction works or an average of both? Based on the fact that 2D drawings were produced without accounting on construction and deformation tolerances, the decision of producing the BIM model with the same principle was taken. This model somehow represented the final position of structural elements after all the deformation had already taken place.

Since poor rock mass quality was predicted, a great numbers of rock bolts and spills were prescribed to satisfy the standards requirements (Figure 1). While modeling all of these elements, some issues that could be divided in two main groups have appeared:

– Problems with project attributes – managing/checking of attributing consistency
– Problems with element rendering, as a combination of hardware and software limitations.

Despite using smart object filtering it has been a difficult task to check if object had the right parameters assigned, or a human or other kind error had occurred. Problems were detected especially in case or rock bolts and spills which together took around 50% of the whole model size. Rendering of the model due to automatic software hiding of elements was noticeable and different from program to program. Moreover, the loading time of the model exceeded user-friendly time frame. All these issues could rise doubts if the project was delivered as it should have been.

During project modelling we have noticed other issues that were not crucial at that point of the project, but would have affected project modelling in future project processes. The complicity of the project would cause a major problem during generation of 4D and 5D project representations. In essence the large quantity of repeating elements slows down the model, but does not contribute to rising the model value. Furthermore, the client wanted to follow the construction works with BIM technology. That is why, it wished for a simpler model which would be easier to adapt to the project changes in the execution phase.

It was confirmed that the decision of modelling the tunnel geometry on the basis of the tunnel cross section profile without deformation tolerances, was appropriate. The major advantage noted was, it was easier to compare the BIM model quantities with quantities derived from 2D drawings. Moreover, it was easier to check if the geometry of the primary lining model and the inner lining model were well coordinated.

After the revision of the project the client has confirmed the quality of the delivered models. Nevertheless, before the next project phase we (designers and client together) have thought about how to improve the model in the next project phase. Founded on the written conclusions, we have prepared a set of new specifications for BIM modelling of primary lining.

We have decided to divide the model in two parts. One would consist of all the supporting elements modeled in 3D for the length of two excavation steps. The other would account for the project quantities and it would consist of elements of lining sprayed concrete and would run throughout the whole tunnel alignment (Figure 2). This would enable project material quantification with the usage of smart attribute assignments.

Afterwards, another idea about color coding was confirmed for a faster and more intuitive detection of stability of the problematic rock mass zones. Again, we have thought about the geometry of the tunnel cross section, which would be the base for our final design model. Based on the fact that the 2D drawings, in the final design phase, have considered the construction and deformation tolerances, we have decided to model the BIM model on the same principle, considering construction and deformation tolerances. Large tunnel lining deformations were predicted in the final numerical analysis of 0,5 m range. The result was a significant change in the tunnel lining diameter compared to the previous model, which did not consider all the tolerances. Tunnel diameter enlargement resulted in an increased number of rock bolt installed in the case of adopting the tunnel cross section with accounting of tunnel tolerances. We were aware that a possible 3D scan of the tunnel primary lining would differ from the BIM model in the range of the tunnel deformations that have taken place after the support installation.

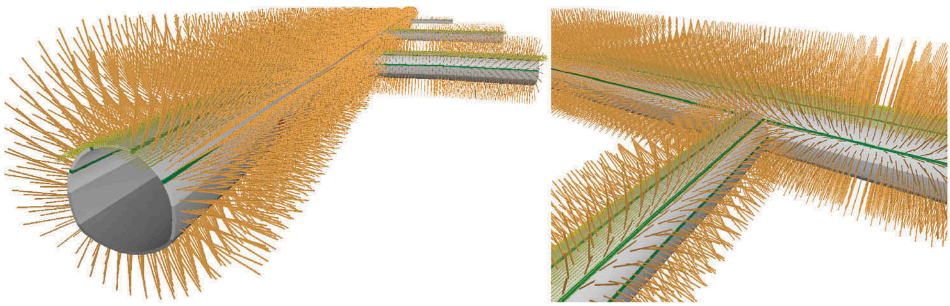

Figure 2. Representation of the BIM model of the primary support.

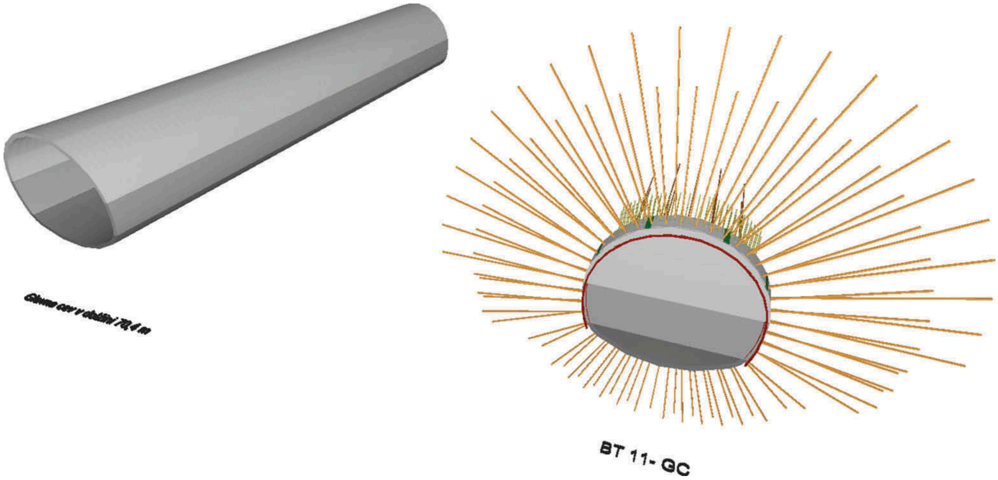


Figure 3. An example of the model prepared in accordance with the client.

Even though we have optimized the modelling procedure, we still maintained all the advantages that BIM brings – clear representation, precise quantities derivation, the possibility of 4D and 5D construction representation and finally producing a well-structured database of the tunnel. The model has shown to be consistent, manageable and reliable. With the introduced changes we have solved the issues that appeared in the previous design phase.

## 4 CHARACTERISTICS AND COMPARISION OF BOTH MODELS

### 4.1 *Model with emphasis on geometry modelling*

As mentioned before, the model that emphasizes on the geometry modelling was modeled with the LOD 300 requirements. We have followed the LOD specification for the year 2015 as it was specified in the contract. In the LOD specifications it was specified to follow and incorporate principles from other described construction elements in case of tunnel structure elements. The result was a model of all the tunnel supporting elements designed for the project. The model was divided in two parts: one would account for tunnel rock mass excavation and the other for tunnel supporting measures (Figure 3). Furthermore, the tunnel supporting measures model was divided in five partial models of the total size of 821 MB. It consisted of rock bolts, spills, rock bolt in tunnel face, deformation elements, reinforcement mesh, steel

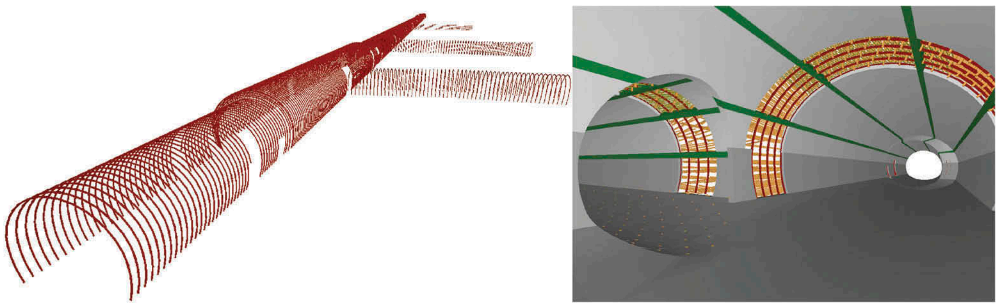

Figure 4. Renders from the model with the emphasize on tunnel element geometries.

arches, sprayed concrete in top heading, bench invert and tunnel face. The majority of the model size is represented by the rock bolt and spills which are joined in one partial model of 408 MB size, which represent 49,7% of the whole model size.

The model was somehow similar to a standard BIM model in which all the structure elements are modeled. Attributes were attached to all the model elements, describing their properties. Beneath can be seen an example describing a rock bolt. The rock bolt is described by its location in space, failure load, yield load, length, type of bolt and the pay item (Figure 4).

The model of the rock mass excavation was divided into excavation steps for the top heading, bench and invert. Beside the support type attribute of the lining segment, other attributes were added, which derive from the matrix method. These are: length of the line 1a, excavation area, rating area, deformation tolerance and other data linked to the excavation quantity (Figure 5).

### 4.2 *Final design model based on smart attribute assignment*

The model was prepared based on the proposal that we have prepared together with the client (Figure 2). The resulting model is divided in two parts, one accounts for tunnel rock mass excavation and the other for tunnel supporting measures (Figure 3). The model for tunnel support is divided in two parts one accounts for tunnel support quantities, the other for 3D support representation and elements properties definition. The model for representation of supporting measures is composed of rock bolts, spills, bolts in excavation face, steel arches, deformation elements, reinforcement mesh, sprayed concrete in top heading, bench, invert and tunnel face. The model was enhanced with color coding based on the parameter »behavior type«. The geometry of the model is based on a cross section that considers the displacement and construction tolerances. Based on an additional request from the client, the representations of supporting measures models are positioned in line with the tunnel axis (Figure 6). The whole model was composed of 38 partial models with the total size of 233 MB. From which 35 partial models represents different supporting type measures with the total size of 190 MB. As per agreement with the client, every support type representation should be placed in its own file.

The model that accounts for support elements quantities is built in the way that every support element pay item attribute is prescribed to an element of sprayed concrete besides the quantity of the element/Pay item (Pay_item_N...) (Figure 7). The quantities can be

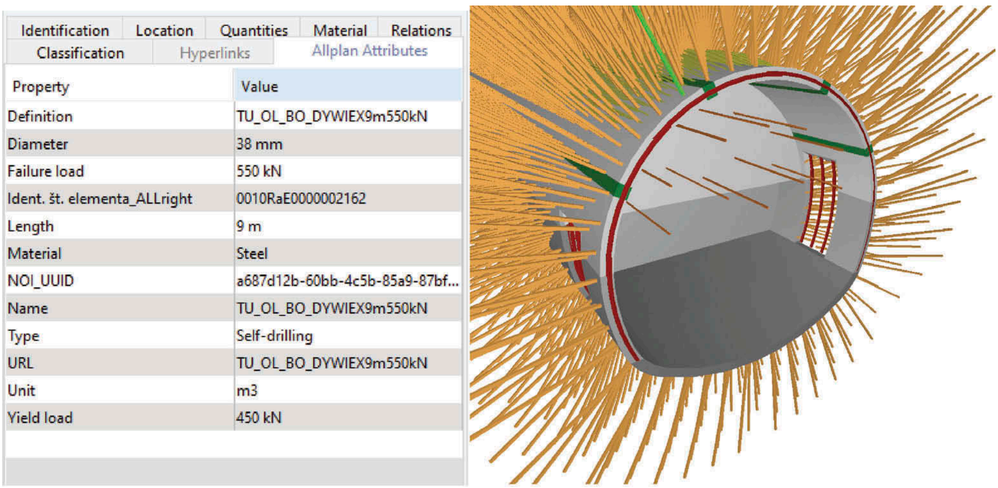


| Property | Value |
|---|---|
| Definition | TU_OL_BO_DYWIEX9m550kN |
| Diameter | 38 mm |
| Failure load | 550 kN |
| Ident. št. elementa_ALLright | 0010RaE0000002162 |
| Length | 9 m |
| Material | Steel |
| NOI_UUID | a687d12b-60bb-4c5b-85a9-87bf... |
| Name | TU_OL_BO_DYWIEX9m550kN |
| Type | Self-drilling |
| URL | TU_OL_BO_DYWIEX9m550kN |
| Unit | m3 |
| Yield load | 450 kN |

Figure 5. Representation of the attributes used in the model in case of a rock bolt.

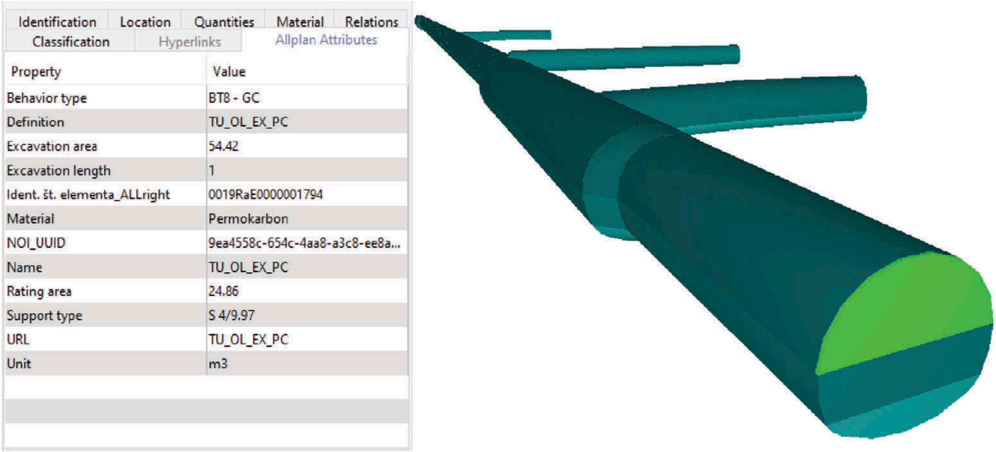


Figure 6. Representation of the rock mass excavation model and attributes used to describe one segment of top heading excavation.

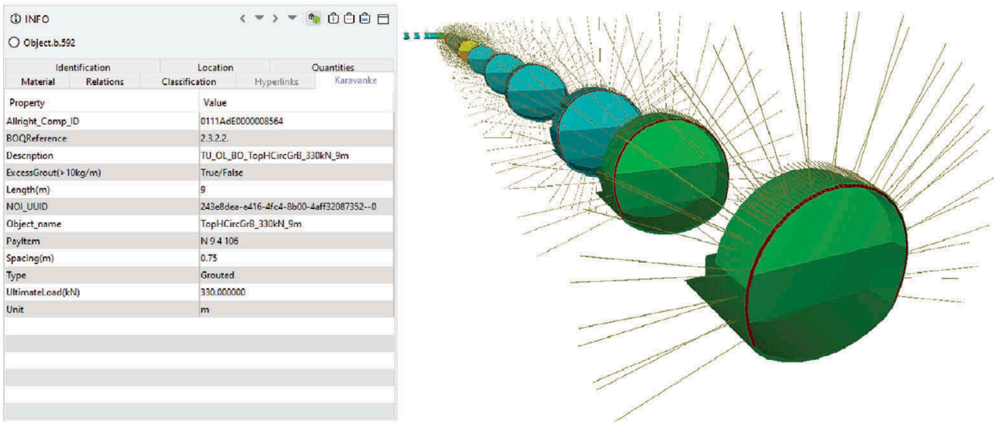


Figure 7. Representation of the supporting measures and attributes for a rock bolt - final design model.

derived from the tunnel support measures model, or transcribed from quantities written in 2D drawings. As can be seen from the figure bellow, an attribute named »Support type« is added to the attribute collection. It is meant as the classification number within the matrix method.

The model of rock mass excavation differs from the previous version mainly by introduction of color coding which is linked to the attribute named »Support type«. The model for rock mass excavation is divided in excavation steps for top heading, bench and invert. Other attributes linked to the matrix method are prescribed as length of line 1a, excavation area, rating area, deformation tolerance and other data connected with the excavation quantity.

The described final design model is well organized, attribution allocation is transparent, while the benefit of 3D support representation is preserved. Furthermore, the model enables a relatively simple way to develop 4D and 5D construction representations and an easy way to input the installed supporting measure during construction phase. The model has shown to be reliable, manageable and useful even when using older, less efficient hardware, always preserving all the benefits of 3D representation and the accuracy in analyzing project material quantities.

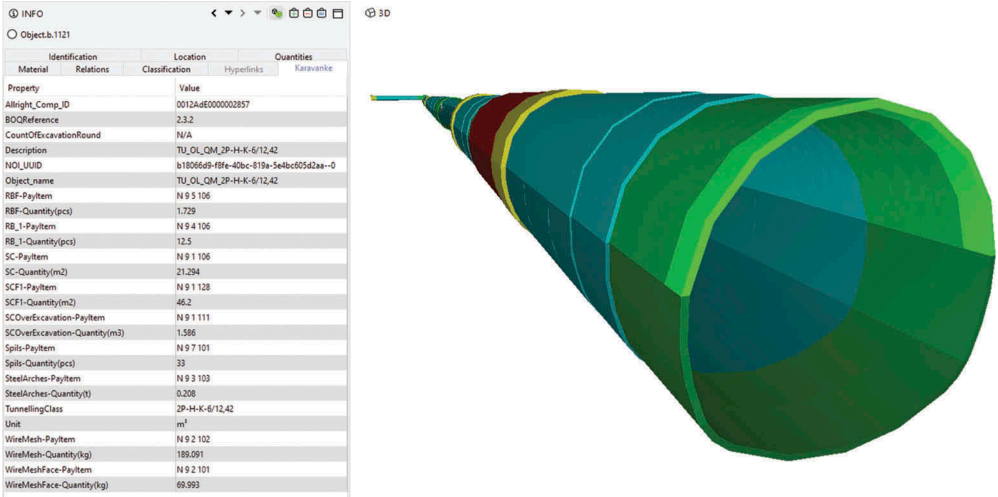


Figure 8. Representation of the model that accounts for support elements quantities – final design model.

#### 4.2.1 *Attribute structure*

Beneath, two out of all quantity model attributes are presented. The pair of attributes is added to one of the sprayed concrete elements (Figure 7) and represents the quantity and type of installed rock bolts:

- RB_1_PayItem – label of the attribute which describes the supporting element type. The label is uniquely defined by the pay item that is written in the quantification schedule. All the pay items can be found in a project database.
- RB_1_Quantity(pcs) – label of attribute that describes the quantity of a support measure element in one excavation step. The attribute label prescribes the unit in which the quantity should be expressed. Quantities are expressed in numbers or text in case of Yes/No input.

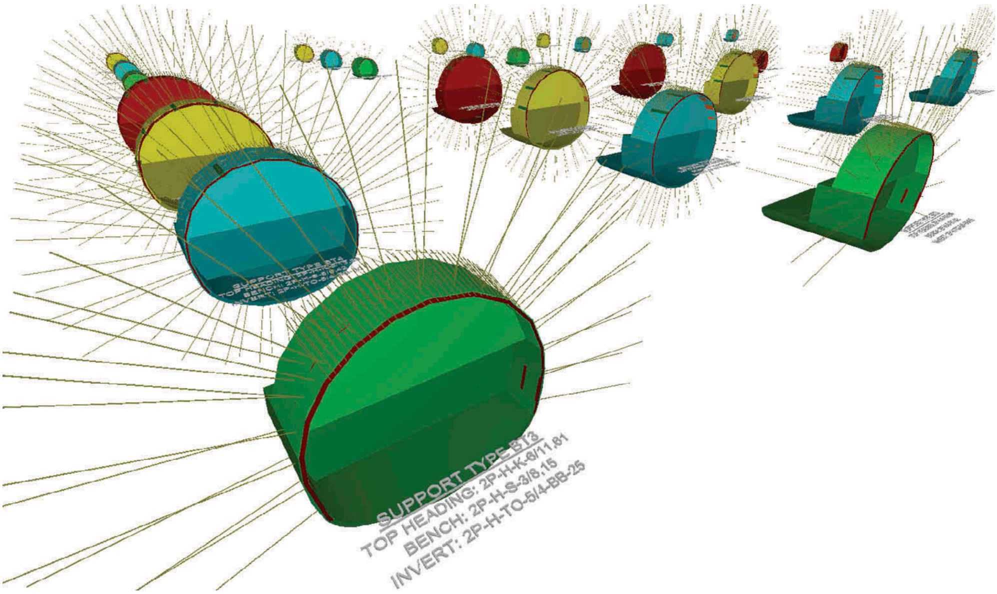


Figure 9. Special model for representation of every supporting measure used in the project.

### 4.3 *Possibilities of improving the models*

While modelling the primary support system some other ideas came across our heads, that could make the model better, but they were not included in the project because of certain disagreements between engineers or with the client. One of them is producing a model that would include all the support type models, which means moving the support models from the tunnel axes to the sides of the axes (Figure 8). Every support type model has its support type written in 3D letters in front of the model. Doing so we facilitate the visual inspection of the model.

The next idea is about material takeoff procedure. We would not assign every material quantity to a primary lining element. Instead we would prescribe just two essential attributes »Support type« attribute and the volume of the lining element. The quantity of a running meter of supporting measure would be derived from the 3D supporting measure models. Afterwards, the final quantity would be calculated by simply multiplying the support element quantity for a running meter with the length of the tunnel segment, which would be derived from the volume of elements from the tunnel support quantity model.

$$l = V_{SUM}/V_1$$

where $l$ = is the length of the tunnel segment with a specific support type; $V_{SUM}$ = total volume of lining element for a specific support type; $V_1$ = volume of a running meter of the lining element.

## 5 CONCLUSION

BIM modelling of the tunnel primary support system is a complex challenge which differs from the standard BIM modelling procedure. Because of the uncertainties in the boundary conditions which are a consequence of the surrounding ground behavior and the probabilistic approach to describe it, it is not possible to model the tunnel excavation and support in the BIM environment in the standard way. While modelling the Karavanke tunnel project we have used two different principles to produce the BIM model. With the first approach we emphasized on the geometry of supporting measures, with the second on the smart attribute assignment. Both approaches resulted to be feasible and both reached the desired goals of accurate 3D representation, project coordination feasibility and precise quantity takeoff derivation. On the other hand, the geometry emphasized approach resulted to be more size consuming and hardware demanding. The model based on smart attribute assignment resulted to be more versatile in case of project changes and more manageable from the point of element quantity and information that they carry. Nevertheless, we believe there is still room for improvement in the modelling approach, as explained in the previous chapter. In our opinion the client has made the right decision when requiring BIM approach in the project. It was proven several times, that project inconsistencies were discovered when modelling or analyzing the BIM model. These might have remained unresolved if BIM approach would not have been used in the project. Cases of discordances were wrong element naming, errors in element property description, conflicts between references in 2D drawing and material takeoff reference, discrepancies between various cross section of the same supporting type, errors in calculating the volume and area of elements and adoption of a wrong principle of tunnel face rock bolt quantity calculation. Based on these examples we can conclude that BIM has contributed to a more accurate project material takeoff. Furthermore, the 3D representation of the support structure with the belonging attributes has shown to be a well usable database of the project structures. Despite the noticeable differences between the common buildings BIM approach modelling and BIM modelling of tunnel excavation and tunnel supporting measures the client observed all the benefits of a standard BIM project. At the end they truly did get a better coordinated and defined project with a more precisely defined material takeoff. By adopting BIM technology to the project, we have produced a useful base for future investments in maintenance of the tunnel structure and have made a step forward in empowering good relations between client and construction companies in charge of excavating and constructing the Karavanke Tunnel project.

## REFERENCE

BIM Forum. 2015. Level of Development Specification. Specification BIM Forum.

*Tunnels and Underground Cities: Engineering and Innovation meet Archaeology, Architecture and Art, Volume 5: Innovation in underground engineering, materials and equipment - Part 1 – Peila, Viggiani & Celestino (Eds)*


# Design and construction of cast in-situ steel fibre reinforced concrete headrace tunnels for the Neelum Jhelum Hydroelectric project

B. Ashcroft, G. Peach & J. Mierzejewski
*Multiconsult Norge AS, Oslo, Norway*

B. De Rivaz & M. Yerlikaya
*Bekaert, Kortrijk, Belgium*

ABSTRACT: Twin 10 km long parallel headrace tunnels were excavated as part of the headrace tunnel system for the Neelum Jhelum Hydroelectric Project, using two Tunnel Boring Machines (TBMs). The permanent support normally comprised a shotcrete lining applied over initial support elements. However, concrete lining was required in certain areas of extremely poor ground conditions. Once placement of conventionally reinforced concrete commenced, it was found to be taking longer than anticipated, prompting a search for alternative solutions. Steel Fibre Reinforced Concrete (SFRC) proved to be the most viable option for accelerating the concrete lining programme. This paper briefly outlines the requirement for a concrete lining in the aforementioned areas. It includes an assessment of the suitability of a conventionally reinforced concrete lining versus an SFRC lining, the design basis, and the actual design itself. A comparison of the costs and durations to install the two types of lining is also presented.

## 1 PROJECT DESCRIPTION AND OVERVIEW

The Neelum Jhelum hydroelectric project is located in the Muzaffarabad district of Azad Jammu & Kashmir (AJK), in northeastern Pakistan. Geographically, the area consists of rugged terrain between 500 and 3 200 m in elevation within the Himalayan foothill zone known as the Sub-Himalayan Range.

The project is a run-of-river one, employing 28.6 km long headrace and 3.6 km long tailrace tunnels to cut off a major loop in the river system, transferring the waters of the Neelum River into the Jhelum River, for a total head gain of 420 m (Figure 1). The headrace tunnels comprise both twin (69 %) and single (31 %) tunnels, while the tailrace tunnel consists of a single tunnel. Design capacity of the waterway system is 283 cumecs.

The project, which was completed in 2018, has an installed capacity of 969 MW, generated by four Francis-type turbines located in an underground powerhouse.

At commencement of construction in 2008, all tunnels were to be excavated using conventional drill & blast techniques. However, it soon became apparent that with the equipment being employed, a 13.5 km long section of the headrace twin tunnels underlain by high terrain that precludes construction of additional access adits, would take too long to excavate.

Consequently, the construction contract was amended to allow the operation of two 8.5 m diameter open gripper hard rock TBMs to each excavate some 10 km of the twin headrace tunnels (Figure 1), with an initial centre-to-centre lateral spacing of 33 m, later increased to 55.5 m.

The tunnel excavation diameter was 8.5 m diameter giving a total face area of 56.75 $m^2$. Excavation direction was upstream to promote drainage, with a typical gradient of 0.8 %.

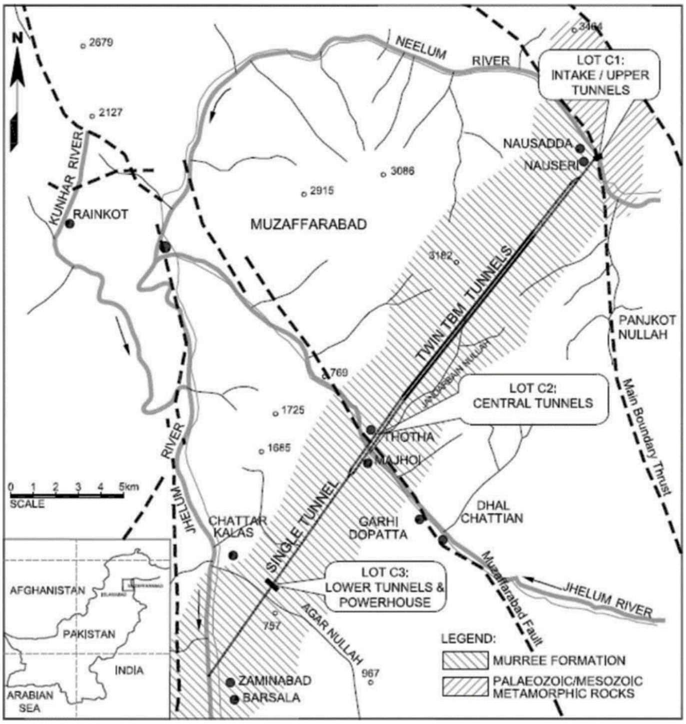


Figure 1. Neelum Jhelum project layout showing TBM Twin tunnels (in bold), major faults (dashed) and alignment geology.

The open gripper design was selected to give the most flexibility for the expected conditions – possible squeezing ground given the relatively weak rock mass and overburden up to 1 870 m, and the potential for rockbursts in the stronger beds. Excavation of the TBM tunnels commenced in January 2013 and was completed in May 2017.

The initial design for the entire project had employed a shotcrete lining throughout, but with short sections of full concrete lining in zones of poor ground, estimated during the feasibility study to add up to about 10 % of the total length.

However, shortly after commencement of the project, the change was made to a full concrete lining for all headrace tunnels, with the exception of the TBM portion, which retained a shotcrete lining for a number of reasons. Specifically, it was judged that the TBM excavation method had several advantages over the Drill & Blast method that resulted in a significantly less-disturbed rock mass, a much smoother tunnel profile, a circular rather than horseshoe shape, and the ability to spray a much more uniform shotcrete layer.

Nevertheless, it was recognized that some sections of concrete lining placed over the shotcrete lining would be required in zones of poor ground, albeit with a shorter aggregate length than the original 10 % estimate, judging by conditions in the early tunnels. It must also be stated that the importance of such local reinforcements had been unavoidably highlighted by the issues encountered on the Glendoe project in Scotland a few years earlier.

It is these sections of concrete lining, which of necessity had to be mostly completed before tunnel excavation had finished, that are the subject of this paper.

### 1.1 *Geological setting*

The entire project was excavated in the molasse-type sedimentary rocks of the Murree Formation, which is of Eocene to Miocene age. The succession comprises intercalated beds of sandstone, siltstone and mudstone that have been tightly folded and tectonized, with generally steep bedding dips and a northwesterly regional bedding strike, rarely far from perpendicular to the tunnel azimuth. Weakness zones and local faults were commonly observed, and were invariably oriented parallel to the regional bedding strike.

### 1.2 *TBM configuration and rock support installation*

The two TBMs were conventional in their layout, and were based on the successful Gotthard Base TBMs. Nearly all rock support elements, including rock bolts, mesh, channel sections and TH ring beams, but with shotcrete application limited to the maximum extent possible, were installed in the so-called L1 zone immediately behind the shield.

The shotcreted tunnel invert was installed between the L1 and L2 zones, while the majority of shotcrete was sprayed in the L2 zone, some 60 m behind the face, using robots installed outside a cylindrical shield that kept workers and equipment free of overspray and rebound.

## 2 TBM EXCAVATION

### 2.1 *Progress*

Both TBMs started headrace tunnel excavation in early 2013 with completion by the first TBM in October 2016 and the second TBM in May 2017. The lengths of the left and right tunnels, respectively (looking downstream), were 10.428 km and 9.893 km, giving an average daily excavation rate of 8.02 m and 6.37 m. For simplicity, the chainages used in this report start at zero where TBM excavation commenced, and increase in the direction of advance. (In practice, construction records reflect actual chainages, which decreased with upstream advance, and which took into account a section of drill & blast tunnel upstream.) Over most of the excavation programme, the left TBM was generally the lead TBM.

### 2.2 *Encountered ground conditions*

Overall, encountered ground conditions were better than expected, in that the squeezing conditions anticipated in the weaker mudrocks were never encountered, despite an overburden of up to 1 870 m. The most likely explanation is that the closely intercalated nature of weak and strong lithologies meant that there was always a 'skeleton' of stronger sandstones and siltstones that provided support for the excavation. Also of benefit to the excavation was the almost complete absence of groundwater ingress.

Furthermore, with the exception of a single major fault, encountered some 1.5 km into the drives, and described below, no other major faults were encountered. Small-scale faulting was common, as were shear zones along beds of weak mudstone, but the strike of most of these features followed the regional bedding strike, which the alignment usually beneficially intersected close to perpendicularly (with the notable exception of the location of the largest rockburst).

On the negative side, however, the incidence of rockbursts was significantly higher than had been anticipated, primarily it is thought because of the existence of elevated horizontal stresses that were unanticipated. It is these rockbursts that primarily contributed to the overall low daily production rates. The left tunnel experienced 937 documented rockbursts, ranging from small to major violent events, while the (usually trailing) right tunnel experienced 590 rockbursts. The zone of the most intense rockbursts persisted for approximately 3 km, before diminishing relatively abruptly.

The two longest sections that required concrete lining were the major fault encountered in both drives, and the location of the largest rockburst experienced on the project, which was named '5/31′ after the day on which it occurred, May 31$^{st}$, 2015. Both features, which are described in more detail below, necessitated construction of concrete lining in both tunnels for over 120 m.

The junction with an access adit, A2, required 48 m of concrete lining in the left tunnel to ensure stability and improve hydraulics. Additional, shorter sections of concrete lining were required in the left tunnel only. Two of these sections were in sheared mudstone that was judged to require additional support, and one was in an area of badly delaminated shotcrete lining. The sections of concrete lining that were placed in the TBM tunnels are shown in Table 1. They amount to 612 m of tunnel, or 3.0 %, significantly lower than the approximately 10 % estimated during the feasibility study.

### 2.3 *Encountered geological features requiring extensive concrete lining*

Two geological features required concrete lining in both tunnels in excess of 100 m length. The first is a 95-110 m wide zone of highly sheared mudstone that unusually was associated with groundwater inflows of up to 10 L/min. During the initial encounter by the left TBM, a cavity formed above and ahead of the cutterhead, and the TBM subsequently became jammed at Ch. 1+430 m by the pressure of the collapsed fault gouge on the shield. Stabilizing the excavation and freeing the TBM required installation of a pipe roof canopy, followed by excavation of a top-heading above the cutterhead, and extensive chemical and cement grouting to consolidate the ground ahead of the TBM.

The second feature was the 5/31 rockburst that occurred in the right TBM tunnel, which at the time was trailing the left TBM by 180 m, separated by a 24.5 m wide pillar. The event had a calculated energy release equivalent to a Richter magnitude 2.4 earthquake, causing extensive damage to the TBM, ancillary equipment and rock support over a 60 m section of tunnel as well as significant damage to the tunnel lining of the already-excavated neighbouring TBM tunnel. It disabled the TBM for 7.5 months.

### 2.4 *Requirement for rapid construction of concrete lining*

Given the obstacles posed by everyday rockbursts, not to mention the catastrophic 5/31 event, it is perhaps not surprising that the tunnel excavation programme slipped significantly behind schedule, and that as the commissioning date approached, it had become one of the project structures (but by no means the only one) on the critical path.

To meet project deadlines, as much of the concrete lining as possible had to be placed within each tunnel while the TBMs were still operational. Failing that, remaining installation had to proceed after completion of the excavation, but while parts of the TBMs were being removed and other tunnel finishing works, such as grouting, were being completed.

Throughout the lining installation, full tunnel logistical access by way of the rail track had to be maintained. These factors significantly influenced the methodology selected. Principally, the solution was to install the additional concrete lining in two stages. Stage one consisted of the installation of the upper 270° of the concrete lining, while maintaining full tunnel access

Table 1. Summary of TBM tunnel sections with concrete lining installed.

| Tunnel | Chainages | Length (m) | Lining Type | Reason for Lining |
|---|---|---|---|---|
| Left | 6+022 to 5+854 | 168 | Conventional RC | 5/31 rockburst |
| Right | 5+818 to 5+698 | 120 | Conventional RC | |
| Left | 1+649 to 1+553 | 96 | Conventional RC | Major Fault |
| Right | 1+512 to 1+404 | 108 | Conventional RC | |
| Left (U/S) | 1+710 to 1+698 | 12 | SFRC | Adit A2 Hydraulic Improvements |
| Left (D/S) | 1+698 to 1+662 | 36 | SFRC | |
| Left | 1+327 to 1+303 | 24 | SFRC | Sheared mudstone 1 |
| Left | 1+188 to 1+164 | 24 | SFRC | Sheared mudstone 2 |
| Left | 0+466 to 0+442 | 24 | SFRC | Delaminated shotcrete |
| TOTAL | | 612 | | |

for other tunnel related work. Stage two consisted of the installation of the lower 90°, after the tunnel rail track had been removed and was no longer required.

### 2.5 *Locations of additional concrete lining*

Concrete lining works commenced at the upstream end of the tunnel and worked backwards downstream. However, it gradually became apparent that the logistical complexity of the operation, with the various concrete lining sections distributed in discrete zones often hundreds of metres apart, all the while maintaining rail access, was delaying completion more than anticipated. One way of streamlining the process was to prioritise construction of the remaining lining sections further downstream initially. This became the driver for assessing and developing alternative concrete lining methodologies.

A major task in conventionally reinforced concrete lining construction involves the careful installation of reinforcing bars at their required locations. It was realized that considerable time could be saved by the implementation of a SFRC lining, and this technique rapidly became the preferred acceleration option.

A comprehensive design review was initiated for the remaining concrete lining locations, and the computations showed that SFRC met all the required specifications, so much so, that its use for most of the required concrete lining sections would have been possible from the start.

The design methodology used for the SFRC lining is presented in detail below.

## 3 DESIGN

### 3.1 *Introduction*

Although the majority of the reinforced concrete tunnel linings on the Neelum Jhelum project had been done so with conventional steel bars, steel fibres were considered as a suitable alternative for certain sections within the TBM tunnels since:

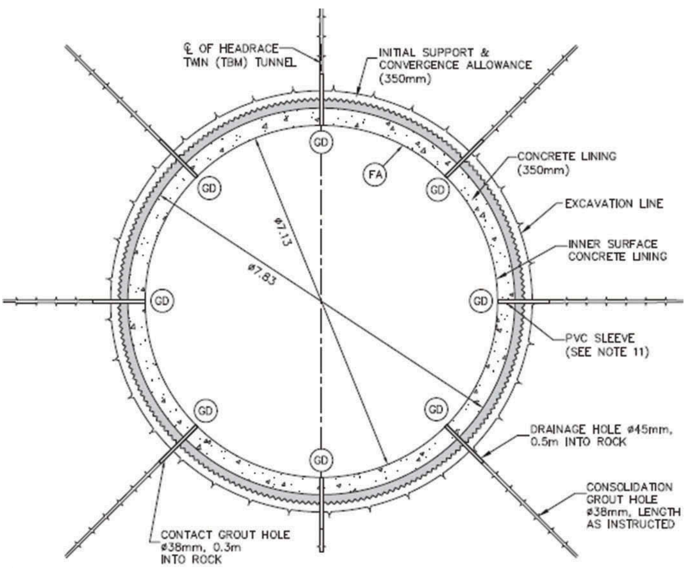


Figure 2. Cross-section of concrete lining.

- The lining shape was circular (as opposed to the horseshoe shape of the portion of the tunnels excavated by Drill & Blast)
- High compressive axial forces would act on the lining with low bending moments
- Steel fibres work to prevent the formation and widening of cracks

### 3.2 *Geometry*

As previously mentioned, the excavated diameter of the TBM tunnels was 8.53 m. Due to the severity of some of the ground conditions encountered, large quantities of initial support had been installed in sections where a permanent concrete lining was required, e.g. heavy steel ring beams at 700 mm centres longitudinally along the tunnel and thick layers of shotcrete. A generous allowance of 350 mm had therefore been stipulated for the initial support and any convergence. The minimum design concrete lining thickness was specified as 350 mm. This thickness was a compromise between finding a constructible solution that achieved the design intent, whilst reducing the cross-sectional area of the waterway as little as possible in order to minimize the head loss and thereby the hydraulic penalty.

### 3.3 *Design loads and tunnel design cases*

The design loads and tunnel design cases applied in the design are summarised in Table 2.

Table 2. Design loads (with their factors) assumed to act on the lining.

| Tunnel Design Cases | Constr-uction Case | Filling Case | Operational Static Case | Transient Water Hammer Case | Dewatering Case | Faulted Ground Special Case |
|---|---|---|---|---|---|---|
| Design Loads: | | | | | | |
| Dead Load | 1.1 | 1.1 | 1.3 | 1.1 | 1.1 | 1.1 |
| Contact Grouting Pressure | 1.4 | | | | | 1.4 |
| External Water Pressure | 1.4 | 1.4 | | | 1.4 | 1.4 |
| Transient Water Pressure | | | | 1.1 | | |
| Wedge Failure Of Rock | 1.2 | 1.4 | 1.4 | | 1.4 | |
| Faulted Ground | | | | | | 1.2 |

### 3.4 *Structural analysis of the lining and design assumptions*

Elastic continuum, closed form analysis was used to determine the stresses acting on the lining. The analysis is based on excavation and lining of a hole in a stressed isotropic and homogeneous elastic medium.

Once bending moment and ring thrust in a lining have been determined, or a lining distortion estimated based on rock-structure interaction, the lining must be designed to achieve acceptable performance. Since the lining is subjected to combined normal force and bending, the analysis is carried out using the moment-axial force capacity curve, (U.S. Army Corps of Engineers, 1997).

Due to local areas of overbreak or variations in the convergence and thickness of initial support, the concrete lining may in reality deviate slightly from the actual design value. As well as obviously affecting the centroid radius value of the tunnel, the thickness of the lining affects the second moment of area, $I$, of the lining. The second moment of area is also affected by the reduced stiffness effect of having joints in the lining (the upper 270° is placed first and then the lower 90° is cast below the advancing formwork). In this analysis, as well as calculating the standard value of $I$ based on the thickness of the lining, a sensitivity analysis with different scenarios was also performed where upper and lower bound values were calculated by taking a percentage variation of the 'standard' value.

## 3.5 *Design of conventionally reinforced and fibre reinforced lining*

### 3.5.1 *Material properties*

The material properties employed in the design are presented in Table 3:

Table 3. Material properties used for design.

| Material | Property | Value |
|---|---|---|
| Concrete | Specified compressive strength of concrete (MPa) | 30 |
| | Modulus of elasticity of concrete (GPa) | 25.74 |
| | Poisson's ratio | 0.15 |
| Steel reinforcement bars | Specified yield strength of reinforcement (MPa) | 400 |
| | Tensile strength of reinforcement (MPa) | 620 |
| | Elastic Modulus of steel (GPa) | 200 |
| Steel fibres | Fibre length (mm) | 35 |
| | Fibre diameter (mm) | 0.55 |
| | Aspect ratio l/d | 65 |
| | Tensile strength (MPa) | 1345 |
| | Young's modulus (GPa) | 210 |
| | Minimum Dosage (kg/m$^3$) | 40 |
| | CMOD 0.5mm, $f_{R1,m}$ (MPa) | 3.7 |
| | CMOD 1.5mm, $f_{R2,m}$ (MPa) | 3.9 |
| | CMOD 2.5mm, $f_{R3,m}$ (MPa) | 3.6 |
| | CMOD 3.5mm, $f_{R4,m}$ (MPa) | 3.2 |

### 3.5.2 *Serviceability Limit State (SLS) design*

#### 3.5.2.1 SERVICEABILITY LIMIT STATE (SLS) DESIGN FOR CONVENTIONALLY REINFORCED LINING

The minimum required cover according to the applicable standards was 75 mm for the structure. #8 (25 mm diameter) and #6 (19 mm diameter) reinforcement bars were specified at centres of 175 mm in the circumferential and longitudinal directions respectively. This reinforcement configuration satisfied the minimum reinforcement requirements and other durability considerations stipulated in the relevant standards such as:

- Minimum reinforcement
- Requirements for flexural crack control
- Requirements for temperature and shrinkage reinforcement

#### 3.5.2.2 SERVICEABILITY LIMIT STATE (SLS) DESIGN FOR STEEL FIBRE REINFORCED LINING

Crack control is one of the main benefits provided by steel fibres to structural elements. If these cracks do not exceed a certain width, they are neither harmful to a structure nor to its serviceability. The limitation of crack width means that steel fibres provide a post crack strength to the concrete.

Fibres may have been originally introduced for strengthening of the matrix, without distinguishing the difference between material strength and material toughness. (Toughness is used for describing the post-peak response of structural members that quantifies the energy absorption characteristics.) The most significant effect of fibre addition to the brittle cementitious matrix is the enhancement of toughness.

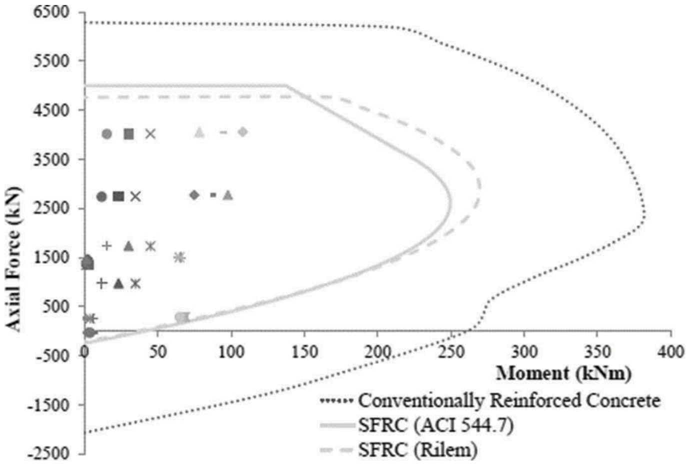


Figure 3. Moment - Axial Force Interaction Diagram - Circumferential Direction from Elastic Continuum Method.

One of the greatest benefits to be gained by using steel fibre reinforcement is improved long-term serviceability of a structure. SFRC in a tunnel lining offers: a) Excellent ductility, b) Reduction in the shrinkage of concrete, c) Elimination of mistakes in conventional reinforcing, d) Shorter construction periods compared to traditional ones, e) Increased tensile and flexure strengths that are equal in all directions, f) Easy crack control and high absorbed energy after matrix failure.

The distance between steel fibres is much smaller than typical spacing between traditional bars. Unlike reinforced concrete, fibres are distributed throughout the whole section. Hence, there is no concrete cover without reinforcement. Furthermore, stresses in the root of a crack can be picked up more quickly. This is why crack propagation and crack patterns change when compared to plain or even reinforced concrete (Vitt, 2005).

#### 3.5.3 *Ultimate Limit State (ULS) design*

The ULS axial loads and bending moments were determined for each type of scenario for each tunnel design case. The moment – axial force capacity curve for the conventionally reinforced section was plotted assuming that there was an equivalent area of circumferential reinforcing steel of 2805 $mm^2$/m in each face of a column under combined axial load and bending. The moment – axial force capacity curves for the SFRC lining were generated using both the Rilem Method and the method detailed in Appendix A of ACI 544.7 These curves are plotted in Figure 3. The singular points on the diagram are the results from the elastic continuum analysis for different scenarios for each of the tunnel design cases listed in Table 2. Figure 3 shows that the points fall within the capacity curves.

The shear was checked using the equation: $V_{max} = [(M_{max} - M_{min})/R]$

The shear capacity of the concrete alone (without separate shear reinforcement or taking the beneficial effect of the fibres into account) was found to be easily adequate, even for the maximum factored shear force of 58 kN.

## 4 DURABILITY CONSIDERATIONS WHEN USING SFRC

SFRC is often used for concrete structures subject to severe exposure conditions e.g. bored tunnels exposed to saline ground water containing high levels of sulphates (Edvardsen, 2018). Two phenomena need to be examined when analyzing the durability of SFRC:

- The reinforcement has to provide good “tightness” against infiltration of water by controlling in situ crack opening
- Corrosion of the reinforcement should not cause a notable reduction in the bearing capacity of the lining

Two different configurations must be taken into account when analyzing the corrosion of steel fibres and its consequences:

1. The fibre does not cross a crack emerging on the surface
2. The fibre crosses a fracture crack on the surface

In the first case, apart from some stains which affect the appearance of the structures, corrosion of the fibres does not lead to any serious problems for the durability or the bearing capacity of these structures in SFRC.

In the second case, the bearing capacity of the SFRC is not reduced significantly with crack openings of 250 μm or less.

The corrosion resistance of SFRC is governed by the same factors that influence the corrosion resistance of conventionally reinforced concrete. Processes such as carbonation, penetration of chloride ions and sulphate attack are in direct proportion to the permeability of the cement matrix.

As long as the matrix retains its inherent alkalinity and remains intact, deterioration of SFRC is not likely to occur. It has been found that good quality SFRC, when exposed to conditions conducive to reduced alkalinity, will only carbonate to a depth of a couple of millimeters over a period of many years (Kern & Schorn 1991, Hannant & Edgington 1975).

## 5 COMPARISON OF COSTS AND DURATIONS

### 5.1 *Comparison of time and cost of different methodologies*

The requirement to meet a completion date necessitated the implementation of a detailed project management system to record all aspects of the concrete lining. This data was recorded by both design and supervision teams, and the key points are presented in Table 4.

The sections numbered 1 to 4 refer to additional concrete lining sections constructed using concrete with steel reinforcement bars, or what may be considered the conventional methodology. Sections numbered 5 to 9 refer to the sections of lining constructed using SFRC.

The sections numbered 1, 2, 3, 7, 8 and 9 were installed whilst maintaining full logistical access for other tunnel works by way of the rail track. Sections 4, 5 and 6 were the last sections to be installed when there was no requirements to maintain tunnel access for other works. Furthermore, they were located directly adjacent to access Adit A2, affording uninterrupted access to surface facilities. (It should be noted that while section 4 was one of the last to be placed, it was one of the first to be designed and issued to the contractor, hence the use of conventionally reinforced concrete rather than SFRC.)

### 5.2 *Comparison by time*

Table 4 presents three columns relating to time required for lining installation. “Time per Section” provides the total time for the concreting works required for that section length. “Time per Lm” is the average time taken to install one linear metre of tunnel lining. “Delays during concrete placement” presents the extent of production delays for each section and is expressed as a percentage of the total time.

### 5.3 *Findings from time data*

The data from Table 4 shows that lining installation using conventionally reinforced concrete ranged from 43 to 175 minutes per linear metre. However, section 4, as mentioned previously,

Table 4. Comparison by Time and cost of Lining Types per Unit Length.

| No. | Reason for Lining | Length (m) | Lining Type | Time per Section (hours) | Time per Lm (minutes) | Placement Delays | Cost per Lm |
|---|---|---|---|---|---|---|---|
| 1 | 5/31 Rockburst (Left) | 168 | Conventional RC | 465.25 | 166* | 35% | Special |
| 2 | 5/31 Rockburst (Right) | 120 | Conventional RC | 350 | 175* | 28% | Cases |
| 3 | Major Fault (Left) | 96 | Conventional RC | 214 | 134 | 26% | 100% |
| 4 | Major Fault (Right) | 108 | Conventional RC | 76.5 | 43 | 9% | 82% |
| 5 | Adit A2 Strengthening and | 12 (u/s) | SFRC | 19.5 | 98 | 9% | 35% |
| 6 | Infill for hydraulic improvement (Left) | 36 (d/s) | SFRC | 45 | 75 | 2% | 35% |
| 7 | Sheared Mudstone 1 (Left) | 24 | SFRC | 24.75 | 62 | 3% | 41% |
| 8 | Sheared Mudstone 2 (Left) | 24 | SFRC | 69 | 173 | 13% | 41% |
| 9 | Delaminated lining (Left) | 24 | SFRC | 34 | 85 | Nil | 33% |
| | Total: | 612 | | | | | |

* *Values have been adjusted to account for the fact that the volumes of concrete placed per linear metre for these sections were larger than the other sections due to the enlarged tunnel profile that resulted from the 5/31 rockburst event. The adjustment allows for a just comparison of the values.*

enjoyed direct access to concrete trucks via Adit A2, resulting in a far more favourable result. Consequently, section 4 should be discounted, and the results from sections 1, 2 and 3 (i.e. 134 to 175 minutes per linear metre) are adopted as a more typical time per linear metre for conventionally reinforced concrete.

The associated time delays when using the conventionally reinforced concrete varied from 9% to 35%. However, once again the result from section 4 should be ignored, and the results from sections 1, 2 and 3 (i.e. 26 to 35%) should be regarded as more representative.

The data from Table 4 shows one outlier, at 173 minutes per linear metre for SFRC. This anomaly was a result of some of the batches of SFRC being rejected and extensive stoppages due to the blockages of pipes during placement and is therefore only shown here for the sake of completeness. Excluding this outlier (section No. 8), the time taken to install the SFRC lining ranges from 62 to 98 minutes per linear metre giving an average of 77 minutes per linear metre, offering a significant time saving over conventionally reinforced lining installation.

The associated typical time delays using the SFRC lining type range from 0 – 9% (discounting the outlier).

### 5.4 *Findings from cost data*

The details of the costs for each section are presented in the last column of Table 4. Information for sections 1 and 2 has been excluded and noted as 'special cases' because these sections required lining as a result of the 5/31 severe rockburst, which caused near-complete destruction of the existing shotcrete lining and surrounding strata. A far more extensive effort was therefore required to repair these two sections, making a comparison with other sections misleading.

The first section of concrete lining to be completed was section 3, associated with the major fault. This has been taken as the reference point for the costs analysis, i.e. this cost is expressed as 100% and all other costs are compared to this bench mark.

The data from Table 4 shows that the lining installed using conventionally reinforced concrete ranged from 82 to 100%.

The data from Table 4 shows that the lining installed using fibre reinforced concrete ranged from 33 to 41% of the reference cost of section number 3, a very significant saving.

## 6 CONCLUSIONS

In summary, the adoption of SFRC over conventional reinforcement proved to be a notable success. Not only did SFRC lining meet the same design criteria as a conventionally reinforced lining, it offered the following advantages:

- Saving cost over the actual quantity of steel employed
- Saving time by being quicker to install
- Producing a lining with smaller crack widths and improved durability over the life of the structure
- Producing a lining that is more efficient at resisting stresses due to groundwater loads and ground loads than conventionally reinforced concrete

## REFERENCES


American Concrete Institute. 2016. *544.7R-16 Report on Design and Construction of Fiber-Reinforced Precast Concrete Tunnel Segments*. Farmington Hills: American Concrete Institute.

Department of the Army, U.S. Army Corps of Engineers. 1997. *Engineer Manual EM 1110-2-2901, Tunnels And Shafts In Rock*. Washington: US Army.

Edvardsen, C. 2018. Consultant's view of durable and sustainable concrete tunnel constructions in the Middle East. *World Tunnel Congress*: *Dubai*.

Hannant, D. & Edgington, J. 1975. Durability of steel fibre concrete. *Proceeding, RILEM Symposium on Fibre reinforced cement and concrete*, *Vol 1*, September 1975: pp 159–169.

Kern, B. & Schorn, H. 1991. 23 Jahre alter Stahlfaserbeton, *Beton and Stahlbetonbau*, V 86, September 1991: pp 205–208.

Rilem TC 162-TDF. 2003. *Test and design methods for steel fibre reinforced concrete: σ-ε design method*. Mater. Struct. 36 (262): pp 560–567.

Vitt, G. 2005. Crack control with combined reinforcement: from theory into practice. *The 1st Central European Congress on Concrete Engineering: Fibre Reinforced Concrete in Practice. Graz*, *8–9 September 2005*. Berlin: Ernst & Sohn.

*Tunnels and Underground Cities: Engineering and Innovation meet Archaeology, Architecture and Art, Volume 5: Innovation in underground engineering, materials and equipment - Part 1 – Peila, Viggiani & Celestino (Eds)*


# Analysis of two-component clay sand backfill injection in Japan

P.J. Ashton, S. Takigawa, Y. Kano & Y. Masuoka
*TAC Corporation, Okayama, Japan*

ABSTRACT: Ground subsidence is one of the main concerns contractors and engineers have when undertaking tunnel excavation projects. Particularly vulnerable from subsidence are older as well as landmark buildings, which form major focal points in cities worldwide. It is with a view to protecting these structures during tunneling that a two-component injectable non-hardening Clay Sand system was envisaged 30 years ago in Japan. This paper will analyze the journey of this "Made in Japan" method from its inception, to industry acceptance and finally it's widespread application in major tunneling projects. We will seek to show, via the analysis of real-world data, the multipurpose nature of this method for enabling excellent thrust stability during sharp curve excavation and for applications with EPB and Slurry TBMs alike. We will also show how this injectable Clay Sand material is evolving to meet the needs of bigger and more complex tunneling sites in the future.

## 1 INTRODUCTION

### 1.1 *Early problems with tunneling in Japan.*

With the success of the first Shield Machine excavated tunnel in Japan in 1922, the almost 100-year long evolution of tunneling technology to the present day had begun. TAC Corporation's own journey within the shield construction industry started in 1976. As the Japanese tunnel market grew, so did TAC's successes with continuous improvements of technologies and materials specifically developed to prevent subsidence at every new opportunity, earning the company the reputation and motto of "Pursuing Zero Ground Subsidence in Shield Construction". In Japan, it was with the evolution of the Shield machine into the two main modern types, Slurry and EPB; and the invention by TAC of simultaneously injected two-component air entrained backfill grout, that the quite regular occurrence of 30–40cm subsidence caused by the deficiencies of Blind shield tunneling in the predominantly ultra-soft clay ground commonly found in Japan, was finally reduced to around 5cm, after the tail of the shield machine had passed, which at the time, was an all-time low. However, it was through an unexpected discovery that subsidence during excavation would be brought under control to virtually zero. Unlike the rapidly hardening two-component cement based backfill grout system that TAC was famous for at the time, this final reduction in subsidence would be achieved by implementing and modifying the use of a non-hardening thixotropic gel material initially invented for its friction reducing properties.

### 1.2 *Solutions for reducing subsidence.*

In the 1970's, TAC was busy developing a quick setting, air entrained, high flow two-component grout, while the rest of the industry worldwide was generally utilizing single-component, relatively slow setting, sand or gravel-based grouts. This new Shield Thixotropic-gel Grout System, was very well accepted in Japan because of its ability to reduce ground settlement in ultra-soft clayey-sand type ground conditions. Two-component grout injection, became the cornerstone of the foundation for the technical skills to finely control the modulation of A:B

Liquid injection ratios that would eventually be required to tame Clay Sand into a workable solution for further reducing subsidence in the future.

Backfill grout used to be almost exclusively be applied via injection through the segment to stabilize the tunnel segments during excavation. A shift in industry practice in the 1980s saw some machine makers start to inject grout via the tail skin using a simple tube in the skin of the machine which opened into the tail void. However, these systems were prone to blockages, even when properly maintained. In 1982, TAC developed a new kind of cleanable injection pipe. This reliable, easily maintainable injection pipe further decreased the rate of subsidence occurring in tunnel construction, however, it was insufficient to totally eliminate uncontrolled settlement occurring in tunnel construction. Eventually, the inspiration for the development of a two-component Clay Sand solution injection as a subsidence prevention material came from a phenomenon noticed post-project completion.

## 2 PAST APPLICATIONS

### 2.1 *Subsidence control as a side effect.*

In the early 1983, Nishimatsu Construction Company was working on the construction of a 1.3 km section of the Osaka City, Midosuji Subway Line with a 6.98m Kawasaki Heavy Industries slurry shield machine. During the design phase, concerns were raised as to perceived problems arising from the combination of driving through a curve, while also ending the drive, since the final part of the drive included a R=160m curve. Nishimatsu Construction Corporation requested TAC to create a solution to mitigate the risks posed by the overcut in such a vulnerable position. Two solutions were presented; The first was to apply a high air content backfill grout mixture containing 80% air which was to be sacrificed, once hardened, as the machine moved around the curve; however, this was discarded due the fact that once the machine began to drive through the curve, the sacrificed grout on one side of the machine would be replaced by a new void on the opposite side of the machine, thus negating the effect of the injected material in the first place. The second, to use a combination of clay-sand, fly ash and thickener to create a non-hardening material with high viscosity, and low friction resistance to lubricate the machine through the curve was adopted. This option would flow freely around the whole of the machine during the drive under the pressure applied from the movement of the machine. The material called “Clay-Shock”, was adopted in conjunction with a segment stabilization system called the “Mini-Packer Method”, and the difficult curve was driven through, completing the tunnel as planned (Figures 1–2).

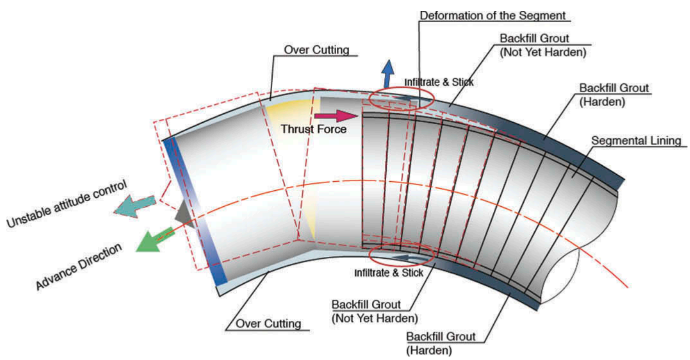


Figure 1. The problem with sharp curve construction. Ground surrounding the TBM during a curve must be filled quickly with grout. The segmental lining must be fixed properly to the ground to ensure stability of TBM attitude. Due to unsatisfactory ability to fill tail void with grout sufficiently, the segmental lining may become unstable due to the thrust of the TBM.

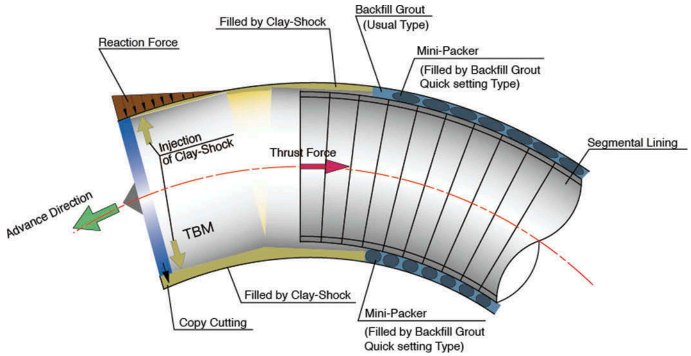


Figure 2. Sharp curve construction using Clay Shock and the Mini-Packer Method. Clay Shock is injected into the overcut to ease the frictional resistance around the TBM, while also preventing the collapse of the overcut wall. Thrust needed to drive the TBM through the curve is reduced. Mini-Packer bags are inflated with quick setting, high strength grout to transfer the thrust force directly into the ground, without affecting the segmental lining. TBM attitude control is improved.

It was only some weeks after the tunnel had been completed, and the final data was analyzed by Osaka City office that a noticeable variation in settlement between the shield machine during a straight drive and a curved drive was discovered. During the straight drives there had been a measurable settlement in places of 3–5mm, and during the curved drives it was expected to be even more. However, the settlement during the curved drive had been reduced to zero. The only difference was the injection of Clay-Shock into the overcut during the curved drives. Based on that result, a new non-hardening process to limit settlement during tunneling had been discovered. This discovery was to become the foundation of a new branch of material research for TAC, which would guide the next 30 years of material development for the company.

### 2.2 *Clay Shock acceptance and uptake.*

Consensus for the application of Clay Shock in the Japanese tunnel market was not immediately forthcoming, even after quantifiable laboratory and field results had been presented. Clay Shock was utilized effectively for curved drives and as a subsidence reducing material at 5 different sites between 1983 and 1989 leading to the hypothesis that instead of being used exclusively to surround the machine, this new material could possibly be used as an additive for EPB shield machines.

In 1989, Maeda Construction Company was constructing a drainage tunnel in Kakogawa City, Hyogo Prefecture, Japan using a 2.28m EPB machine. The 1.37 km tunnel was to be driven through a mostly coarse gravel and cobble layer with very low silt and clay content, and what was predicted from boring data to be low water content. In reality, the machine's progress was hindered severely by high water content during the initial drive, so much so that tunnel operations were halted. TAC was contacted, and the research which had been undertaken into the properties of the new Clay Shock product started to yield results. Rigorous lab testing of various concentrations and combinations of A & B liquids had produced reliable data showing Clay Shock to be able to produce consistent results, shown in Table 1 and Figure 3. It had also been found that when Clay Shock when prepared to the ratio shown in Table 2, could support up to a 1kg weight on its surface (Figure 4)

Based on the research, the general contractor chose to apply Clay Shock as an additive. Due to the gelling properties of the mixture, it was decided to adopt a similar backfill grout two-component injection method via the tail skin for Clay Shock, using a mixing nozzle arrangement to thoroughly mix the A and B liquids. The forward-facing nozzles on the Shield machine were also repurposed and Clay Shock was injected around the side of the machine

Table 1. Clay Shock β and βII Viscosity Test Results.

| Clay Shock β | | | | | | | Clay Shock βII | | | | | | |
|---|---|---|---|---|---|---|---|---|---|---|---|---|---|
| A Liquid (1m$^3$ batch) | | | B Liquid % | | | | A Liquid (1m$^3$ batch) | | | B Liquid % | | | |
| Clay Sand | Water | Viscosity dPa·s | | | | | Clay Sand | Water | Viscosity dPa·s | | | | |
| | | 0% | 1% | 3% | 5% | 7% | | | 0% | 1% | 3% | 5% | 7% |
| 419kg | 839L | 0.4 | 45 | 150 | 170 | 100 | 308kg | 881L | 3 | 80 | 150 | 170 | 120 |
| 454kg | 826L | 0.6 | 55 | 250 | 300 | 200 | 347kg | 867L | 5 | 90 | 270 | 350 | 250 |
| 488kg | 813L | 0.8 | 70 | 300 | 400 | 300 | 384kg | 853L | 8 | 130 | 400 | 470 | 380 |
| 520kg | 800L | 1.0 | 100 | 400 | 500 | 400 | 419kg | 839L | 15 | 200 | 550 | 700 | 600 |
| 552kg | 788L | 1.5 | 150 | 500 | 750 | 650 | 454kg | 826L | 30 | 300 | 700 | 900 | 850 |
| 582kg | 777L | 10 | 250 | 800 | 1200 | 1050 | | | | | | | |

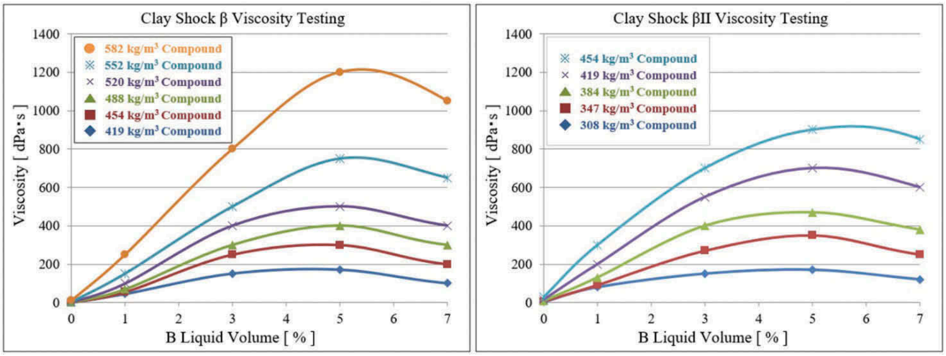


Figure 3. Graph of Clay Shock tests with concentrations and viscosities of various A:B liquid combinations.

Table 2. Mix design for 1m$^3$ of Clay Shock used for Kakogawa City drainage tunnel project.

| A Liquid | | B Liquid | Viscosity |
|---|---|---|---|
| Clay Sand | Water | Sodium Silicate | |
| 520kg | 800L | 50L | 500 dPa·s |

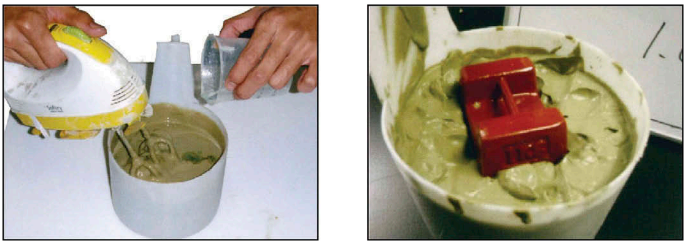

Figure 4. Mixing and testing of Clay Shock compound until viscous enough to support a 1kg weight on its surface.

through to the cutterhead. This facilitated the penetration of the chamber, and upon machine restart, the coarse gravel and cobble layer was transported through the machine (Figure 5). Clay Shock's secondary property of water resistance (Figure 6), also contributed to the success of this project. Owing to the flow of Clay Shock around the tail skin and through into the cutterhead, a percentage of the material ended up filling the cracks and crevices in the ground in front of the excavation face. Previously unachievable on the project, this flowability, combined with resistance to wash out and dilution with water, limited water ingress significantly, which enabled the stable extraction of spoil from the screw conveyor.

It had now been proved on site that Clay Shock was a versatile material solution, with many possible applications. In the 7 years between its development in 1983 and 1990, Clay Shock had been used at a total of 7 sites across Japan mainly as a friction reduction material but also as an additive. Between 1990 and 2000, widespread acceptance of Clay Shock as not just a product, but as a distinct tunneling method, had led to its use at 40 sites within a ten-year time-span. Furthermore, due in part to the official registration of Clay Shock Method with the Japanese Ministry of Land, Infrastructure, Transport and Tourism's New Technology Information System (KT-16002-A), the uptake of Clay Shock between 2000 to 2010 had risen to over 140 sites across Japan with applications as wide and varied as preventing water ingress during machine launch and breakthrough at arrival shaft; settlement control; ground stabilization when passing though fluvial sand layer; as an additive when mining in mixed ground; mining bedrock under high water pressure; to prevent leakage of slurry via fractures in bedrock; preventing collapse of the excavation face in unstable ground; to maintain pressure during cutter head interventions of shield machines; use in pipe jacking sites in fractured ground and Clay Shock had even been used onsite to course correct jammed TBMs in severe nose down scenarios.

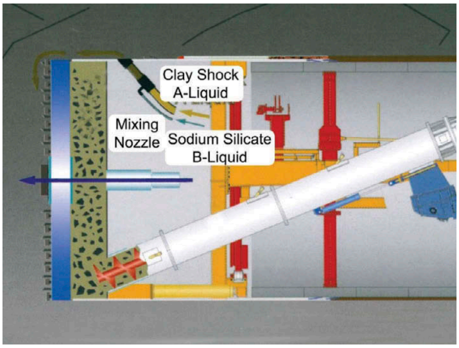


Figure 5. Injection of Clay Shock through the Tail Skin, to the front of the EPB machine.

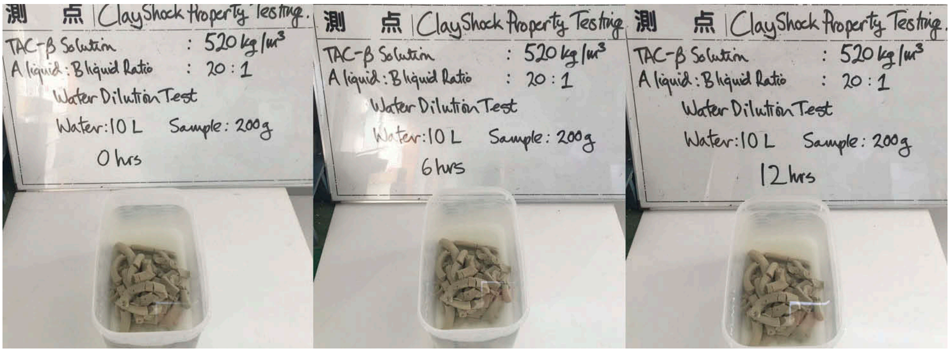


Figure 6. 0h, 6h and 12h dilution testing of Clay Shock.

## 3 RECENT APPLICATIONS

### 3.1 *Breaking new ground.*

In 2010 the Hanshin Highway Corporation began construction of a brand-new highway bisecting South Osaka connecting the two ends of the Osaka Loop Line Highway. Called the Yamatogawa Route, the new highway would stretch 9.7 km under one of the most densely populated cities in the world, below 11 separate over ground railway lines, and to within 2.2m beneath one of the busiest subway lines in Osaka, the famous Midosuji Line. This 6.8 m diameter tunnel holds the main Osaka Metro North-South line, travelling 24.5 km through the center of Osaka, and carries 1.2 million people daily. (Figure 7).

The two main contractors, Daitetsu JV and Obayashi JV, shared the task of excavating the eastbound and westbound Yamatogawa Route tunnels respectively, with the segments between the two tunnels having a minimum separation in places of only 1m. The tunnels would be excavated with a single IHI made (now JIM Technology Corporation), 12.54m EPB Shield machine, with TAC providing the Backfill Grout above ground batching plants and underground support machinery, Backfill Grout Injection Pipes, Additive and Foam generation equipment and control panels. The construction would also incorporate TAC's Clay Shock Method to ensure the perfect passing of the EPB Shield Machine under the Midosuji Line.

While passing beneath the Midosuji Line, the EPM would be driven twice, (once for the north tunnel, and once for the south tunnel), through a combination of Ds (Diluvial Sandy Soil) and Dc (Diluvial Clay Soil) layers, (Figure 8). The upper half of the cutterhead would pass though the diluvial sandy soil layer, which has a minimum Coefficient of Uniformity of 8.2, and a minimum fine grain content of 2.4%. Through experience of past tunnel construction in the area, it is known that this kind of soil is very prone to disintegration upon excavation. (Shima, Minamikawa, Nishiki, Nishimori & Miyake, 2015). This would be further compounded by the double passing of the TBM through the high-risk zone under the Midosuji subway tunnel, creating possibly high stresses close to the calculated limits of the segment structure itself.

### 3.2 *Understanding subsidence caused by TBMs and Shield Machines*

The key to the success of the Yamatogawa Tunnel was the accuracy of pressure management of the EPB and backing that up with subsidence prevention of the earth surrounding the shield machine. With the Shield Machine within 100m of the Midosuji underpass section, it was decided to test the actual settlement in the ground without using Clay Shock. A settlement meter was placed 2 m above the crown of the cutter head, and a normal drive was commenced,

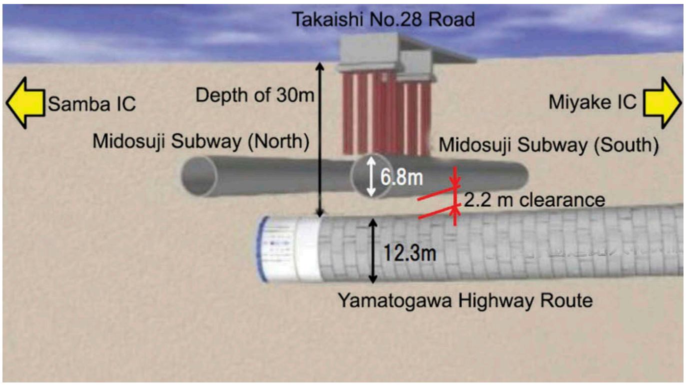


Figure 7. Yamatogawa Route Tunnel passing under the Midosuji Subway Line Tunnel.

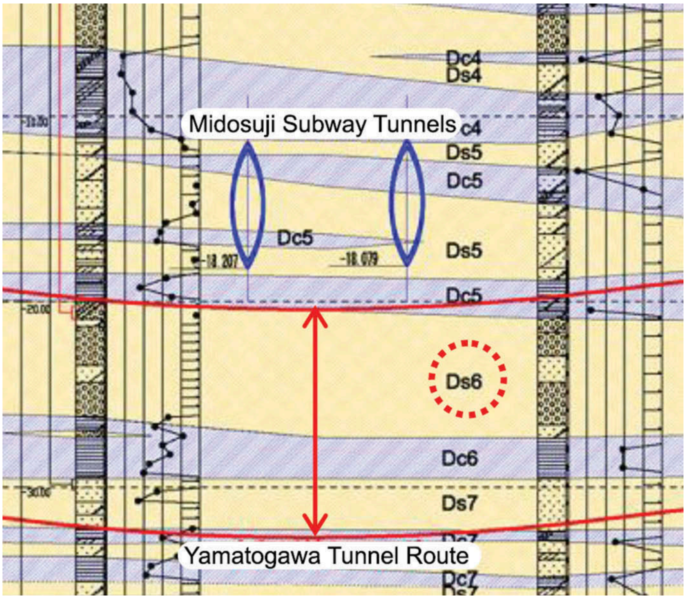


Figure 8. Longitudinal section of soil at the underpass point of the Yamatogawa and Midosuji tunnels clearly showing the multitude of Dc and Ds layers present at the site.

readings were then taken of the subsidence which occurred during the passing of the Shield machine, and continually until 1 day after the machine had passed. An initial measurement of 1.5 mm of subsidence was observed, increasing to 2.6 mm in 1 day. A secondary effect of the subsidence was an overall increase of thrust force of the shield machine during the drive to 144,000 kN, 70–80% of the maximum thrust of the machine (Shima et al., 2015). This field data influenced the general contractor to inject Clay Shock simultaneously via 8 injection ports on the machine during the drive under the Midosuji tunnel. (Figure 9).

The construction plan for the Yamatogawa Tunnel accounted for a maximum subsidence of -10.2 mm while passing under the Midosuji tunnels, but by injecting Clay Shock around the machine and managing the earth pressure correctly, the Yamatogawa Tunnel was driven under the Midosuji line with a final measurement, once the EPB Shield machine had driven

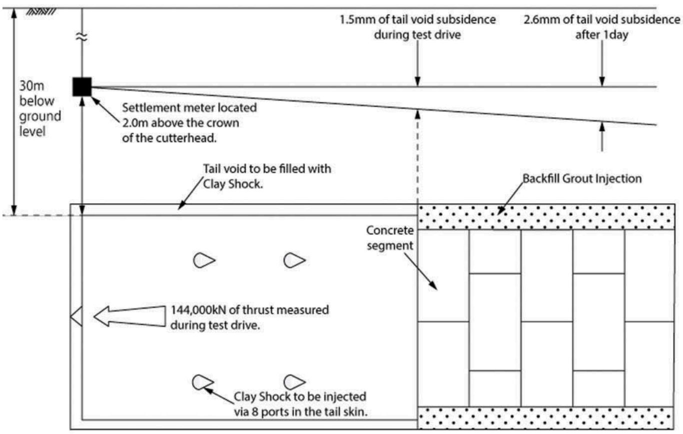


Figure 9. Measuring the actual settlement and thrust force without use of Clay Shock.

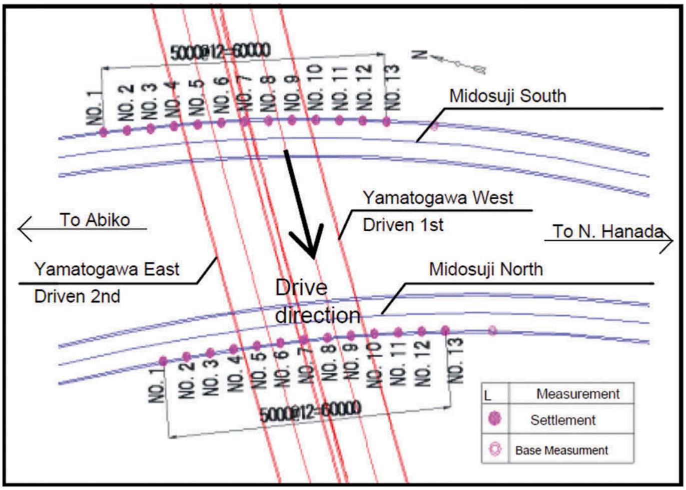


Figure 10. Settlement meter placement, for Yamatogawa Tunnel.

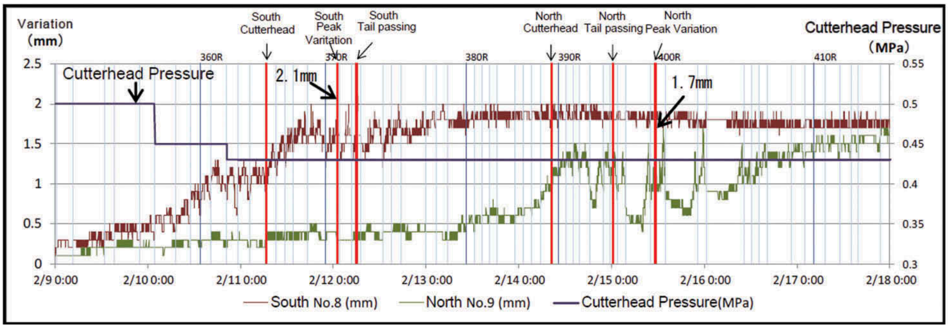


Figure 11. Settlement meter reading during drive under Midosuji Tunnel.

through and the segments were in place, that showed a maximum level increase of +2.1 mm for the North bound tunnel, and +1.7 mm for the South bound tunnel. (Shima et al., 2015) The increase had been due to the cutterhead pressure, and once the cutterhead had passed, the Clay Shock had held the ground in place until the void was subsequently filled with backfill grout as soon as the segment had left the rear body of the machine, (Figures 10–11). Undoubtedly, the application of Clay Shock had been a resounding success resulting in zero ground subsidence in the most sensitive part of this project.

### 3.3 *Use of Clay Shock for slurry pressure management with Slurry TBMs.*

Applications of Clay Shock didn't stop at EPB machines. Slurry Shields, inherently thought to be stable due to the flow of slurry around the machine, have been shown as they increase in diameter to have an inherent imbalances of slurry pressure the further away from the cutterface, and the further towards the crown of the machine pressure is modelled. The vertical gradient of pressure generated by slurry density as shown by (Van Eeklen, Van der Berg, Bakker, 1997), as well as the pressure of slurry in such a shield system (Ngoc-Anh, Dias, Oresta and Djeran-Maigre, 2013) indicates the need for a filler material, which can maintain pressure in larger diameter machines. The pressure differentials in Slurry shield machines make Clay Sand based, waterproofed fillers a viable solution to this reduce this differential, (Figure 12).

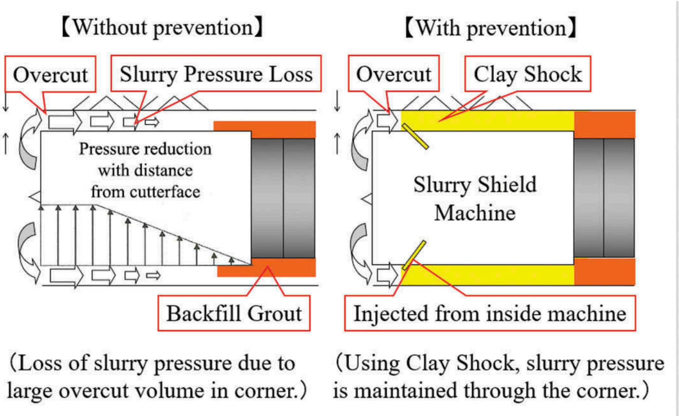


Figure 12. Use of Clay Shock to reduce pressure differential of Slurry Shield Machines.

Clay Shock use in Japan, in Slurry Shield for this purpose is well accepted, with Maeda Construction Corporation using such a system for a Kawasaki Heavy Industries made 10.30m Slurry Shield Machine used to excavate a 990m flood prevention tunnel for Tokyo Water Board in Tachiaigawa in 2008. This tunnel passed through three R=30m curves, two of which were S-curves. Slurry pressure loss through these sensitive turns was controlled by the injection of Clay Shock, which in turn limited subsidence in the middle of heavily populated area in downtown Tokyo. (Masuda, 2011)

## 4 FUTURE APPLICATIONS

### 4.1 *Hardening Clay Shock for pipe jacking.*

With a quarter of the 1400 or so construction sites in Japan and overseas where TAC has been active in the last 40 years having adopted the Clay Shock Method, there is a strong amount of data to back up the efficacy of the method and material itself. The real asset the material has been its ability to adapt into numerous situations and be effective in providing real solutions to real problems in tunneling. As with any product, it is the evolution of the product, and the search for the "next big thing" which drives progress. The next evolution for Clay Shock has been in producing hardening variants of what had become known as a non-hardening material.

Clay Shock has generally been associated with Shield machine applications, however pipe jacking, where frictional resistance should be low, but once the mining is complete the filler should solidify, is a very interesting future field to explore. Generally, this kind of construction has been completed using a two-step approach, using a low friction gel component, which is then replaced by a grout type component in a two-part process. With a hardening type of Clay Shock, it was thought that this process could be reduced to only one step. The following mix design was tested in the laboratory, see Table 3.

Table 3. Clay Shock Hard Mix Design and UCS and Viscosity test results.

| | A Liquid for $1m^3$ batch | | | | B Liquid | UCS Test $N/mm^2$ | | |
|---|---|---|---|---|---|---|---|---|
| Mix Design | Slag | Clay Sand | Retarder | Water | Sodium Silicate | σ28d | σ56d | σ91d |
| Mix 1 | 120kg | 350kg | 10kg | 814L | 25L | 0.30 | 0.60 | 1.20 |
| Mix 2 | 120kg | 350kg | 10kg | 814L | 50L | 0.14 | 0.25 | 0.30 |

## 5 CONCLUSIONS

This paper has attempted to show the progression over many years of one single product with in the tunneling industry in Japan, from inception to final acceptance and on into its future research and development by using real world examples to paint a picture of research and testing in Japan. The hope is this has deepened an interest in Japanese solution-based engineering, which can possibly lead to collaborative research in the future.

The Clay Shock Method was developed at a time when the economic bubble was just about to burst. When it did burst, it sent the burgeoning Japanese construction and civil engineering sector into free fall. On the back of this, many large general contractors were looking for more cost-effective ways to construct tunnels for less money, but without cutting back on safety and reliability, Clay Shock became a very viable alternative to other ground conditioning methods for reducing subsidence in tunneling, especially at sites where it would prove impractical to shut down roads, such as in the center of major cities. In particular, Clay Shock has been successfully applied to complex geology, hard rock and loose soil mixed layers, as well as diluvial clay and diluvial sand split-layer tunneling projects with great success in Japan and overseas. In Singapore, Clay Shock has been used for Land Transport Authority projects not only as a subsidence limiting material, but also as a face stabilization material for both EPB and Slurry shield machines, where stabilization of the face is essential in preventing subsidence during interventions. (Shirlaw, 2008)

The evolution of applications for the use of Clay Shock is based on the feedback of General Contractors, Project Directors, Engineers, Designers and City Officials who have supported this method and challenged TAC to develop more complex and innovative solutions for the problems which occur in tunneling. It is this kind of collaborative atmosphere which helps innovation thrive, not only in Japan but worldwide. Facing future on-site challenges head on, with a spirit of inquisitiveness and a passion for doing the seemingly impossible, is what will enable the further evolution of new materials within the field of tunnel engineering fueling the next generation of growth and success for us all.

## REFERENCES

Ngoc-Anh, D. Dias, D. Oreste, P. Dejeran-Maigre, I. 2013. *3D Modelling for Mechanized Tunneling in Soft Ground-Influence of the Constitutive Model*. American Journal of Applied Sciences. 10 (8): pp.863–875

Masuda, M. 2011. *Sewage Tunnel Construction with a Large Diameter (φ 10.3 m) Shield Machine and Sharp Curve Excavation*. Maeda Construction Company presentation at 55$^{th}$ NPR, Shield & Tunnel Construction Technique Workshop, 2011. (in Japanese)

Shima, T. Minamikawa, S. Nishiki, O. Nishimori, F. Miyake, S. 2015. *Excavation Management of a Large Diameter (φ 12.5 m) Shield Tunnel, Constructed with a Minimum Separation of 2.2m Beneath a Subway Tunnel Structure*. Osaka City Transportation Bureau, Japan Civil Engineering Society, National Conference, 2015. (in Japanese)

Shirlaw, N. 2008. *Mixed Face Conditions and the Risk of Loss of Face in Singapore*. ICDE, Singapore, 2008.

Van Eekelen, S. Van de Berg, P. Bakker, K.J.C. 1997. *3D Analysis of Soft Tunneling. Proceedings of the fourteenth international conference on solid mechanics and foundation engineering*., Hamburg, 1997.

*Tunnels and Underground Cities: Engineering and Innovation meet Archaeology, Architecture and Art, Volume 5: Innovation in underground engineering, materials and equipment - Part 1 – Peila, Viggiani & Celestino (Eds)*
*© 2020 Taylor & Francis Group, London, ISBN 978-0-367-46870-5*

# Durability of precast concrete tunnel segments

M. Bakhshi & V. Nasri
*AECOM, New York, USA*

ABSTRACT: In one-pass lining systems, the durability of tunnel structure is directly related to durability of concrete segments acting as both the initial support and the tunnel final lining. In this paper, most-frequent degradation mechanisms of concrete linings are discussed including chloride- and carbonation- induced corrosions, sulfate, acid and freeze-and-thaw attacks, and alkali-aggregate reactions. Mitigation method for each specific degradation mechanism is explained. A durability factor specific to railway and subway tunnel known as stray current corrosion is presented. Mitigation methods for this specific corrosion together with coupling effects with other conventional damage mechanisms are explained. Prescriptive approaches for durability design based on major codes and standards are explained and comparison is made between these methods. Exposure classes as the main inputs to the prescriptive approaches are elaborated and requirements specified by the codes and standards are presented and analyzed. The need to move on from prescriptive approach and embrace performance-based approaches for durability design of tunnel segmental lining is demonstrated and future studies are discussed.

## 1 INTRODUCTION

Tunnels as important underground structures are typically designed for a service life of more than 100 years. Mechanized tunneling method with Tunnel Boring Machines (TBMs), as the most common excavation method, is often associated with continuous installation of one-pass precast concrete segments in the form of rings behind TBM cutterhead. In these tunnels, durability of tunnel is directly related to durability of concrete segments acting as both the initial support and the tunnel final lining. In this paper, most-frequent degradation mechanisms of concrete linings are briefly discussed. This includes corrosion of reinforcement by chloride attack and carbonation, as well as sulfate, and acid attacks as major deterioration processes caused by external agents. Alkali-aggregate reactions caused by internal chemical reactions and frost attack and freeze-and-thaw damages are also explained. Stray current-induced corrosion as one major durability concern specific to railway and subway tunnel linings is discussed. Mitigation methods for different durability factor are discussed. Stray current corrosion mitigation method including use of FRC segments are presented and durability of segments under coupling effects of stray current with other conventional degradation factors are explained. Prescriptive approach for durability design based on European standard (EN 206-1:2013, Eurocode EN 1992-1-1:2004) and American Code ACI 318 (2014) is explained and comparison is made between two methods. Exposure classes related to environmental actions as the main inputs to both prescriptive approaches are explained separately. Conforming to these two major standards, recommendations made on concrete to ensure typical service life of tunnels are explained including concrete strength, maximum water-to-cement (w/c) ratio, minimum cement content and minimum air content.

## 2 DEGRADATION MECHANISMS IN TUNNEL LININGS

Possible degradation and damage mechanisms in bored tunnels include corrosion of reinforcement by chloride attack and carbonation, sulfate and acid attacks, alkali-aggregate reactions, freeze-and-thaw damages as well as stray current corrosion.

## 2.1 *Chloride-induced reinforcement corrosion*

Chloride-induced corrosion of reinforcement is the main cause of degradation in tunnels lined with reinforced concrete. Table 1 presents thirteen major tunnels that are significantly damaged and corroded due to chloride ingress before the year 1991 (ITA 1991; Abbas 2014). Chloride-induced corrosion is even a greater durability issue specifically in sub-sea, sea outfall, and road/rail tunnels. In sub-sea and outfall tunnels, and tunnels exposed to brackish groundwater, the intrusion of chloride ions present in sweater and salt water into reinforced concrete can cause steel corrosion. In cold region road/rail tunnels, major durability issue is the ingress of chloride ions present in deicing salts sprayed from vehicles during the snow fall. Chloride induced corrosion due to water infiltration initiates from the lining extrados, while corrosion due to de-icing salts sprayed from vehicle tires starts from lining intrados. Rust as the reaction product has a greater volume than the steel and cause expansion resulting in excessive tensile stresses, cracking, delamination, and spalling in the concrete (Figure 1).

## 2.2 *Carbonation -induced reinforcement corrosion*

Carbonation-induced corrosion in general is considered as a minor durability issue in reinforced concrete structures compared to chloride-induced corrosion. This is mainly due to limited impact area of carbonation and reduced strength zone limited to the extreme outer layer. In bored tunnels, carbonation is unlikely to occur due to the fact that generally extrados of tunnel lining is limited impact area of carbonation and reduced strength zone limited to the extreme outer layer. It is well-known that high rates of carbonation occur when the relative humidity is maintained between 50% and 75% (PCA 2002). In a lower relative humidity, the degree of carbonation is insignificant and above this range, moisture in concrete pores restricts penetration of $CO_2$ (ACI 201.2R 2016). In tunnels, only portal areas and entrance zones can maintain a relative humidity in the aforementioned range as lining in such areas is exposed to cyclic wet

Table 1. Damaged/Corroded tunnels due to chloride ingress (ITA 1991; Abbas 2014).

| Tunnels | Location | Tunnel type | Diameter | Completion year |
|---|---|---|---|---|
| Basel/Olten Hauenstein | Switzerland | Railway | - | 1916 |
| Northern Line Old Street to Moorgate | U.K. | Metro | 3.5 m | 1924 |
| Shimonoseki/Moji Kanmon | Japan | Railway | - | 1944 |
| Mikuni National Route 17 | Japan | Highway | 7.6 m | 1959 |
| Uebonmachi-Nipponbashi | Japan | Railway | 10 m | 1970 |
| Dubai | U.A.E | Roadway | 3.6 m | 1975 |
| Tokyo Underground | Japan | Roadway | - | 1976 |
| Berlin Tunnel Airport | Germany | Roadway | - | 1978 |
| Second Dartford | U.K. | Roadway | 9.6 m | 1980 |
| Mass Transit Railway | Hong Kong | Metro | 5.6 m | 1980 |
| Ahmed Hamdi | Egypt | Roadway | 10.4 m | 1980 |
| Stockholm Underground | Sweden | Metro | - | 1988 |

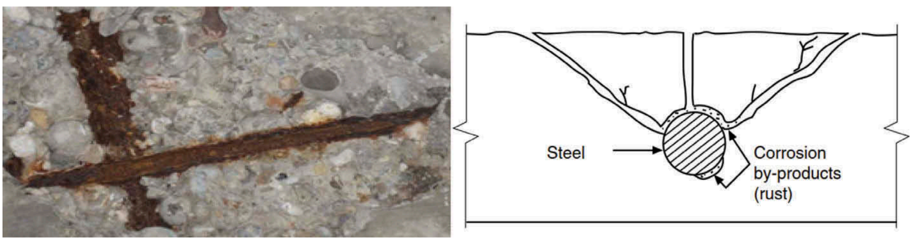


Figure 1. Loss of reinforcement section and cracks caused by chloride-induced steel corrosion (PCA, 2002; Romer, 2013).

and dry conditions. Also high rate of carbonation requires elevated atmospheric carbon dioxide ($CO_2$) levels which is only a case in heavily trafficked road runnels because of $CO_2$ emission from car exhaust. Therefore, carbonation is a major durability factor in portal areas and entrance zones of heavily trafficked road runnels. Carbonation can also occur in tunnel linings exposed to bicarbonate ($HCO_3$) ground water which often formed by the reaction of carbon dioxide with water and carbonate bedrocks such as limestone and dolomite.

Chloride- and carbonation-induced corrosion can be mitigated using low w/c ratio, high compressive strength and high cement content. This in conjunction with considering a sufficient concrete cover over reinforcement provide with a high quality and dense concrete that can delay the initiation time of corrosion also known as propagation time beyond the service life of structure. Other effective mitigation methods that are not in the codes include using cements with high amount of $C_3A$, and addition of corrosion inhibitors to the concrete mix.

### 2.3 *Sulfate attack*

Sulfate attack is a major durability issue for concrete structures in contact with soil or water containing deleterious amounts of water-soluble sulfate ions. Tunnels as underground structures, regardless of their specific use, can be exposed to external sulfate attack from common sources such as sulfates of sodium, potassium, calcium, or magnesium found in in the surrounding ground or dissolved in natural ground water. Ancient sedimentary clays and the weathered zone (< 10m) of other geological strata, as well as contaminated grounds and groundwater generally contain significant sulfate concentrations (BTS 2004). In tunnel linings exposed to such conditions, sulfate attack is a major concrete degradation mechanism. In tunnels, usually ettringite and gypsum can be produced as a result of a sulfate attack which in turn results in expansion of cement (e.g. ettringite volume is ~2.2 times higher in volume than the reactants). As a result concrete cracks and loses strength. It is expected that damages in tunnel linings due to sulfate attack start on segment extrados and at the interface between lining and the ground where sulfate from ground or groundwater can penetrate the concrete.

Sulfate attack can be mitigated by using cements with low amount of $C_3A$ (<8%), use of high content of active mineral components, low w/c ratio and use of blended cements with pozzolans. Codes and standards recommendations to mitigate sulfate attack are based on using a concrete with low w/c ratio, high compressive strength and high cement content. In addition codes require use of sulfate-resisting cements such as type II portland cement (ASTM C150 2017) or in severe cases type V (ASTM C150 2017) plus pozzolan or slag cement.

### 2.4 *Acid attack*

Acid attack is a chemical attack that can be a major durability issue when concrete structure is exposed to high concentrations of aggressive acids with high degrees of dissociation. The deterioration of concrete by acids is primarily the result of decomposition of the hydration products of the cementitious paste (ACI 201.2R 2016). Sulfuric and hydrochloric nitric acids are main inorganic (mineral) acids, and acetic, formic and lactic acid are main organic acids with rapid rate of attack on concrete at ambient temperature. Acids reduce the pH or alkalinity of the concrete, and once the pH reduces to less than 5.5 to 4.5, severe damages are imminent as cement hydration products such as Portlandite (CH, $Ca(OH)_2$) and C-S-H starts to decompose when pH drops to around 12 and 10, respectively (ACI 201.2R 2016). This is the main reason that no concrete materials have a good resistance to acids.

In tunnels, the rapid deterioration of concrete only normally occurs when concrete is subject to the action of highly mobile acidic water (BTS 2004). With external acidic groundwater this is rarely the case, since ground waters are not usually highly mobile. Regarding internal sources for acid attack, flow of acid-containing runoff from outside the tunnel is not a major concern. However, sulfuric acid solutions result from decay of organic matter by bacterial action in sewage and wastewater tunnels is the primary mechanism of degradation in these tunnels. This is due high attack rate of sulfuric acid and continuous movement of the acidic materials inside the tunnel as gravitational flow of sewage in these tunnels is always guaranteed. Sewage is not aggressive to concrete buy itself but hydrogen sulfide produced by anaerobic bacteria reaction with the sludge is subsequently oxidized by aerobic bacteria to form sulfuric acid. In addition to decomposition of the cement hydration products, sulfuric acid is particularly aggressive to concrete because the calcium sulfate formed from the acid reaction may drive sulfate attack of adjacent concrete that was unaffected by the initial acid attack (ACI 201.2R 2016; PCA 2002).

Acid attacks can be mitigated with providing a dense and high quality concrete by lowering w/c ratio and increasing compressive strength and cement content. Codes and standards provide specific limits to achieve very high density and relatively impermeable concrete to reduce the damage due to acid attack. Type of cement has an insignificant role on mitigation of acid attacks. When concrete is exposed to very server acid attacks, a surface protection method such as coatings, waterproofing membranes or a sacrificial layer should be considered.

### 2.5 *Alkali-Aggregate Reaction (AAR)*

AAR as a chemical attack can be a major durability concern when concrete aggregates contain materials that can be reactive with alkali hydroxides in cement phase. The AAR generates expansive products and may result in damaging deformation and cracking of concrete over a period of years. AAR has two main forms of alkali-silica reaction (ASR) and alkali-carbonate reaction (ACR). ASR is often major concern compared to ACR as aggregates containing reactive silica are more common (PCA 2002) whereas aggregates susceptible to ACR are less common and usually unsuitable for use in concrete. Reactive forms of silica can be found in aggregates such as chert, volcanic glass, quartzite, opal, chalcedony, and strained quartz crystals. Damage to concrete only normally occurs when concrete alkali content is high, aggregate contains an alkali-reactive constituent, and concrete is under wet conditions (BTS 2004). ASR reactions can be summarized as:

Alkalis + Reactive Silica → Gel Reaction Product
Gel Reaction Product + Moisture → Expansion

PCA (2002) reports the internal relative humidity of 80% as a threshold, below which the alkali-silica reactivity can be virtually stopped. AAR does not depend on the specific use of each tunnel. Sub-sea tunnels may be more susceptible due to exposure to warm seawater containing dissolved alkalis which may aggravate alkali-silica reactivity. AAR can be mitigated by using inert aggregate, controlling the amount of soluble alkalis in concrete, and using blended cements with pozzolans.

### 2.6 *Frost attack and freeze-and-thaw damages*

Frost attack and freeze-and-thaw damages are durability concerns in concrete structures built in cold regions. Water expands by about 9% when it freezes and as a result, the moisture in concrete capillary pores exerts pressure on the concrete solid skeleton. This leads to development of excessive tensile stresses in the concrete and rupture of cavities. Successive cycles of freeze-thaw can disrupt paste and aggregate and eventually cause significant expansion and cracking, scaling, and crumbling of the concrete (PCA 2002). Frost damage is considerably accelerated by deicing salts (ACI 201.2R 2016).

Surface scaling is the only frost damage that can possibly occur in precast tunnel segments. Since the increase in volume when water turns to ice is about 9%, more than 90% of capillary pores volume must be filled with water in order for internal stresses to be induced by ice formation (BTS 2004). Moisture content near saturation level is usually the case for tunnel linings as often times tunnels are built under the water table and concrete lining can be near saturation level. However, along most of tunnel alignment, the temperature rarely falls under the freezing point because tunnel is embedded in the ground. Tunnel entrances, portals and shafts are parts of tunnel system that should be designed for exposure to cycles of freezing and thawing because of saturation level and exposure to freezing temperature.

Freeze–thaw attacks are mitigated by controlling w/c ratio, compressive strength and cement content. Controlling air content in the mix to a minimum 4% using air-entraining admixtures is the most effective mitigation method. Codes and standards often provide limits for maximum w/c ratio and minimum compressive strength, or require frost-resistant aggregates (EN 206-1 2013).

## 2.7 *Stray current corrosion*

Stray current corrosion is a type of corrosion specific to rail tunnels where corrosion is caused by traction current resulting in accelerated oxidation of metals and rapid migration of the chloride ions (ITA 1991). Inspection of removed segments from tunnels with high conductivity between running rails and lining reinforcement such as Bucharest Metro has shown an extensive corrosion of the outer reinforcement layer (Buhr et al. 1999).

Government agencies around the world are promoting electric trains and all modern railway systems take advantages of railway electrification. Power transmission is provided by overhead catenary wire or a conductor rail also known as third rail. The running rail connected to nearby substations is often used as traction loop through which the return circuit is made. The running rail has a limited conductivity, and insulation between the rail and the ground is sometimes reduced or constructed poorly form the beginning. This causes a fraction of the traction current to leave the rail, leak into the ground and flow back along the running rail on the return path to the traction substation by the earth diversion, which is referred to as stray current. Figure 2(a) shows a simplified electronic circuit of the electric railway system for modeling the stray current. In this figure, $I_T$, $I_R$ and $I_s$ represent the train (overhead catenary system) current, stray current and the current flowing through the running rail, respectively. $R_R$ is the running rail resistance, $R_s$ is the ground resistance at the traction substation, and $R_T$ is the ground resistance as seen at the train. It's evident that reduced $R_T$ or $R_s$ results in increased stray current. When train runs in a lined tunnel, stray current leaks to the tunnel lining and through the concrete reinforcement. This is shown schematically in Figure 2(b) with a cathode formed at reinforcement where stray current enters the rebar and an anode is formed where stray current leaves the rebar and flows back to substation. Figure 2(c) shows that in cathode, rebar is disengaged from the concrete due to trapped hydrogen isostatic pressure, and in the anode, the rebar is oxidized in contact with electrolytic material, i.e. concrete, and accumulation of corrosion products exerts excessive pressure leading to cracking (Wang et al. 2018). This type of corrosion is not limited to rebar in concrete lining but also metal utilities and steel pipelines embedded in the ground in the proximity of tracks.

General mitigation methods for this type of corrosion are based on reducing the amount of stray current by decreasing rail resistance, improving rail to ground insulation using isolated rail

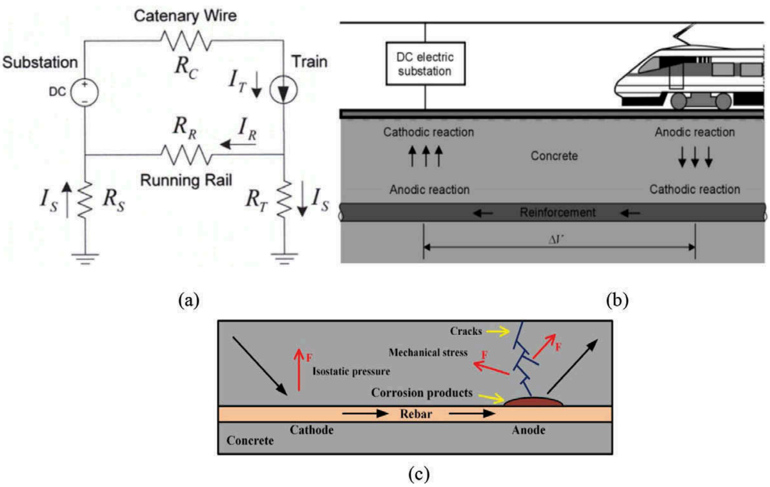


Figure 2. a) Modeling stray current leakage with simplified electronic circuit (Niasati & Gholami 2008); b) Schematics of stray current from a train overhead catenary system picked up by reinforcement in concrete (Bertolini et al. 2007), c) corrosive effect of stray current (Wang et al. 2018).

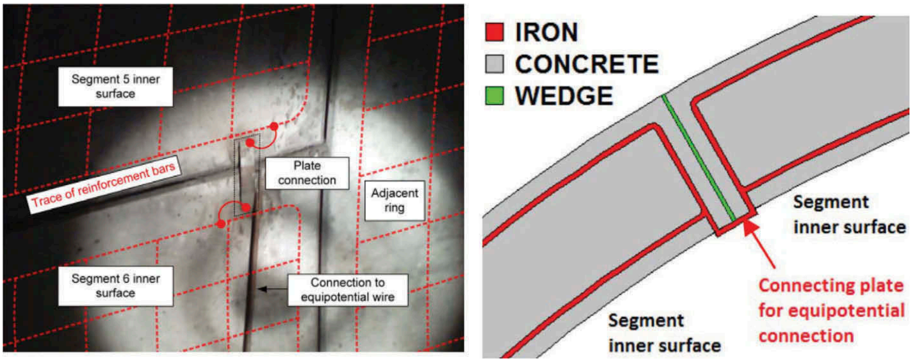


Figure 3. Stray current mitigation using equipotential connection provided by copper plates/straps connecting reinforcement cages of segments by Dolara et al. (2012).

fastening systems or pads, keeping the substation as close to the point of maximum current as possible, developing monitoring systems, devices and measurement apparatus (Brenna et al. 2010).As shown in Figure 3, stray current corrosion can be also mitigated using equipotential connection provided by copper plates/straps connecting reinforcement cages of segments. The equipotential connections between the reinforcing bars of all segments in a ring constitute a path with extremely low electrical resistance that allows the current to flow from a segment to the adjacent one without passing into the ground. The equipotential connection reduces bar-to-ground voltage to values well below the standard limits (EN 50122-2 2010) for corrosion initiation, and provides an effective method to prevent stray current corrosion in segments.

Another mitigation method for stray current induced corrosion is use of fiber-reinforced concrete (FRC) segments (Tang 2017). Results of studies on stray current corrosion of FRC show that steel bars are more likely to pick up current than short steel fibres under same conditions (Edvardsen et al. 2017). This can be due to the fact that the chloride threshold for the corrosion of steel bars in concrete is between 0.15–0.6% by mass of cement (ACI 318 2014). However, steel fiber-reinforced concrete demonstrates a higher corrosion resistance compared to steel bar reinforced with a chloride threshold level for corrosion at 4% by mass of cement (Tang 2017). The discontinuous and discrete nature of steel fibres or the length-effect is the main factor to be accounted for this higher corrosion resistance as fibers rarely touch each other and there is no continuous conductive path for stray currents through the concrete (ACI 544.1R-96 2009).

## 3 DURABILITY UNDER COUPLED DURABILITY FACTORS

Precast concrete tunnel segments may be subjected to the coupling effects of degradation factors such as carbonation, sulfate and chloride-induce corrosion of steel bars by groundwater and surrounding ground. For subway tunnel, stray current is another major factor that accelerates the steel corrosion. A summary of these different major degradation mechanisms together with their mitigation methods are shown in Table 2. A literature review on experiments conducted on coupled effect of stray current and other degradation factors reveals that the majority of previous works (Xiong 2008) has been focused on the material scale level which cannot truly reflect the durability aspects of full-size concrete members (Zhu & Zou, 2012; Geng and Ding, 2010). Coupling effects of multi factors on durability of segments in large-scale were studied by Li et al. (2014). These factors include carbonation, sulfate, chloride ion penetration and stray current corrosion. Study was conducted on segments made of concrete with water–cement ratio of 0.28–0.33, compressive strength of 60–70 MPa, and steel bars of 6.5mm diameter with yield and ultimate strengths of 472 and 586 MPa. Extrados side of segments was immersed in solutions of 3.5% NaCl for simulation of exposure to chloride ions, and 3.5% NaCl + 5% $Na_2SO_4$ for simulation of exposure to both chloride and sulfate ions. Segment intrados was exposed to a carbonation setup simulating $CO_2$ environment with concentration of 20%, temperature of 20°±5, and relative

Table 2. Summary of major durability factors for tunnel linings, their sources and mitigation methods.

| Degradation mechanism | Type of tunnels susceptible to this factor | Main sources of degradation | Specific location of tunnel prone to this factor | Mitigation method |
|---|---|---|---|---|
| Chloride-induced corrosion | - Sub-sea tunnels<br>- Sea outfall tunnels<br>- Transportation tunnels in cold region | - Sea/salt water<br>- Sea/salt water<br>- Deicing salts sprayed from vehicle tires | - Lining extrados | Delay corrosion initiation by:<br>- Sufficient cover over rebar<br>- Dense/high quality concrete:<br>. Low w/c ratio<br>. High compressive strength<br>. High cement content<br>- Cement w/high $C_3A$ content<br>- Use of corrosion inhibitors |
| Carbonate-induced corrosion | - Heavily-trafficked roadway tunnels | $CO_2$ emission from car exhaust | - Lining intrados near portals, entrance zones, shafts | Delay corrosion initiation by:<br>- Sufficient cover over rebar<br>- Dense/high quality concrete:<br>. Low w/c ratio<br>. High compressive strength<br>. High cement content<br>- Sufficient cover over rebar<br>- Cement w/high $C_3A$ content<br>- Use of corrosion inhibitors |
| | - All types of tunnels embedded in carbonate bedrock such as limestone or dolomite | Bicarbonate (HCO3) groundwater formed by reaction of water & carbonate bedrock | - Lining extrados | |
| External sulfate attack | - All types of tunnels embedded in ancient sedimentary clays or<br>- All types of shallow tunnels exposed to weathered zone (<10 m) of other geological strata<br>- All types of tunnels exposed to sulfate contamination | Formation of ettringite due to sulfate reacting with calcium aluminates or $Ca(OH)_2$ | - Lining extrados | - Dense/high quality concrete:<br>. Low w/c ratio<br>. High compressive strength<br>. High cement content<br>- Cement w/low $C_3A$ (<8%)<br>- Pozzolans/Blended cement |
| Internal acid attack | - Sewage/Wastewater tunnels | Formation of H2S and oxidization to sulfuric acid | - Lining intrados | - Dense/high quality concrete<br>- Coatings<br>- Sacrificial layers<br>- Use calcareous aggregates |
| Alkali aggregate reaction (AAR) | - All types of tunnels built with reactive silica aggregate | Volcanic glass<br>Opal/chalcedony<br>Deformed quartz | No specific location | - Use inert aggregate<br>- Control amount of soluble alkalis in concrete<br>- Pozzolans/Blended cement |
| | - Sub-sea tunnels | warm seawater containing dissolved alkalis | - Lining extrados | |
| Frost attack/ Freeze-thawing | - All types of tunnels in cold region | Surface scaling due to increase in volume when water turn to ice near saturation | - Lining intrados near portals, entrance zones, shafts | - Dense/high quality concrete:<br>. Low w/c ratio<br>. High compressive strength<br>. High cement content<br>- Air-entraining admixtures |
| Stray current corrosion | - Subway tunnels<br>- Railway tunnels | OCS current leaking into lining when returning from running rail | - Near rebar | Reduce amount of current:<br>- Decrease rail resistance<br>- Improve rail/ground insulation<br>- Substation close to max current<br>Use of straps connecting bars<br>Use fiber reinforcement |

humidity of 70%±5%. Figure 4a shows the dimension of segments and arrangement of reinforcement. Figure 4b shows schematics of the test setup demonstrating series connections between 6 segment samples in a group to ensure equal current flow of 1A among all segments. Segment reinforcement as anode and stainless steel tube placed in corrosion pools as cathode were connected to DC power supply to simulate the stray current. After casting and standard curing, samples were immersed in corrosion solution for 18 days and were exposed to carbonation setup for 28 days. Free chloride ion was determined from powders collected using drilling at 5mm intervals along the segment thickness. Results show that stray current accelerates the migration of chloride ions. Stray current corrosion also changes the penetration distribution of chloride ion in the section resulting in the largest concentration of chloride ions to be at the reinforcement level instead of the exposure surface which is the case for general chloride ion exposure without stray current. Also chloride ion concentration is higher for segments immersed in chloride solutions ($Cl^-$) than the ones immersed in solution with both chloride and sulfate ($Cl^- + SO_4^{2-}$). This can be due to the concrete pores that may be filled by ettringite produced by reaction of $SO_4^{2-}$ ions in the solution with hydration products, resulting in obstruction of channels through which chloride ions migrate. Another argument is that $SO_4^{2-}$ ions firstly react with $C_3A$ producing ettringite while decreasing the opportunity of integration of $Cl^-$ ion and $C_3A$. As a result it is more likely to be absorbed by C-S-H, altering the combination form of $Cl^-$ ions (Li et al. 2014). Another major outcome is that carbonation depth is only 1–4 mm, leading to a conclusion that carbonation is not a controlling durability factor for concrete segments compared with the chloride and sulfate ions and stray current corrosion. A typical corroded steel cage under coupled durability factors using this setup is shown in Figure 4d. Another major conclusion specific to reinforcement is the more significant corrosion of the reinforcement layer near the extrados compared to intrados, and more corrosion damage on stirrups than main transverse reinforcing bars. Considering results of this study, one can conclude that coupling factors of chloride ion penetration and stray current has the most detrimental effect on the durability of concrete tunnel segments.

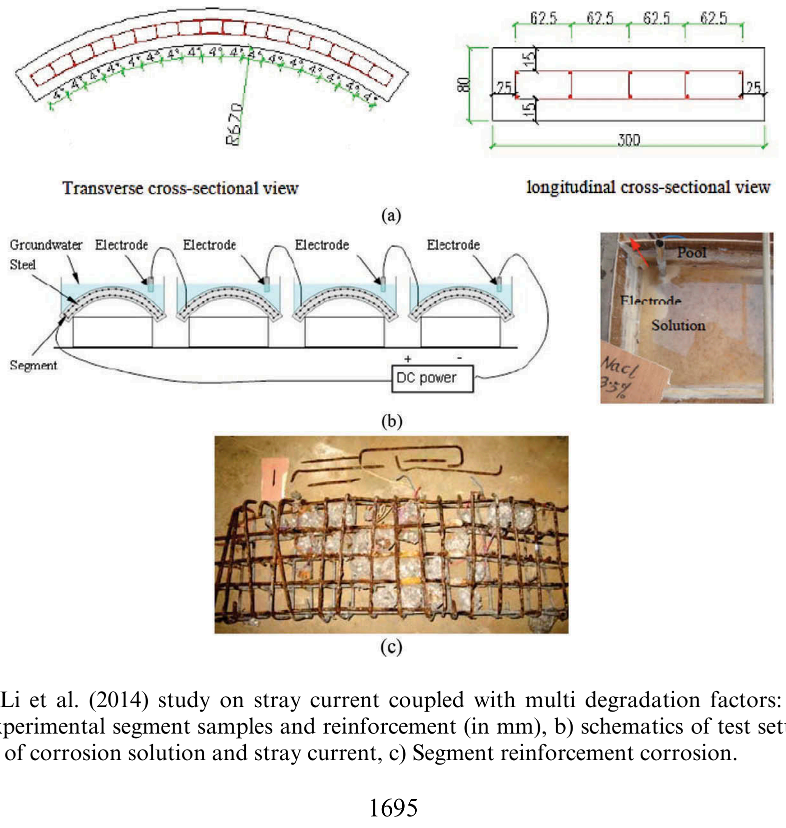


Figure 4. Li et al. (2014) study on stray current coupled with multi degradation factors: a) size and layout of experimental segment samples and reinforcement (in mm), b) schematics of test setup for combined effect of corrosion solution and stray current, c) Segment reinforcement corrosion.

## 4 PRESCRIPTIVE-BASED APPROACHES

Durability design according to prescriptive approaches is the most-common method in tunnel and concrete industries that are performed in accordance with major national and international structural codes (EN 206-1 2013; EN 1992-1-1 2004, ACI 318 2014). Inputs to these methods are environmental exposure classes and outputs to these methods are required concrete characteristics such as concrete strength and maximum w/c ratio. Following Euro standards (EN 1992-1-1 2004), for specific case of tunnel linings, suggested exposure classes according to Helsing and Mueller (2013) for $CO_2$ carbonation are XC3 to XC4, for seawater chloride-induced corrosion is XS2 to XS3, for deicing salt chloride-induced corrosion is XD2 to XD3, for frost exposure is XF3 to XF4 and for harmful ions other than chloride ($Mg^{2+}$, $SO_4^{2-}$) is XA1 to XA3. This is mainly due to the fact that this standard includes assumption of design service life of 50 years, and exposure classes should be increased by 2 in order to consider 100 years as minimum tunnel service life. Exposure category C2 in ACI 318 (2014) can be compared to above-mentioned XC, XD/XS exposure classes in EN 206-1 (2013) and EN 1992-1-1 (2004), and categories F2 and F3 with XF3 and XF4. Similarly, considering sulfate attack, ACI 318 (2014) exposure categories S1 to S3 can be compared with EN categories XA1 to XA3. A case example for an extreme exposure to chloride-induced corrosion (ACI category C2 vs. EN class XS3/XD3) shows that ACI would require a maximum w/c ratio of 0.4 and a minimum compressive strength of 35 MPa. On the other hand, EN would require a maximum w/c ratio of 0.45, a minimum compressive strength of 35 MPa, and a minimum cement content of 340 kg/m$^3$. Concrete cover specified by ACI 318 (2014) as minimum 38 mm (1.5 in) for reinforcement size of No. 19 or smaller (<imperial #6) can be compared with 45 mm required by EN 1992-1-1 (2004). This indicates that concrete requirements set forth for concrete by either ACI or EN would be very similar and most likely would result in a concrete specification with similar if not identical quality.

The major flaw of prescriptive apaches is lack of connection between the limiting requirements and main source of degradation mechanisms for each specific type of concrete damage. In contrast, performance-based design approaches despite all challenges related to these methods provides significant benefits to designers by focusing on the specific sources of concrete damages in a project-specific fashion (Swiss Standard SIA 262 2003). In order to achieve a performance design, rapid, easy, and reliable test methods are needed to assess properties of structural concrete. Future studies are needed to develop a performance-based design approach with reference to different major tunnel segment projects. While this design approach is not discussed in this paper, studies such as Rashidi & Nasri (2012), Sigl et al. (2000) and Li et al. (2015) provide important new insight into such design method for wastewater, subway and sub-sea road tunnels, respectively. In addition, durability recommendations of national and international tunnel segment guidelines should be analyzed and compared in future studies.

## 5 CONCLUSION

Degradation mechanisms of concrete linings include chloride- and carbonation- induced corrosion, sulfate and acid attacks, alkali-aggregate reactions, and frost attack. All these mechanisms are introduced and mitigation methods are explained. Stray current-induced corrosion as one major durability concern specific to railway and subway tunnel linings is discussed. Mitigation methods for stray current corrosion including use of FRC segments are discussed and durability of segments under coupling multi-factors is explained. Coupled factors of chloride ion penetration and stray current are presented as the most detrimental for service life of tunnel precast segments. Prescriptive approaches for durability design based on major codes and standards are presented and compared. The need for developing a performance-based design approach for tunnel linings is explained. Future studies should include also comparison of current durability recommendations by national and international tunnel guidelines.

## REFERENCES


Abbas, S. 2014. Structural and durability performance of precast segmental tunnel linings. PhD Dissertation, The University of Western Ontario, London, Ontario, Canada.

ACI 201.2R. 2016. Guide to durable concrete. American Concrete Institute.

ACI 318. 2014. Building code requirements for structural concrete and commentary. American Concrete Institute.

ACI 544.1R. 2009. Report on fiber reinforced concrete (Reapproved 2009). American Concrete Institute.

ASTM C150/C150M-17. 2017. Standard Specification for Portland Cement, ASTM International, West Conshohocken, PA, 2017, www.astm.org.

Bertolini, L. & Carsana, M. & Pedeferri, P. 2007. Corrosion behaviour of steel in concrete in the presence of stray current. Corrosion Science, 49(3):1056–1068.

Brenna, M. & Dolara, A. & Leva, S. & Zaninelli, D. 2010. Effects of the DC stray currents on subway tunnel structures evaluated by FEM analysis. Power and Energy Society General Meeting: IEEE:1–7.

BTS. 2004. Tunnel lining. Design guide. British Tunnelling Society (BTS).

Buhr, B. & Nielsen, P. V. & Bajernaru, F. & McLeish, A. 1999. Bucharest metro: dealing with stray current corrosion. Proceedings of the Tunnel Construction and Piling Conference, 99.

Dolara, A. & Foiadelli, F. & Leva, S. 2012. Stray current effects mitigation in subway tunnels. IEEE Transactions on Power Delivery, 27(4):2304–2311.

Edvardson, C. & Müller, S. & Nell, W. & Eberli, M. 2017. Steel fibre reinforced concrete for tunnel lining segments – design, durability aspects and case studies on contemporary projects. Proceedings of STUVA Conference 2017, Stuttgart, Germany: 184–189.

EN 206-1. 2013. Concrete – Specification, performance, production and conformity. European Norm (EN).

EN 1992- 1-1 Part 1. 2014. Eurocode 2: Design of concrete structures - Part 1-1: General rules and rules for buildings. European Norm (EN).

EN 50122-2. 2010. Railway applications - Fixed installations - Electrical safety, earthing and the return circuit Part 2: Provisions against the effects of stray currents caused by d.c. traction systems. European Norm (EN).

Helsing E. & Mueller U. 2013. Beständighet av cement och betong i tunnelmiljö (Resistance to cement and concrete in tunnel environment). Seminarium Vatten i anläggningsbyggande (Seminar on Water in Construction). Göteborg, Sweden. Nov 27, 2013.

Geng, J. & Ding, Q.J. 2010. Transport characteristics of chloride ion in concrete with stray current. Journal of Building Materials, 1:121–124.

ITA. 1991. Report on the damaging effects of water on tunnels during their working life. Tunnelling and Underground space technology, 6(1):11–76.

Li, K. & Li, Q. & Wang, P. Fan, Z. 2015, September. Durability assessment of concrete immersed tube tunnel in Hong Kong-Zhuhai-Macau sea link project. Concrete Institute of Australia Conference, 27th, 2015, Melbourne, Victoria, Australia.

Li, Q. & Yu, H. & Ma, H. & Chen, S. & Liu, S. 2014. Test on durability of shield tunnel concrete segment under coupling multi-factors. Open Civil Engineering Journal, 8:451–457.

Niasati, M. & Gholami, A. 2008. Overview of stray current control in DC railway systems. International Conference on Railway Engineering - Challenges for Railway Transportation in Information Age, ICRE, Hong Kong, 2008:1–6.

PCA. 2002. Types and causes of concrete deterioration. PCA IS536.

Rashidi, S. & Nasri, V. 2012. Mitigation of the corrosion risk for large concrete sewer tunnels. ITA-AITES World Tunnel Congress (WTC) 2012, Bangkok, Thailand.

Romer, M. 2013. Durability of underground concrete. Workshop on Underground Infrastructures: Challenges and Solutions, June 27, 2013, LTA, Singapore.

Sigl, O. &, Raupach, M. & Rieker, L. 2000. Durability design of concrete tunnel lining segments. 25th Conference on Our World in Concrete and Structures: 23–24 August 2000, Singapore.

Swiss Standard SIA 262. 2003. Concrete structures. Swiss Society of Engineers and Architects.

Tang, K. 2017. Stray current induced corrosion of steel fibre reinforced concrete. Cement and Concrete Research, 100:445–456.

Wang, C. & Li, W. & Wang, Y. & Xu, S. & Fan, M. 2018. Stray current distributing model in the subway system: A review and outlook. International Journal of Electrochemical Science, 13:1700–1727.

Xiong, W. 2008. Study on deterioration characteristics of reinforced concrete in the presence of stray current and chloride ion. PhD dissertation, Wuhan University of Technology, Wuhan, China.

Zhu, Y.H. & Zou, Y.S. 2012. Influence of stray current on chloride ion migrates in concrete. Journal of Wuhan University of Technology, 7:32–36.

*Tunnels and Underground Cities: Engineering and Innovation meet Archaeology, Architecture and Art, Volume 5: Innovation in underground engineering, materials and equipment - Part 1 – Peila, Viggiani & Celestino (Eds)*
 *ISBN 978-0-367-46870-5*

# Relieved specific energy estimation using FLCM and PLCM linear rock cutting machines and comparison with rock properties

C. Balci, H. Copur & D. Tumac
*Mining Engineering Department, Istanbul Technical University, Maslak, Istanbul, Turkey*

R. Comakli
*Mining Engineering Department, Nigde Omer Halisdemir University, Nigde, Turkey*

ABSTRACT: Specific energy is defined as the amount of work required to break a unit volume of rock and used to predict the performance of mechanical miners. This value can be obtained from full-scaled laboratory linear (FLCM) or portable linear rock cutting (PLCM) experiments at different cut spacings and depths, respectively. For this purpose, full-scaled linear and portable linear rock cutting experiments are performed on 5 different blocks of rock samples including Beige marble, Kufeki limestone, Travertine, Sandstone and Limestone. Cutter forces acting on a cutter in three orthogonal directions (cutting force, normal force, and sideway force) and, specific energy values are measured during testing. In addition, some physical and mechanical property testing are carried out and the relationships between optimum specific energy values and rock mechanical properties are analyzed using regression analysis. Statistical analyses suggest that the relieved specific energy values can be predicted reliably from rock mechanical properties to select the most efficient mechanical miners for a given rock or mineral.

## 1 INTRODUCTION

Prediction of the excavation performance of any mechanical excavator such as roadheaders, continuous miners and shearers for any geological formation is one of the main concerns in determining the economics of a mechanized mining and/or tunneling operation. There are several methods of performance prediction and the best approach may be the use of more than one of these methods. These methods may be generally classified as full-scale linear cutting test, small-scale cutting test (core cutting), empirical approach, semi-theoretical approach and field trial of a real machine.

Empirical performance prediction models are mainly based on the past experience and the statistical interpretation of the previously recorded field data. Collection of field data is very important for developing empirical performance prediction models. The accuracy and reliability of these models depend on the quality and amount of the data. It is usually difficult to collect large amount of and high quality data in the field (Balci, 2009; Balci and Bilgin 2007; Balci and Tumac, 2012).

It is widely accepted that efficiency of mechanical excavators such as roadheaders, continuous miners, and shearers are measured based on specific energy value for a given rock and cutter type. Specific energy concept provides a realistic measure of rock cuttability and a simple method for a quick and informative performance (production) capacity of all types of mechanical excavators. The specific energy is best obtained from full-scale rock cutting tests, which fulfills the gap and weaknesses of the theoretical and empirical models. The basic disadvantage of full-scale rock cutting tests is that it requires large blocks of rock samples (around 1x1x0.6 m), which are usually difficult, too expensive or impossible to obtain. Therefore, the core sample based cuttability tests are preferred in many cases, even though their predictive abilities are lower than full-scale rock cutting tests. Specific energy values were correlated, in the past, with rock properties by different researchers. However, these researches were usually limited to one rock type, one machine type and/or one index rock property. Therefore, this study focuses on the prediction of specific energy based on core based index tests including a wide range of rock, mineral and ore types. Portable and Full-scale rock cutting tests and physical and mechanical property tests are performed on the rock samples collected from different mine and tunnel sites. The relationships between the specific energy and rock properties such as compressive strength, tensile strength values are investigated by using regression analysis.

## 2 FLCM AND PLCM LINEAR ROCK CUTTING TESTS AND PROCEDURES

Laboratory testing program includes portable and full-scale rock cutting tests and physical and mechanical property tests. The tests are performed in the laboratories of Istanbul Technical University, Mining Engineering Department. The testing equipment, procedures and parameters are introduced and discussed in this section.

Full scale linear rock cutting machine (FLCM) is presented in Figure 1. Cutting (drag or rolling) force, acting parallel to the surface being cut and tool travel (cutting) direction, is directly related to the torque requirement of a mechanical miner, and used to estimate specific energy, which is defined as energy (work) required to excavate a unit volume or mass of rock (Pomeroy 1963, Roxborough 1973). Normal (thrust) force, acting perpendicular to the surface being cut and tool travel direction, is used to estimate required effective mass and thrust of the excavator to keep the tool in a desired depth of cut (penetration). Sideways force, acting perpendicular to the tool travel direction and the direction of normal and cutting forces, may be used along with normal and cutting forces to balance tool lacing for minimizing machine vibrations.

One of the portable rock-cutting devices was developed in the Mining Engineering Department of Istanbul Technical University (Bilgin et al. 2010). In the new generation of PLCM all mini scale cutters (mini discs, mini conical and chisel cutters) can be used in the rock cutting experiments (Balci et al.2016, Comakli et al. 2015). The cutter is attached to the dynamometer with a tool holder. Experiments are performed at 3 cm/s cutting speed and forces are measured with a data logger system. Before performing the experiments, surface of the rock is trimmed or conditioned with the cutters. All experiments are replicated 3 or 4 times. In Figure 2, a photographic view of the testing machine is given.

Figure 1. Full-scale linear cutting machine (FLCM) in ITU Laboratories.

Figure 2. A new generation portable linear rock cutting machine in ITU Laboratories.

A groove is cut on the surface of a rock sample with a small disc cutter with a certain depth of cut. The table of the portable linear rock-cutting device is moved by a hydraulic cylinder. Block rock samples in 20 × 20 × 10 cm in size or core samples split into two pieces (two halves) are attached to the table with a special mechanism or cast in a sample box with a flat surface on top to cut the rock with a minidisc. The forces acting on the cutter and specific energy values are measured using triaxial force transducer (dynamometer). Dynamometers equipped with strain gauges have been designed and developed for this special application, reaching a precision in the order of 1 kN and covering a range from 0 to 100 kN. The force dynamometer is calibrated with a hydraulic cylinder by applying known forces. The tests should be replicated at least 3 times for more reliable results in a given rock type. Using the new generation PLCM different cutter tools can be used for rock cutting tests. CCS type mini discs used with PLCM are shown in Figure 2.

### 2.1 *Estimation of optimum specific energy from laboratory cutting experiments*

Specific energy concept provides a realistic measure of rock cuttability and a simple method for a quick and informative performance (production) capacity of all types of mechanical excavators. The specific energy is best obtained from small-scale or full-scale rock cutting tests, which fulfills the gap and weaknesses of the theoretical and empirical models.

The production rate of a given mechanical miner is calculated by the following equation:

Net cutting rate can be calculated using Equation 1 below:

$$ICR = k.\frac{P}{SE_{opt}} \tag{1}$$

where ICR = net cutting rate in $m^3/h$; P = power consumed in optimum conditions in kW; k = energy transfer ratio from cutterhead to tunnel face usually taken as 0.85–0.90, (Rostami et al., 1994); SEopt = optimum specific energy, $kWh/m^3$.

The predicted net cutting rate by using Equation 1 is valid for competent rock conditions and does not include the effect of rock mass properties (Bilgin et al., 2014). Energy transfer ratio (k factor) is also selected for competent rock to be 0.85 -0.9 (Rostami et al., 1994). It is obvious that the geological discontinuities will increase or decrease the net excavation rate to a certain level. Low RQD or water income in rock formation with high amount of clay will decrease the daily advance rate due to regional collapses, face instability and chocking the cutters etc.

The effect of the spacing between the cuts and depth of cut on the cutting efficiency/specific energy is also explained in Figure 3. If the line spacing is too small (a), the cutting is not efficient due to over-crushing the rock. If the line spacing is too wide (c), the cutting is not

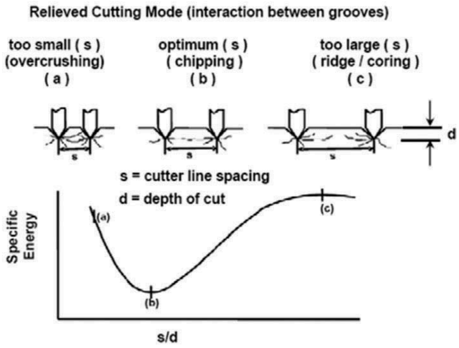


Figure 3. Effect of line spacing and depth of cut on specific energy.

efficient since the cuts cannot generate relieved cuts (tensile fractures from adjacent cuts can not reach each other to form a chip), creating a groove deepening situation or forming a bridge/rib between the cuts. The minimum specific energy is obtained with an optimum spacing to depth of cut ratio (b). The optimum ratio of cutter spacing to depth of cut varies generally between 1 and 5 for pick (drag) cutters. The specific energy (SE) is calculated as follows using Equation 2 below:

$$SE = \frac{FC}{Q} \tag{2}$$

where, SE = specific energy in MJ/$m^3$; FC = mean cutting (drag) force in kN; Q = yield per unit length of cut in $m^3$/km. Cutting force and yield are functions of rock properties, bit type and cutting geometry.

## 3 PHYSICAL AND MECHANICAL PROPERTIES OF ROCKS

The physical and mechanical properties of the rock sample is determined according to ASTM (2005) for acoustic velocity, for the rest of the physical and mechanical property tests standards of ISRM (Ulusay and Hudson, 2007). Physical and mechanical property tests include uniaxial compressive strength, Brazilian tensile strength, static elasticity modulus, acoustic velocity test (dynamic elasticity modulus, Poisson's ratio). Uniaxial compressive strength tests are carried out on grinded core samples with a length to diameter ratio of 2. The stress rate applied to core samples is 0.5 kN/s. Brazilian tensile tests are performed on core samples with 0.25 kN/s stress rate and the ratio of a length to diameter of 1. The results of physical and mechanical properties of the beige marble is given in Table 1.

Table 1. Results of the rock mechanics tests.

| | Travertine | Limestone | Beige marble | Sandstone | Kufeki limestone |
|---|---|---|---|---|---|
| UCS (MPa) | 9.10 ± 1 | 70.2 ± 12.5 | 160.7 ± 10 | 120.6 ± 21.5 | 15.6 ± 3.3 |
| BTS (MPa) | 3.17 ± 0.26 | 7.73 ± 1.33 | 7.82 ± 1.82 | 11.94 ± 1.32 | 1.14 ± 0.16 |
| $\gamma$ (gr/$cm^3$) | 1.92 ± 0.06 | 2.7 ± 0.01 | 2.7 ± 0.01 | 2.8 ± 0.01 | 2.16 ± 0.02 |

$\gamma$ = Natural unit weight (density), UCS = Uniaxial compressive strength, BTS = Brazilian (indirect) tensile strength.

## 4 SPECIFIC ENERGY COMPARISON OF FLCM, PLCM RESULTS AND ROCK PROPERTIES

The independent linear cutting test variables in this study consist of five major constant variables: rock type (five blocks of samples), cutting mode (relieved), cutter penetration (1, 1.5, 2, 3, 4, 5 mm for relieved cutting mode), and line spacing (relieved mode) and cutter type (432 mm in diameter CCS type disc cutter with 18 mm tip width and 144 mm in diameter CCS type mini disc cutter with 2 mm tip width). The dependent variables are average cutter forces (rolling and normal force), and specific energy. The constant parameters through the testing program are cutting sequence (single-start), cutting speed (12.7 cm/s in FLCM 3 cm/s in PLCM), and data sampling rate (2,000 Hz). Each cut is replicated at least 3 or 4 times. Mean forces (rolling and normal forces) and yield (the volume of rock obtained per unit length of cut cutting) are recorded in each cut. Specific energy is obtained by dividing mean cutting force to yield. Results of the rock cutting tests with FLCM with 432 mm in diameter CCS type disc cutter and 144 mm in diameter CCS type mini disc cutter in unrelieved cutting modes is presented in Table 2.

The results of the specific energy obtained from FLCM and rock properties were correlated with the result of the specific energy obtained from PLCM and rock properties for144 mm in diameter mini disc cutter in unrelieved cutting conditions (Balci et. al, 2017). Relationships between UCS and specific energy for PLCM and FLCM in relieved cutting conditions at 5 mm depth of cut are given in Figures 4 and 5.

Table 2. Results of the rock cutting tests obtained from FLCM and PLCM in relieved cutting conditions.

| | PLCM (CCS) | | | FLCM (CCS) | | |
|---|---|---|---|---|---|---|
| Rock formation | SE (kWh/m$^3$) | FN (kN) | FR (kN) | SE (kWh/m$^3$) | FN (kN) | FR (kN) |
| Beige marble | 12.07 | 11.91 | 2.03 | 5.58 | 142.94 | 4.50 |
| Kufeki limestone | 4.13 | 5.29 | 0.86 | 1.18 | 26.34 | 2.57 |
| Travertine | 6.41 | 13.77 | 3.07 | 1.81 | 66.26 | 8.47 |
| Sandstone | 10.62 | 12.00 | 3.11 | 5.09 | 108.82 | 9.77 |
| Limestone | 8.94 | 13.76 | 3.27 | 3.37 | 61.28 | 5.60 |

FN = Experimental mean normal forces; FR = Experimental mean rolling forces; SE = Specific energy.

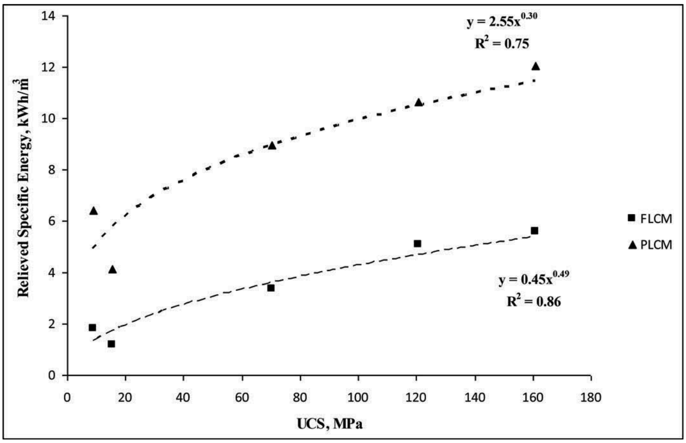


Figure 4. Relationships between UCS and specific energy for PLCM and FLCM in relieved cutting conditions at 5 mm depth of cut.

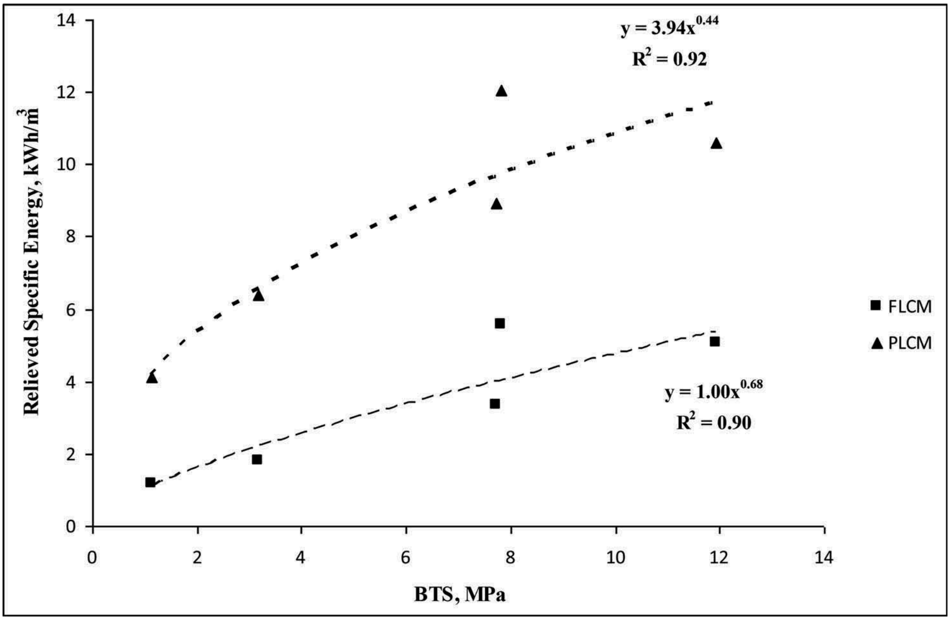


Figure 5. Relationships between BTS and specific energy for PLCM and FLCM in relieved cutting conditions at 5 mm depth of cut.

It is seen from the figures that the best-fitted relationships are found to be best represented by power functions. The correlation coefficients between unrelieved specific energy from FLCM and PLCM and uniaxial compressive at 5 mm depth of cut values is found to be 0.75 and 0.86, respectively. The correlation coefficients between unrelieved specific energy from FLCM and PLCM and Brazilian tensile strength at 5 mm depth of cut values is found to be 0.92 and 0.90, respectively.

## 5 CONCLUSION

This paper summarizes the results obtained with a new developed portable linear cutting machine (PLCM). A recently developed rock cutting testing device named as Portable Linear Cutting Machine (PLCM) is used in this study to measure normal and rolling forces acting on mini-scale cutting tools for mini disc, and specific energy. This machine minimizes the disadvantages of FLCM and can be used for predicting performances of the mechanical excavators used for hard rocks such as tunnel boring machines (TBMs), roadheaders, surface miners and, shearers. PLCM tests can be performed faster compared to the other full scale linear rock cutting machines and do not require too much manpower and large blocks of rock samples; thus it is comparatively cheaper.

The results indicate that specific energy values obtained from PLCM and FLCM by using disc cutters are very well-correlated with UCS and BTS for five different rock types. Relieved specific energy values can be predicted by BTS and UCS parameters reliably. The performance parameters of mechanical excavators such as thrust force, cutterhead power, and net cutting rate of known machines are theoretically estimated with using the PLCM test results.

The studies are still continuing with some other rock types, other cutter types (conical and chisel), and different experimental conditions in both laboratory and field for developing more reliable predictive models and verification purposes. Scale effect due to the cutters geometry (size, cutter ring tip width, the cutter ring diameter, cutting velocity etc.) is under analysis for further investigations.